

EVAPORATION AND SPUTTERING
PROCESSES FOR Se-CdO
PHOTOVOLTAIC CELL STRUCTURES

by
Ziad A. Shukri

*A thesis submitted to the Faculty of Graduate Studies
and Research in partial fulfillment of the requirements
for the degree of Master of Engineering.*

Department of Electrical Engineering
McGill University, Montreal, Canada
October 1989.

**EVAPORATION AND SPUTTERING
PROCESSES FOR Se-CdO
PHOTOVOLTAIC CELL STRUCTURES**

ACKNOWLEDGEMENTS

The author wishes to express his sincere appreciation to his supervisor, professor C.H. Champness, for his valuable guidance, advice and patience throughout this work and also for his dedication to his students.

The author also extends his thanks to J. Foldvari, A. Limoges and B. Dicso for preparing the mechanical parts for the experiments. Thanks are also due to J. Mui for his help with photographic work.

Many thanks are extended to G. Rodrigue for his valuable efforts in maintaining the vacuum systems in the laboratory in good working condition and to Y. Go for his assistance in preparing the curve fitting calculations.

The financial support of this work by the Fonds pour la Formation de Chercheurs et l'Aide a la Recherche (FCAR), is greatly acknowledged.

To my father, mother, sister and brother whom have given me all their love, respect, support and encouragement, throughout the years and to whom I have much love and admiration, I can only do the least and dedicate this thesis to them.

ABSTRACT

A study has been made of certain features of the fabrication of a Se-CdO photovoltaic cell having a layer structure usually of the form Al-Bi-Se-CdO-metal. It was found that increasing the substrate temperature during the selenium deposition between 80 and 140°C increased the illuminated short circuit current density in the cell. This clearly demonstrated the necessity of having well-crystallized selenium, as opposed to amorphous selenium, as the active absorber layer in this cell. The CdO layer was normally deposited by d.c. reactive sputtering from a cadmium target in an ambient of argon plus residual air and, as a result of optimizing experiments, a conversion efficiency of about 2% was obtained under an illumination of 100 mWcm⁻². The CdO layer was also deposited by r.f. magnetron sputtering from a CdO target. This produced satisfactory cells but with lower shunt resistance values than in the d.c. sputtered devices. It was found that the electrical resistivity of the CdO layer was decreased with increase of r.f. power and with decrease of sputtering pressure. Exploratory Se-CdO cells were also fabricated on glass substrates using d.c. reactive sputtering. By connecting these electrically in series, a photovoltaic panel was constructed and incorporated as the power source in a small pocket calculator, which was found to function satisfactorily under indoor lighting. An inverted structure of the form CdO-Se-metal was also fabricated and shown to function as a photovoltaic device.

RESUME

Nous avons examiné certaines caractéristiques du procédé de fabrication d'une cellule photovoltaïque de Se-CdO comportant une structure de couche de type Al-Bi-Se-CdO-métal. On a découvert qu'entre 80° et 100°C, l'augmentation de la température du substrat pendant la déposition du sélénium faisait augmenter la densité du courant du court-circuit sous éclairage dans la cellule. On a ainsi clairement démontré que la couche absorbante de la cellule doit se composer de sélénium bien cristallisé et non de sélénium amorphe. La couche de CdO a été normalement déposée par pulvérisation réactive en courant continu à partir d'une cible de cadmium et en présence d'argon et d'un peu d'air résiduel. Les expériences d'optimisation ont permis d'obtenir un rendement de conversion de 2% sous éclairage de 100 mWcm⁻². La couche de CdO a été également déposée par pulvérisation magnétron à haute fréquence à partir d'une cible de CdO. On a ainsi obtenu des cellules satisfaisantes, qui présentent des valeurs de résistance shunt plus faibles qu'avec le procédé de pulvérisation en courant continu. On a constaté que la résistivité électrique de la couche de CdO diminuait en fonction de l'augmentation de la puissance à haute fréquence et de la diminution de la pression de pulvérisation. Des cellules préliminaires de Se-CdO ont également été fabriquées sur des substrats de verre par pulvérisation réactive en courant continu. En reliant ces cellules en série, on a pu construire un panneau photovoltaïque qui a été incorporé à une calculatrice de poche comme alimentation. Cette calculatrice a fonctionné de façon satisfaisante sous éclairage artificiel. Nous avons aussi fabriqué une structure inversée de CdO-Se-métal; cette nouvelle structure s'est comportée comme un dispositif photovoltaïque.

TABLE OF CONTENTS

ACKNOWLEDGEMENTS	i
ABSTRACT	ii
RESUME	iii
TABLE OF CONTENTS	iv
1 INTRODUCTION	1
2 OVERVIEW OF SPUTTERING	5
2.1 INTRODUCTION	5
2.2 GLOW DISCHARGE	6
2.3 DIODE d.c. SPUTTERING	7
(a) Sputtering Power	8
(b) Sputtering Pressure	8
(c) Target-to-Substrate Separation	9
(d) Target and Substrate Temperature	9
2.4 DIODE r.f. SPUTTERING	10
2.5 REACTIVE SPUTTERING	12
2.6 MAGNETRON SPUTTERING	13
3 MEASUREMENT TECHNIQUES	14
3.1 INTRODUCTION	14
3.2 MEASUREMENT OF CELL CHARACTERISTICS	14
(a) Illuminated j-V Characteristics	14
(b) Dark j-V Characteristics	15
(c) Photoresponse	15

TABLE OF CONTENTS (Cont'd)

3.3 MEASUREMENT OF LAYER CHARACTERISTICS	16
(a) Selenium Film Thickness	16
(b) Se-CdO Cell Inter-stripe Cell Resistance	17
(c) CdO Film Thickness	17
(i) Films in cells	17
(ii) Films on glass substrates	17
(d) CdO Film Resistivity	18
4 EFFECT OF SUBSTRATE TEMPERATURE ON Se-CdO CELLS	21
4.1 INTRODUCTION	21
4.2 SAMPLE PREPARATION	22
(a) Aluminum Substrate Preparation	22
(b) Bismuth Evaporation	22
(c) Selenium Evaporation	23
(d) CdO Reactive d.c. Sputtering	24
(e) Wood's Alloy Evaporation and Soldering of Leads	25
4.3 EXPERIMENTAL RESULTS	26
(a) Effect on Illuminated j-V Characteristics	27
(b) Effect on Dark j-V Characteristics	28
(c) Effect on Photoresponse	28
(d) Effect on Selenium Morphology	29
4.4 DISCUSSION	30
5 PRELIMINARY STUDIES ON R.F. SPUTTERED Se-CdO CELLS	53
5.1 INTRODUCTION	53
5.2 SAMPLE PREPARATION	54
(a) R.f. Sputtering Apparatus	54
(b) CdO Powder Target Preparation	54
(c) CdO Depositions on Glass Substrates	55
(d) CdO Depositions in Cells	56
(e) Other Cell Fabrication Details	57

TABLE OF CONTENTS (Cont'd)

5.3 EXPERIMENTAL RESULTS	57
(a) CdO Films Deposited on Glass	57
(i) Effect of sputtering pressure	57
(ii) Effect of sputtering power	58
(b) R f. Sputtered Selenium CdO Cells	58
(i) Uniformity of CdO depositions	58
(ii) Effect of sputtering pressure	59
(iii) Effect of deposition time	61
(iv) Accidental change of device characteristics	61
5.4 DISCUSSION	62
(a) Uniformity of CdO Depositions	62
(b) Effect of Sputtering Pressure	62
(c) Effect of Deposition Time	64
(d) Effect of Sputtering Power	64
(e) Device Performance Change	65
6 EXPLORATORY Se-CdO PHOTOVOLTAIC PANELS	87
6.1 INTRODUCTION	87
6.2 PREPARATION OF NORMAL PANELS	88
(a) Substrate Preparation	89
(b) Bismuth Deposition	90
(c) Selenium Deposition	90
(d) CdO Deposition	91
(e) Wood's Alloy Deposition and Interconnects	91
(f) Panels with Configurations D, E, F and G	92
(g) Photolithographic Experiments	92
6.3 EXPERIMENTAL RESULTS ON NORMAL PANELS	93
(a) Performance of Panel Cells	93
(b) Overall Panel Performance	94
(c) Glass Substrate Cells versus Aluminum Stud Cells	94
(d) Uniformity of CdO Film	95
(e) Uniformity of Selenium Film	96
(f) Effect of Cell Short Circuit	96

TABLE OF CONTENTS (Cont'd)

6.4	PREPARATION OF INVERTED PANELS	97
	(a) Substrate Preparation	97
	(b) Window Material Deposition	98
	(c) Selenium Deposition	98
	(d) Metal Contact Deposition	99
	(e) Wood's Alloy Contacts and Interconnects	100
6.5	EXPERIMENTAL RESULTS ON INVERTED PANELS	100
	(a) Glass-CdO-Se-Bi Inverted Panels	100
	(b) Glass-Cd-Se-Pt Inverted Panel	101
6.6	DISCUSSION	101
	(a) Normal Structures	102
	(b) Inverted Structures	104
7	OVERALL DISCUSSION OF RESULTS	130
	7.1 EFFECT OF SUBSTRATE TEMPERATURE	130
	7.2 CELLS FABRICATED WITH r.f. SPUTTERING	131
	7.3 Se-CdO PHOTOVOLTAIC PANELS	133
8	CONCLUSIONS AND FUTURE WORK	136
	8.1 CONCLUSIONS	136
	8.2 FUTURE WORK	137
	(a) Selenium Film Deposition	137
	(b) CdO Film Deposition	138
	(c) Normal and Inverted Panels	140
	BIBLIOGRAPHY	141
	CURRENT DENSITY-VOLTAGE RELATION IN CELLS	144

Chapter 1

INTRODUCTION

The Se-CdO photovoltaic cell has been used for more than half a century in the field of photometry, mainly because it exhibits a spectral response closely resembling that of the human eye. However, while these commercial Se-CdO cells are satisfactory for the measurement of lower light levels, their conversion efficiency at higher illumination is somewhat poor. Hence, such photometry cells are not serious contenders for high power photovoltaic applications, such as solar cells. Never-the-less, in a theoretically perfect selenium homojunction, the short circuit current density (j_{sc}) is estimated to be around 18 mAcm^{-2} (from the energy gap of selenium of about 1.85 eV), which is about one order of magnitude larger than that observed in the commercial cells. While homojunctions are not possible in selenium because n-type conduction has not been observed in this material, heterojunctions such as Se-CdO structures can be fabricated. Hence, if the output of the Se-CdO cell could be increased beyond that of the existing commercial photometry cell, it would seem possible that these devices could have potential use in low power applications, possibly in the area of consumer electronics products, such as in pocket calculators and watches. Furthermore, from an economic point of view, the Se-CdO cell would appear to be competitive, since the fabrication steps mainly involve simple low temperature processes and also the raw materials are readily available.

While the Se-CdO photometry cells were fabricated for many years, it was only in 1950 that the first detailed study on these structures was published. Preston [1] reported the fabrication of Se-CdO cells with the CdO layer deposited by d.c. reactive sputtering on a crystallized selenium film. The sputtering from a cadmium

target was carried out in a low pressure ambient of argon with a trace of residual air, intentionally left in the chamber. By adopting the same basic fabrication technique used by Preston [1], work was initiated in this laboratory in an attempt to improve the Se-CdO cell by optimizing the many fabrication variables which affect its performance [2,3,4]. As a result of this work, cells were fabricated with an increase in j_{sc} well beyond that of the commercial photometry cells. The basic cell structure employed in these studies consisted of an aluminum base, as the substrate, on which a layer of bismuth was first evaporated. A layer of crystalline selenium was then deposited by evaporation on to the bismuth and followed by the deposition of four CdO areas on to the selenium layer using d.c. reactive sputtering. Wood's alloy contacts were then deposited on to the CdO for external connections. In recent work, Go [5] studied in detail the important parameters affecting the stoichiometry of the CdO film and found that sputtering pressure, sputtering current and gas flow rate influenced the CdO film stoichiometry in much the same manner, by controlling the deposition rate. This is because in the reactive sputtering process used, the stoichiometry of the deposited CdO depends on the transition time of the oxygen and cadmium atoms and hence on their rate of arrival at the substrate. An optimum set of conditions was therefore needed to obtain the right film stoichiometry to ensure that the CdO film was sufficiently transparent without having too high an electrical resistivity, leading to high series resistance.

While the deposition conditions of the CdO layer were investigated in some depth in previous work, no detailed studies were carried out to optimize the deposition parameters of the underlying selenium layer. This layer is especially important, since it is here that most of photogeneration of the electron-hole pairs takes place. However, some previously unpublished isolated results indicated that cell performance improved when higher substrate temperature was used for the

selenium deposition. The substrate temperature is expected to affect the crystallinity and hence the electrical conductivity of the selenium layer and thus, it would seem to be important to control this parameter. Accordingly, as the first part of this thesis, experiments were carried out in which a number of Se-CdO cells were fabricated under nominally similar conditions but with the selenium deposited at different substrate temperatures. The range of temperatures employed was between 80 and 140°C, so chosen to cover the transition of the selenium film from the amorphous to the crystalline phase.

While the method of d.c. reactive sputtering, employed in fabricating the Se-CdO cells in this laboratory, is satisfactory for the deposition of the CdO, there are other methods that can be utilized for depositing this layer. For example, Shaw and Ghosh [6] employed a radio frequency (r.f.) reactive sputtering technique to deposit the CdO in a slightly different Se-CdO structure and reported conversion efficiencies much higher than those observed in selenium photometry cells. Arising from this, it was considered worthwhile to explore the use of r.f. sputtering and to compare it with the d.c. reactive sputtering method for depositing the CdO film. The r.f. sputtering technique has some apparent advantages over d.c. sputtering, mainly because of the lower working pressures involved. This reduces the contamination in the deposited film and yields a greater film density. Since r.f. sputtering was never employed in this laboratory to deposit the CdO layer, a preliminary investigation of this method was considered to be of special interest. Accordingly, a study was carried out as a part of this thesis, where CdO was first deposited on glass substrates using r.f. magnetron sputtering from a CdO target. Following this, Se-CdO samples were then fabricated with this method. The sputtering parameters varied in this investigation were sputtering pressure, sputtering power and deposition time, and as will be seen later, some interesting results were obtained in these experiments.

While optimization of the fabrication parameters of the Se-CdO cell was not completed in the present work, it was never-the-less thought timely to test the feasibility of making a photovoltaic panel of series-connected cells, to power a small pocket calculator. The series interconnection of cells is necessary because the illuminated open circuit voltage (V_{oc}) of an individual cell is rather small. Accordingly, efforts were directed at constructing such a panel, which requires an insulating substrate, in contrast to the aluminum substrate used in the individual research cells. Several preliminary panels were made and tested and this work is described in the thesis. In an exploratory vein, an inverted cell panel was also fabricated, where in this case the sequence of layer depositions was reversed.

It should be pointed out that, since most of the work in this thesis was experimental and frequently of a preliminary and exploratory nature, detailed analyses of the photovoltaic characteristics of cells are not given.

The organization of this thesis is as follows. Firstly, chapter 2 gives a basic review of sputtering as used in thin film deposition. This is followed, in chapter 3, by a description of the measurement techniques employed in this study. Chapter 4 presents the results of the effect of substrate temperature during selenium deposition on cell performance and in chapter 5, preliminary results, obtained with r.f. magnetron sputtering of the CdO layer, are reported. Exploratory work on the Se-CdO photovoltaic panels is presented in chapter 6, followed by a discussion of all the results in chapter 7. Finally, in chapter 8, a summary is given of the conclusions drawn from this work, as well as a list of possible future studies.

Chapter 2

OVERVIEW OF SPUTTERING

2.1 INTRODUCTION

Sputtering is a versatile process for the deposition of elemental and compound thin film materials on a variety of substrates. The growing popularity of this technique stems mainly from its applicability to a wide range of industrial needs. While thin film sputtering emerged in a major way only in the last three to four decades, the concept of sputtering was known for more than a century. The phenomenon was first observed by Sir W. R. Grove [7] as early as 1852, during experiments on the electrical conductivity of gases, where he referred to the process as cathodic disintegration. Later, in 1908, for the first time, J. Stark [8] proposed that the cathodic disintegration was due to the release of atoms through momentum-transfer by the bombarding particles. In 1921, Sir J.J. Thomson [9] dubbed the process "sputtering" but the "t" was dropped in a scientific paper published two years later. Sputtering was used as early as 1877 to coat reflectors with metallic films. The method employed then was d.c. (direct current) sputtering. While this technique was satisfactory for the deposition of metallic layers, another method, known as r.f. (radio frequency) sputtering, was developed for the deposition of insulating films. Thus, the use of sputtering was expanded to a wide range of non-conducting materials. With improvement in vacuum technology in the last two to three decades, sputtering became a more refined process, allowing for the deposition of large-area, high-purity films of improved reproducibility.

At present, sputtering is used in a number of applications such as in the

fabrication of integrated circuits and hybrid microelectronic components. It is also used in the deposition of protective coatings for industrial and commercial products as well as in ornamental applications. The universality of this process in film deposition has made it a valuable tool for research purposes as well. It is therefore, the object of this chapter to review the basic technique of sputtering as employed in thin film deposition. The emphasis of this chapter is on the important deposition parameters affecting the properties of the sputtered film. This is especially helpful in respect of work done in this thesis.

2.2 GLOW DISCHARGE

The phenomenon of glow discharge plays an important role in sputtering, since it is the environment in which the film deposition takes place. Therefore, it is of interest to review the basic characteristics of a glow discharge.

When a sufficiently large voltage is applied between two electrodes, in a low pressure chamber, the gaseous atoms are ionized by a small amount of residual electrons present in the gas, arising from cosmic rays for example. The resulting positive ions are then accelerated by the electric field to strike the cathode (the negative electrode) and release more electrons as well as some atoms from the cathode surface. The atoms then travel by diffusion to deposit on to fixtures inside the chamber. At the cathode, the electrons released by ionic bombardment are repelled by the negative potential towards the anode, where in transit, they make more ionizing collisions with the gas atoms creating ion-electron pairs. When the electrons emitted from the cathode create enough ions in the gas to release the same number of electrons, the discharge becomes self-sustaining.

While the structure of the classical vacuum-tube glow discharge exhibits

about seven different zones [10], the structure of the discharge normally observed in sputtering shows only two distinct regions. A glowing region (known as the negative glow) extends from the anode to a short distance away from the cathode, and a glow-less region, called the Crookes dark space, extends from the end of the negative glow to the surface of the cathode. The dark space is a region of positive ionic charge, attracted by the negative potential at the cathode and across which most of the applied voltage appears. The width of this region is approximated to be the mean distance travelled by an electron from the cathode before it makes an ionizing collision [11]. This distance is about five to ten times the actual mean free path of the electrons, which includes elastic collisions as well. The larger negative glow region is for the most part electrically neutral, although separate ions and electrons are present. The glow in this region is caused by some electron-atom collisions that result in the excitation of the atoms which then release the excess energy in the form of radiation, giving rise to the characteristic glow. In glow discharge sputtering, the atoms released from the surface of the cathode form the source of material used for the deposition of the film.

2.3 DIODE d.c. SPUTTERING

When it is desired to sputter a thin film of a metallic substance, the diode d.c. sputtering technique is a simple method to use. A solid target of the same material to be sputtered is prepared and placed in a vacuum chamber at the cathode position. A substrate to support the film to be deposited, is placed at the anode, and a suitable gas, such as argon is passed through the chamber at a specific pressure. By applying a negative bias to the cathode, positive argon ions bombard the target and cause the ejection of atoms or molecules from its surface, which then diffuse towards the substrate to deposit as a thin film.

During sputtering, the deposition of the film is influenced by many factors. The more important parameters affecting the properties of the deposited film are the sputtering power, the sputtering (chamber) pressure, the target-to-substrate separation and the temperature of the target and substrate during sputtering. The effects of these parameters are now briefly discussed.

(a) Sputtering Power

The sputtering power can be taken as the cathode potential times the sputtering current, the latter being proportional to the flux of ions at the target surface. Since the sputtering yield, which is the number of atoms ejected per incident ion, increases only slightly with target voltage in the energy range used in sputtering, the discharge current is a more important parameter for determining the deposition rate [12]. Because of this, it is better to sputter at high current and low voltage (rather than low current and high voltage) to make more efficient use of the power supplied. As will be described later, this may be achieved by using a magnetic field which enhances the ionization process in the gas.

(b) Sputtering Pressure

Another parameter that affects the deposition of the film is the sputtering pressure. At a constant power input, increasing the sputtering pressure increases the ion density in the chamber and therefore, also the discharge current. At lower pressure, the deposition rate increases linearly with increasing pressure due to the increase in the discharge current [12]. However, at higher pressure, although the ion density increases further, the rate of deposition of the film decreases due to the scattering of the sputtered material by gas atoms [13]. In fact, at a pressure as high as 130 mTorr, almost half of the sputtered material diffuses back to the target [14]. Since a minimum sputtering pressure is needed to sustain the glow discharge,

only a small operating pressure range between a few mTorr to about 100 mTorr can be employed in sputtering. The optimum pressure in this range yielding the greatest deposition rate must be empirically determined for each application.

(c) Target-to-Substrate Separation

The third important parameter that influences the deposition of the film is the target-to-substrate separation. If this distance is less than the width of the dark space, then essentially no deposition occurs. Therefore, the target-to-substrate separation must be made larger, preferably twice the dark space width to obtain improved uniformity. In fact, for a given sputtering pressure and geometry, an optimum separation exists that yields the best spacial film uniformity [15]. Beyond the dark space, increasing the target-to-substrate separation decreases the deposition rate of the sputtered film. Furthermore, with increase of this distance, the amount of gas incorporated into the growing film decreases [16] and also the amount of heat dissipated at the substrate by secondary electron bombardment is reduced [12].

(d) Target and Substrate Temperature

The deposition of the film is also affected by the temperature of the target and substrate during sputtering. In sputter deposition, it is estimated that only about 1% of the total input power results in the ejection of atoms. As much as 75% appears as heat dissipated in the target by the ion bombardment. The remaining 24% is dissipated at the substrate through the bombardment of secondary electrons [12]. The substrate temperature is known to affect the crystallization of the sputtered film [17], as well as its rate of deposition. For example in the case of germanium [18], it was found that increasing the substrate temperature decreases the deposition rate of the film. Similar results have also

been observed for other materials [18]. In target heating, as the target temperature rises, the sputtering rate is increased [19]. Therefore, it is important to control the temperature of both target and substrate during deposition. The target is usually water-cooled to minimize structural damage that may arise due to the excessive heating. However, while substrate cooling is also possible, it is sometimes desirable to deposit the film at a properly controlled temperature to promote epitaxial film growth for example. According to Chopra [20], when using sputtering, the critical substrate temperature needed for epitaxy is reduced as compared to evaporation. This is attributed to the higher kinetic energy and hence higher mobility of the sputtered atoms, compared to evaporated atoms. A review by Mattox and MacDonald [21] appears to support the above argument. However, a second school of thought seems to contradict the above statement, where it is claimed that at the pressures employed in sputtering, most of the sputtered atoms are thermalized by collisions with the "cold" gas atoms and therefore arrive at the substrate with a *lower* mean kinetic energy than that of atoms evaporated from a hot source in the vacuum [17,22].

2.4 DIODE r.f. SPUTTERING

If a metallic target is replaced by an insulating target in d.c. sputtering, the discharge will no longer be sustained. This is because positive charge build-up at the target surface decelerates the arriving ions, resulting in a reduced emission of secondary electrons and hence the termination of the discharge. One way to overcome this is to apply an a.c. (alternating current) signal to the target, so that in the first half of the cycle, the target is bombarded with positive ions and in the second half with electrons that neutralize the charge build-up. The termination of the discharge often occurs so quickly (of the order of 1 μ sec), so that if a low

frequency a.c. signal (e.g. 60 Hz) is used, the discharge will be off for the most part of the half cycle. Therefore, voltage signals in the higher radio frequency range (5 to 30 MHz) are employed.

The way in which sputtering takes place in a discharge with an r.f. excitation is as follows. If the r.f. signal is applied between two electrodes of equal area, a dark space develops near each electrode and both are sputtered in alternating cycles. However, if it is desired to sputter in one direction only, then the electrode to be sputtered must be of smaller area. This causes the voltage drop across the smaller electrode dark space to become much larger than that across the larger electrode dark space [23]. Furthermore, a capacitor must be connected in series with the r.f. power supply to support the difference in potential between the two electrodes. The polarity of the voltage at each electrode is negative with respect to the discharge [24] but the smaller electrode acquires a larger negative potential. Thus, this electrode acts as the target (cathode) which is sputtered by the positive ions. If the target to be sputtered is an insulator, then the capacitor is no longer necessary. In practice, the substrate is placed at the larger electrode, which is grounded thereby, making it the larger area. Film deposition is then carried out much like d.c. sputtering.

In using r.f. sputtering, certain advantages are obtained. For instance, at the higher frequency range, the ionization efficiency of the electrons oscillating in the discharge is increased so that there is less dependence on secondary electrons to sustain the discharge. Thus at a given power, it is possible to operate at lower pressure. This is advantageous since films sputtered at lower pressure are less porous and hence more dense [17]. In addition, at such pressures, the scattering of the sputtered material by the gas atoms is reduced [13] and hence, higher deposition rates are possible. Another advantage with r.f. sputtering is that the

heat dissipated at the substrate by secondary electrons is about half that dissipated in the case of d.c. sputtering [25].

2.5 REACTIVE SPUTTERING

Reactive sputtering is a technique employed for the deposition of certain compound thin films through a reaction between the sputtered material and the gas used inside the chamber. The formation of oxide and nitride thin films are common examples. Normally, a small quantity of the reactive gas (e.g. oxygen or nitrogen) is mixed with argon and used for sputtering with a metal target. The actual reaction may take place either at the target surface or the substrate surface. When the reactive gas partial pressure is low and the sputtering rate of the target is high, virtually all of the reaction and subsequent film formation occurs at the substrate. In this case, the stoichiometry of the film is determined by the relative rates of arrival of the sputtered material and the reactive gas atoms at the substrate [26]. However, if the gas partial pressure is increased beyond a critical value (in the case of oxygen for example), the reaction shifts to the target. In this case, the film is deposited by sputtering a compound layer from the target surface [27]. A strong decrease in the deposition rate of the film is usually associated with this shift, and thus, it is more desirable to use a lower partial pressure for the reactive gas for a reasonable deposition rate. Reactive sputtering can be employed with both d.c. and r.f. deposition methods, where it may also be used (in the case of r.f. sputtering) to restore the stoichiometry of films deposited from a compound target.

2.6 MAGNETRON SPUTTERING

In a conventional d.c. supported glow discharge, the degree of ionization is somewhat small, of the order of 10^{-4} . Hence, it would seem desirable to increase the ionization efficiency in the discharge. One way to do this is to force the secondary electrons to make more collisions in the gas phase, by travelling a longer distance, so that the probability of an ionizing collision is increased. This can be accomplished, for instance, by using a magnetic field from a permanent magnet placed inside the chamber. One example is the planar magnetron sputtering arrangement in which a flat, two-piece magnet is placed underneath the target. In this case, the lines of magnetic flux confine the electrons to helical paths near to the target surface. This increases the effective mean free path of the electrons so that more electrons are able to ionize the gas atoms and hence obtain a greater discharge current.

In comparison with conventional sputtering systems, a magnetron system generally yields a higher deposition rate of films. For example, in the case of copper, the erosion efficiency of the target, which is the amount of material sputtered per unit input power, was reported to be about three times greater in planar magnetron sputtering than in conventional sputtering [28]. Furthermore, with magnetron sputtering, the amount of heat dissipated at the substrate is reduced, since most of the secondary electrons are trapped by the magnetic field in the vicinity of the target [25]. Currently, many magnetron sputtering arrangements are utilized in both d.c. and r.f. systems to obtain enhanced film deposition.

Chapter 3

MEASUREMENT TECHNIQUES

3.1 INTRODUCTION

In this thesis, results will be presented on many Se-CdO cell structures fabricated in different ways, under different conditions and as separate cells or in small panels. However, the evaluating measurements on the devices were all made in the same manner. Accordingly, it is convenient to describe the measurement techniques at the outset and this is done in the present chapter. Specifically, measurements of illuminated and dark current density-voltage (j - V) characteristics and of photoresponse were carried out on cell structures to evaluate their performance. Measurements were also done to evaluate the selenium and CdO layers of the cell and these were selenium film thickness, Se-CdO cell inter-stripe resistance and CdO film thickness and resistivity. A description of each measurement procedure is now given.

3.2 MEASUREMENT OF CELL CHARACTERISTICS

(a) *Illuminated j - V Characteristics*

Measurement of the illuminated current density-voltage characteristics of the cells was done using the circuit set-up shown in Fig.3.1. A solar simulator (Kratos model LH-150/1), fitted with an AM1 filter was employed to provide 100 mWcm^{-2} of direct illumination. The output characteristics of the cell, registered on an X-Y recorder (Hewlett Packard model 7035B), were obtained by manually changing a variable load resistor connected across the cell, as shown in the circuit. The

current was determined by measuring the voltage across a 100 ohm series sensing resistor; this voltage was measured at the Y terminals of the recorder. The voltage across the sample was measured via the X terminals of the recorder. The value of 100 ohm for the sensing resistor was chosen small enough to yield near short-circuit conditions for the cell with the load resistor set to zero but large enough to give reasonable accuracy. The position of the sample in the divergent light beam from the simulator was adjusted to AM1 as determined using a Solarex reference cell calibrated to yield 124.4 mV under AM1 conditions at room temperature.

(b) Dark j-V Characteristics

While the dark j-V characteristics could also be measured in principle using an X-Y recorder, this was found to be inadequate for the measurement of very small currents at lower voltage. Accordingly, a point-by-point method was employed using a multi-range voltmeter and ammeter. The set-up is shown in Fig.3.2. A Farnell d.c. power supply, together with a potentiometer, was used to provide the voltage bias to the cell in the range between 0 to 1.5 V. The polarity of the voltage source was changed to provide both forward and reverse bias. The current through the cell and the voltage across it were measured using a Keithley model 480 picoammeter and a Keithley model 610C electrometer respectively. The measurement was carried out while the cell was covered with a piece of dark cloth.

(c) Photoresponse

The response of the cells to different wavelengths of the optical spectrum was measured using the arrangement of Fig.3.3. A monochromator (Beckman model 2400) was used to generate the spectrum of wavelengths between 400 and 800 nm from a white light source (Oriol 100 W halogen lamp). Each wavelength

was selected by setting the dial, which controlled the rotation of the prism inside the monochromator. The opening of the exit slit of the monochromator was fixed at 1.5 mm. The response of the sample to incident monochromatic light was taken to be the short circuit current from the sample as measured with the Keithley model 480 picoammeter. This instrument was used in a sufficiently sensitive range to measure the current but one where the terminal resistance was low enough to consider the current to be a "short circuit" value. This measurement was again done in a point-by-point manner. In order to be able to calculate the photoresponse of the cell, the current of a calibrated silicon detector (United Detector Technology model 95289) was measured in the same spectral range. The photoresponse P_{Se-CdO} of the cells was then calculated at a given wavelength using the following formula:

$$P_{Se-CdO} = \frac{I_{Se-CdO} \cdot A_{Si}}{I_{Si} \cdot A_{Se-CdO}} P_{Si} ,$$

where

I_{Se-CdO} is the current generated by the Se-CdO cell,

A_{Se-CdO} is the area of the Se-CdO cell,

I_{Si} is the current generated by the silicon detector,

A_{Si} is the area of the silicon detector (0.2 cm²).

The detector photoresponse P_{Si} at different wavelengths was taken from a calibrated responsivity curve of the silicon detector, supplied by the manufacturer.

3.3 MEASUREMENT OF LAYER CHARACTERISTICS

(a) *Selenium Film Thickness*

The thickness of the selenium film was determined for each sample by chipping off a small piece of the film using a sharp razor blade and erecting it

edgewise on a glass slide edge using some grease. The edge of the selenium film was then viewed through a microscope with an eye-piece having fiduciary lines of predetermined separation. By simultaneously comparing the film edge with the line separation, the thickness of the selenium layer was obtained.

(b) Se-CdO Cell Inter-stripe Resistance

A measure of the resistance of the CdO areas deposited on the selenium film was obtained in the following manner. A Keithley model 169 digital multimeter was used for this purpose. The meter was simply connected to the pair of contact-strips on the same CdO area and the resistance value (R_{st}) registered. The resistance was measured on three different ranges to ensure consistency in the readings.

(c) CdO Film Thickness

(i) Films in cells

The thickness of CdO films in the Se-CdO cells was estimated from the inherent interference colours of the film. By viewing the CdO film under a microscope, the order of the interference colour at the central region was determined. The thickness was then calculated from the following relation $2nd=N\lambda$, where n is the refractive index of CdO (2.49), d is the CdO film thickness, N and λ are the order and wavelength of the colour at the central region respectively.

(ii) Films on glass substrates

The thickness of the CdO film sputtered on glass substrates was determined by a Dektak surface profile measuring instrument. An abrupt edge was created in the central region of the film by using hydrochloric acid as an etchant. The

technique used by the Dektak profiler is one in which the displacement of a stylus, that traces the surface topology of the film, is detected and converted into an electrical signal. The films were placed on a moving base below the stylus and a trace of the edge profile was registered by the instrument on chart paper. The CdO film thickness was then simply derived from the trace.

(d) CdO Film Resistivity

The electrical resistivity of CdO films deposited on the insulating glass substrates was measured using the four-point probe method. By measuring both current (I) and voltage (V), and using the thickness (t) as derived from the Dektak unit, the resistivity of the film ρ was calculated from the formula given by $\rho = 4.53(V/I) t$. During the measurements, it was verified that for zero current, the voltage was zero, and further that it reversed yielding the same magnitude, when I was reversed. The current used in the measurement was maximized without causing short circuits in the CdO film.

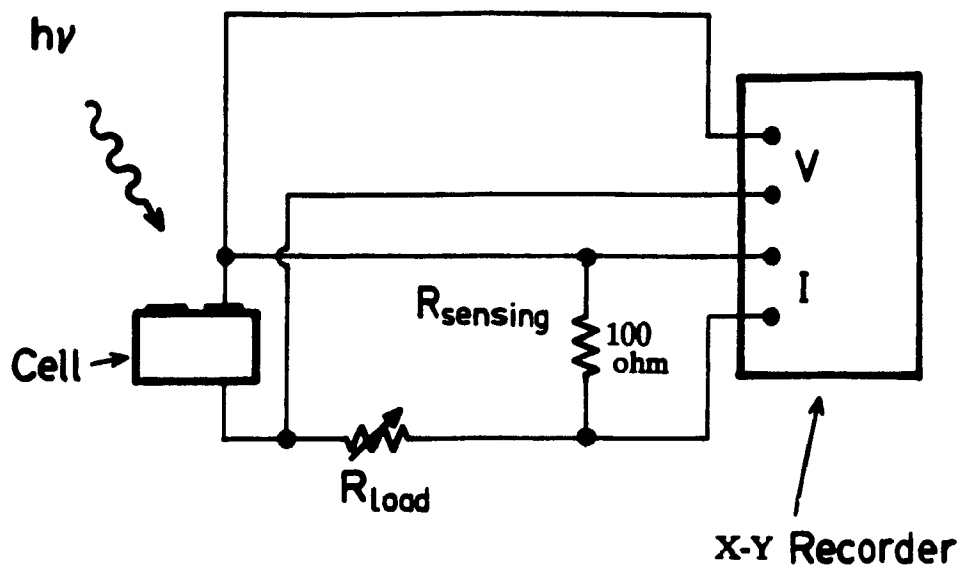


Fig.3.1 Circuit used for the measurement of the illuminated j-V characteristics of a cell.

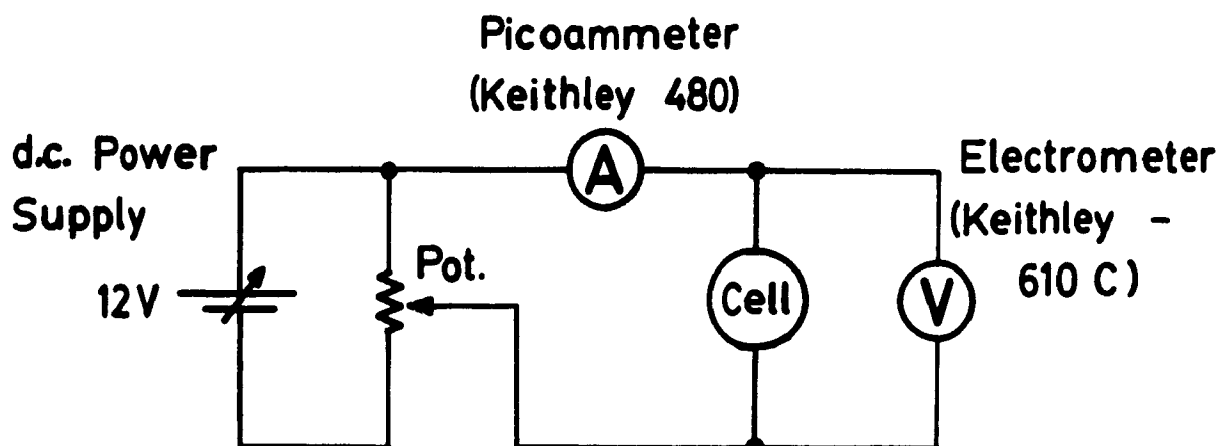


Fig.3.2 Circuit used for the point-by-point measurement of the dark j-V characteristics of a cell.

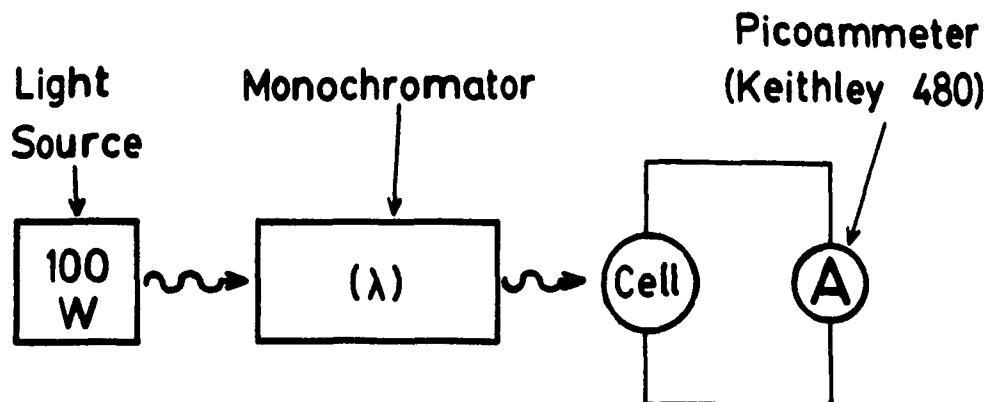


Fig.3.3 Set-up used for the measurement of the photoresponse of a cell

Chapter 4

EFFECT OF SUBSTRATE TEMPERATURE ON Se-CdO CELLS

4.1 INTRODUCTION

As mentioned in chapter 1, the conventional Se-CdO research cell involves a number of fabrication parameters which must be optimized to exploit the full potential of this device. Although many of these parameters were investigated in previous work [2,3,4,5], the effect on cell characteristics of substrate temperature during the deposition of the selenium film was not very clear. Therefore, as a part of the present work, a detailed study of the effect of this parameter on cell performance was carried out and this is the subject of the present chapter. Accordingly, a number of cells were fabricated under otherwise similar conditions but with the selenium deposited at different substrate temperatures ranging from 80 to 140°C. This temperature range covers the transition point of selenium from the amorphous state to the crystalline state and, as will be seen later, some very important results were obtained in this respect.

The Se-CdO samples were prepared by first evaporating a layer of bismuth on a mechanically-roughened cylindrical piece of aluminum. A layer of selenium was then evaporated on to the bismuth, followed by depositing four CdO areas on to the selenium film using d.c. reactive sputtering. Wood's alloy stripes were then evaporated on to the four CdO areas (cells) to define contacts and copper wires attached for external connections. Fig.4.1(a) shows a schematic diagram of the Se-CdO research sample, indicating the four CdO cells deposited on the common substrate. Fig.4.1(b) shows the numbering scheme of these cells with respect to the

base contact. These numbers will be referred to later. The fabrication details of all of the devices made are given in Table 4.1.

4.2 SAMPLE PREPARATION

This section describes the fabrication of the Se-CdO cells prepared with different substrate temperatures.

(a) *Aluminum Substrate Preparation*

The Se-CdO cells were fabricated on a cylindrical aluminum substrate (stud) about 2 cm in diameter and about 1 cm in thickness. Besides acting as the positive electrode of the cell, the substrate also provided structural support for the different cell layers. In order to allow for better adhesion between these layers and the substrate, the surface of the aluminum stud was mechanically roughened by hand, using a piece of sand paper (Canada Sand Papers, grit # 400), under running water for a few minutes and then dried using "Kimwipe" brand tissues. The aluminum surface was then rinsed with propanol and dried in a nitrogen gas stream, so as to minimize surface contamination. This treatment produced a rather clean and smooth aluminum surface, yet grooved enough to obtain good adhesion of subsequent layers.

(b) *Bismuth Evaporation*

Due to the poor sticking between selenium and aluminum at higher temperatures, a layer of bismuth was introduced between the two to improve the adhesion of the selenium film to the substrate. Immediately after substrate lapping, four aluminum substrates were located in a special mounting block and placed inside the chamber of a vacuum system (Edwards model 6E4), with a 6

inch-diameter bell jar. Bismuth pellets (about 3 to 4) were then placed in a self-constructed molybdenum boat, located about 7 cm below the aluminum stud surfaces. The coating system and the schematic evaporation arrangement are shown in Figs.4.2(a) and (b).

After 15 minutes of vacuum pumping to a pressure of well below 10^{-4} Torr, the bismuth was evaporated at a current of 40 A for 5 minutes. Following this evaporation, the samples were allowed to cool down for about 15 minutes before introducing air into the chamber.

(c) *Selenium Evaporation*

The selenium layer is one of two primary layers contributing to photovoltaic action in the Se-CdO cell. Being a vital component, selenium was evaporated with extra care, so as to ensure proper control over film deposition as well as maintaining contamination to a minimum. The evaporation was done for four samples at a time in a 12-inch bell jar vacuum system (Edwards model E12E3) immediately following the bismuth deposition. The samples were mounted in a special graphite holder supported inside the chamber by its own heating element. The holder was then properly positioned, such that it was 7 cm directly above a heated graphite crucible filled with selenium pellets. Inside the chamber one thermocouple was inserted in a tiny hole in the exterior side of the graphite sample holder and a second thermocouple was located in a similar hole in the graphite crucible. Propanol-soaked "kimwipe" tissues were then used to clean up oil-based contaminants from certain parts of the chamber. The selenium evaporation apparatus and the schematic arrangement inside the chamber are shown in Figs.4.3(a) and (b)

After the system was pumped down to a pressure of about 10^{-6} Torr (in 2 to

3 hours), the desired substrate temperature was selected on a temperature controller (Omega, model 1622-0-J). This controller maintained a specific temperature by continuously adjusting the duty cycle of a heating element such that the thermocouple-monitored temperature matched that of the set point. The temperature of the sample was allowed to stabilize for about one hour and then, with the shutter closed (i.e. covering the samples), the temperature of the crucible was raised using a second temperature controller (Marcland). The source temperature was increased to about 245°C (above the selenium melting point of 217°C) and allowed to stabilize for 20 minutes. This was followed by opening the shutter and exposing the samples to the selenium vapor. The evaporation time was taken as the duration between the opening and closing of the shutter.

After the evaporation was completed, the shutter was closed to obstruct further selenium deposition. This was followed by lowering the source and substrate temperatures. The substrate temperature was decreased at a rate of about 2°C per minute, so as to prevent the selenium film from peeling-off. This effect can be caused by the difference in the contraction rates between selenium and aluminum, which produces large stresses in the selenium film. After the temperature of the samples dropped to near room temperature, air was admitted into the chamber and the samples were removed.

(d) CdO Reactive d.c. Sputtering

The CdO layer was deposited on the selenium film by reactive d.c. sputtering using the residual air method. In this method, a cadmium target is used but because of a small amount of air deliberately left in the chamber, the sputtered cadmium reacts with the residual oxygen to deposit a CdO film. A second Edwards vacuum system (model E12E3), shown in Fig.4.4(a), was utilized for this purpose. The sputtering arrangement inside the chamber is shown in Fig.4.4(b).

Following the selenium deposition, each sample was mounted on a custom-made holder (shown schematically in Fig.4.4(b)), which was fitted with a masking assembly. An aluminum mask with four circular openings (Fig.4.6, mask number 1) was inserted into the assembly and brought into contact with the selenium surface of the sample. The holder, with its sample and mask, was then placed inside the chamber and located vertically above a cadmium target. The height of the holder was adjusted such that the surface of the sample was about 1.3 cm above the cadmium target (cathode). The chamber was then pumped down to an initial pressure of about 10 mTorr. At this pressure, the high vacuum valve was then closed and argon was introduced into the chamber via an inlet needle valve. As the pressure rose towards 75 mTorr, the high vacuum valve was re-opened and the chamber pressure was controlled with the opening of the gas inlet valve only. At a valve setting of about 80 units, a pressure of 75 mTorr was established. The sample was sputtered for 3 minutes at a current of 20 mA supplied from a high voltage power source, with a cathode potential of about - 700 volt. As the 3-minute run was completed, air was allowed into the system and after 5 minutes at atmospheric pressure the chamber was pumped down again to 10 mTorr. Sputtering was then carried out for another 3 minutes at 75 mTorr and 20 mA and this process was repeated for 10 cycles yielding a total sputtering time of 30 minutes. At the end of the tenth cycle the holder, with the sample inside, was removed from the chamber.

(e) Wood's Alloy Evaporation and Soldering of Leads

Wood's alloy was used to make contact stripes on each of the four CdO areas of the sample (Fig.4.1(a)). This metal is an alloy made up of 50% bismuth, 25% lead, 12.5% tin and 12.5% cadmium, having a melting point of about 71°C. The evaporation was done using the same system employed for the bismuth

deposition (Edwards model 6E4) with the same type of boat. Mask number 2 (Fig.4.6) was inserted into the mask holder to define a pair of stripes per CdO area of the sample. A small piece of Wood's metal was placed in a boat and the holder was located inside the chamber such that the boat was 5 cm directly below the surface of the sample. The arrangement is shown schematically in Fig.4.5. The chamber was then pumped down to a pressure well below 10^{-4} Torr, followed by an evaporation of 5 to 10 minutes at a current of about 40 A. After completion, the holder was taken out of the chamber and the sample removed.

After completing the deposition of all the layers, the sample was inserted into a custom-made plastic disk and secured with a screw, which also served as the positive electrode of the four cells on the sample. Thin copper wires were then soldered onto each of the eight Wood's alloy stripes on the cells. The other ends of the wires were soldered to eight screws fixed in the plastic casing, each screw acting as a negative electrode. The cells were then complete and ready to be tested. Fig.4.7 shows one of the four Se-CdO cells in a sample, where the CdO appears as a reddish disk on top of a yellowish-golden selenium film. The interference colours are clearly seen at the periphery of the CdO disk. Two wires are also seen soldered to the Wood's metal stripes on the CdO layer.

4.3 EXPERIMENTAL RESULTS

This section presents the results of the effect of substrate temperature on cell characteristics. A number of tests were carried out on the cells to evaluate their performance. The cells were tested in terms of their illuminated j-V characteristics, dark j-V characteristics, photoresponse and selenium film morphology. The results of these tests are given below.

(a) Effect on Illuminated j - V Characteristics

In this section, results for cells under an illumination of 100 mWcm^{-2} simulated solar irradiation are presented. Fig.4.8 shows representative curves of illuminated current density against voltage, for cells fabricated at eight different substrate temperatures. The general trend is seen to be an increase in the output power of the cells with increasing substrate temperature. This increase is more evident at temperatures below 110°C . At higher temperature however, beyond about 120°C , the increase in cell performance seems to be less definite. Cells at lower substrate temperatures, such as 80 and 90°C were also fabricated but are not shown since the short circuit current densities were less than $0.1 \mu\text{Acm}^{-2}$. The highest observed current density in a cell was 8.9 mAcm^{-2} , obtained at a substrate temperature of 140°C (not shown). The variations of short circuit current density j_{sc} and open circuit voltage V_{oc} with substrate temperature are also shown separately in Figs.4.9 and 4.10 respectively. The figures show a rather sharp increase in both j_{sc} and V_{oc} within a small temperature range between 80 and 100°C and, while V_{oc} remained more or less constant beyond 110°C , j_{sc} continued to show progressive increase with temperature.

Fig.4.11 shows the illuminated characteristics of the four cells of sample SH-24, which was fabricated at a substrate temperature of 95°C . The figure also shows a plan view of sample SH-24, where two regions can be distinguished on the selenium film. One of the regions appears to be more crystallized than the other, as evidenced by a higher density of localized crystallization regions. It is seen that the two cells fabricated on the more crystallized side, produced larger values for both j_{sc} and V_{oc} than those on the less crystallized side.

Fig.4.12 shows the illuminated j - V characteristics of cell SH-14-4 tested under both simulated AM1 illumination and actual solar irradiation. The latter

was carried out on October 5, 1987 at 1:20pm in Montreal. It is seen that although the actual solar illumination conditions were less than AM1, the j_{sc} value of the cell was about 7.4 mAcm^{-2} , which is slightly less than the value of around 8.7 mAcm^{-2} obtained under simulated illumination at 100 mWcm^{-2} . The open circuit voltage however, remained more or less unchanged near 0.52 V.

(b) Effect on Dark j-V Characteristics

Fig.4.13 shows typical dark forward characteristics of nine samples fabricated at eight different substrate temperatures. It can be seen that at higher voltage, the forward current increased with increasing substrate temperature. The increase is more evident at temperatures below 100°C . This can also be seen in Fig.4.14, where the forward current at 1.0 volt is plotted against substrate temperature. In this figure, it can be seen that between 80 and 100°C , the curve increased sharply with increasing temperature. Beyond 110°C however the current continued to increase but at a much lower rate up to a temperature of 140°C .

(c) Effect on Photoresponse

The photoresponse (also known as spectral response) of cells fabricated at substrate temperatures between 95 and 140°C is given in Fig.4.15. While the trend is not very definite it seems that, in general, the photoresponse of cells increases with increasing substrate temperature. It also appears that the peak photoresponse of the cells shifts to longer wavelengths with increase of substrate temperature. Both effects are more apparent in Fig.4.16 where the photoresponse of four of the cells fabricated at the substrate temperatures 80 , 90 , 100 and 140°C is shown. In this figure, it can be seen that the change in photoresponse between the temperatures 90 and 100°C is much greater than the change between 100 and 140°C .

(d) *Effect on Selenium Morphology*

A photograph of the surface of a selenium film grown at a substrate temperature of 120°C is shown in Fig.4.17 (see Table 4.1, sample SH-18). The appearance of the selenium layer in this photograph is in fact representative of films deposited at substrate temperatures between 110 and 140°C. The film shown is a polycrystalline one and not amorphous, even though the grain boundaries are not quite apparent at a first glance. Careful examination of the film however, reveals the boundaries as faint and tiny dark twisting lines in the selenium film. At a lower substrate temperature, grain boundaries became more apparent. Fig.4.18 shows three regions of a selenium film grown at a substrate temperature of 100°C. In this temperature range, two types of grains can be distinguished. One has a "crater-like" appearance and is slightly larger than the other type, which appears to be smoother. The density of the two types of grains seems to vary across the selenium film, as can be seen in Figs.4.18 (a), (b) and (c). Region (a) seems to be more dominated by smaller grains, while region (c) seems more dominated by the larger ones. A similar variation in grain density across the selenium film can also be seen in Fig.4.19, where three regions of a selenium film grown at a substrate temperature of 95°C are shown. Here, it is seen that the smaller grains are heavily packed in region (a), while only few of them appear in region (c). In fact, region (c) is largely made up of amorphous selenium. This semi-amorphous region is actually part of a circular shadow of amorphous selenium, which appeared on the four aluminum studs during evaporation, reflecting an image of the crucible opening. This phenomenon was only observed during the evaporation run at 95°C. At a lower substrate temperature the grain density dropped even further, as indicated in Fig.4.20 showing a selenium film grown at a substrate temperature of 90°C. Here, the film is more or less

amorphous except for a few grains scattered here and there. However, the selenium film became entirely amorphous at 80°C (not shown).

Fig.4.21 shows a top view of two Se-CdO cells one with a 100°C crystalline selenium film (a) and the other with an 80°C amorphous selenium layer. The CdO films in the two cells were sputtered under similar conditions at a sputtering current, pressure and time of 20 mA, 75 mTorr and 10x3 min. respectively. A view of the edge of each CdO film shows its interference pattern to yield a third order green colour, indicating a film thickness of about 0.33 μm in the two cells. The interesting observation here is that in the case of the crystalline selenium film, its surface topology did not appear to change after the CdO deposition as compared to the amorphous, 80°C selenium film. In the latter, it was evident that the sputtering action had altered the morphology of selenium surface layer as evidenced by the drastic difference in appearance between selenium underneath the CdO and that with no CdO on top.

4.4 DISCUSSION

A discussion of the results of section 4.3 is now presented and explanations are offered, where possible. It should be mentioned that, unless otherwise stated, the interpretations offered are largely tentative and other explanations may emerge with future work.

Over the range of selenium substrate temperatures of 80 to 140°C it was found that the higher the temperature, the better the output of the cell. By examining the performance of the cells fabricated at lower substrate temperatures, it was evident that photovoltaic action using amorphous selenium was quite small and hence rather difficult to detect. Thus to obtain reasonable photovoltaic output

in the Se-CdO structures, crystalline selenium is needed. This was clearly shown in the sample fabricated at 95°C, which was well crystallized on one side and less crystallized on the other. In this sample, the well crystallized side showed the better photovoltaic performance. The reason for the variation in crystallinity is no doubt due to a small transverse temperature gradient across the substrate during deposition.

Samples fabricated at higher substrate temperatures (all with a well crystallized selenium film), exhibited increasing photovoltaic output with increasing temperature and, in the cells prepared at 140°C, the conversion efficiency was found to be up to about 2%. The improvement in the illuminated j-V characteristics with increasing substrate temperature is perhaps partly due to a reduction in the series resistance of the cell, which is reflected by the increase in short circuit current density. However, the improvement in the open circuit voltage cannot be due to this but could possibly be attributed to an actual increase in the generated photocurrent of the cell. Higher substrate temperature could increase the diffusion length of the minority charge carriers (electrons in p-type selenium), and hence increase the photocurrent generated by the cell.

The reduction in the series resistance of the cell with increasing substrate temperature is evident in the dark j-V characteristics, where it was seen that at a forward bias of 1.0 volt, the current density clearly increased with temperature. The initial sharp rise in the current between 80 and 100°C could be caused by the continuous increase in the crystallization of the selenium film, which in turn results in a reduction in the series resistance. However, beyond 100°C, where the crystallization of the selenium film is believed to be largely complete, the reduction in series resistance is thought to be due to increased hole mobility. This could, for instance, be caused by a reduction in the concentration of trapping centers in the

selenium film.

While the photoresponse measurements were only preliminary, they confirmed a maximum response for the cells at a wavelength of about 550 nm for selenium crystallized in the temperature range of 100 to 140°C. For samples prepared at the lower temperatures of 80 and 90°C, the maximum response occurred at a shorter wavelength of around 450 nm. The much reduced response in this temperature range is speculated to be due to the larger density of trapping centers in the selenium film, which can reduce the photocurrent generated in the cell.

During the deposition of the selenium film at the substrate temperatures of 95 and 100°C, crystalline "grains" were observed of two types, larger "grains" and smaller ones. It is speculated that the larger grains arose from earlier nucleation during the deposition stage of the selenium film. The smaller grains however, were assumed to have been nucleated at a later stage, possibly during the long cooling-down period after selenium evaporation. However, this speculation has yet to be tested experimentally.

Table 4.1

Fabrication Conditions of Se-CdO Cells by d.c. Sputtering

Sample	Bi ¹ Evaporation		Subst. Temp. (°C)	Se ² Evaporation			Voltage ⁴ (V)	CdO ³ Sputtering		Wood's Metal ⁶ Evaporation	Remarks
	No. of pellets	Time (min.)		Time (min.)	Sep. (cm)	Thick. (μm)		Gas ⁵ inlet	Colour (third order)		
SH-7	-	-	140	180	14	15	-	80	Green	-	H.V. valve partially opened
SH-8	-	-	130	180	14	40	-	-	-	-	
SH-13	6	6	140	60	7	20	-	80	Red	-	Poor Se-Al adhesion
SH-14	3	7	140	60	7	20	700	80	Red	10	Good cells
SH-15	4	10	130	60	7	20	700	80	Green	10	Good cells, one area damaged
SH-17	4	10	120	60	7	40	-	80	-	5	
SH-18	3	5	120	25	7	18	700	85	Violet	10	
SH-19	3	5	110	21	7	20	700	85	Green	5	
SH-20	3	5	100	20	7	18	700	82	Green	5	Se crystalline grains apparent
SH-21	3	5	90	20	7	18	700	80	Green	5	Amorphous Se film
SH-22	3	5	100	20	7	18	625	80	Green	5	Se crystalline grains apparent
SH-23	3	5	80	20	7	20	650	80	Green	5	Amorphous Se film
SH-24	3	5	95	20	7	18	650	80	Green	5	Crystalline & amorphous Se regions
SH-25	3	5	130	60	7	15	650	85	Green	5	Good cells
SH-28	3	5	140	60	7	20	650	85	Green	5	Good Cells, two areas damaged

1 Boat current 40 A, sample-to-boat separation 7 cm

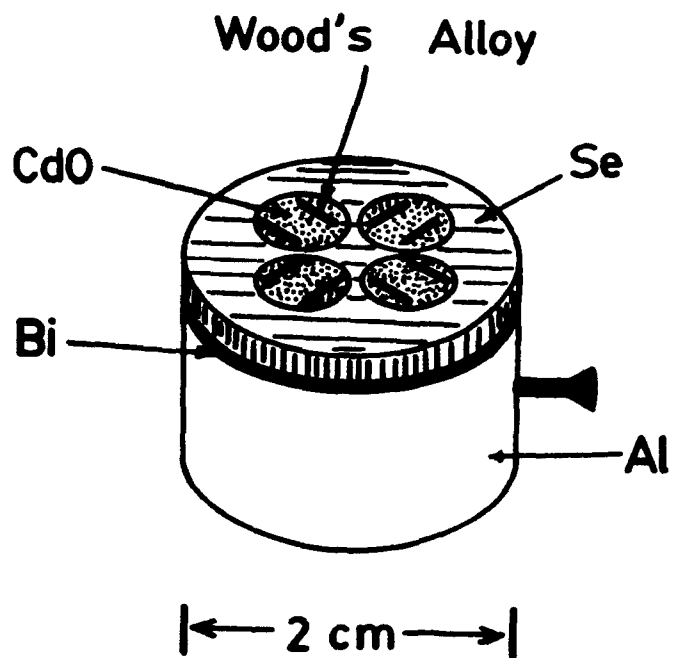
2 Indicated temperature is for substrate, source temperature 245°C, maintained for 1 hour before evaporation
Se contained 69 ppm Cl

3 Sputtering pressure 75 mT, sputtering current 20 mA, sputtering time 10x3 min, initial pressure 10 mT, H V valve fully opened, pressure control with gas inlet valve only

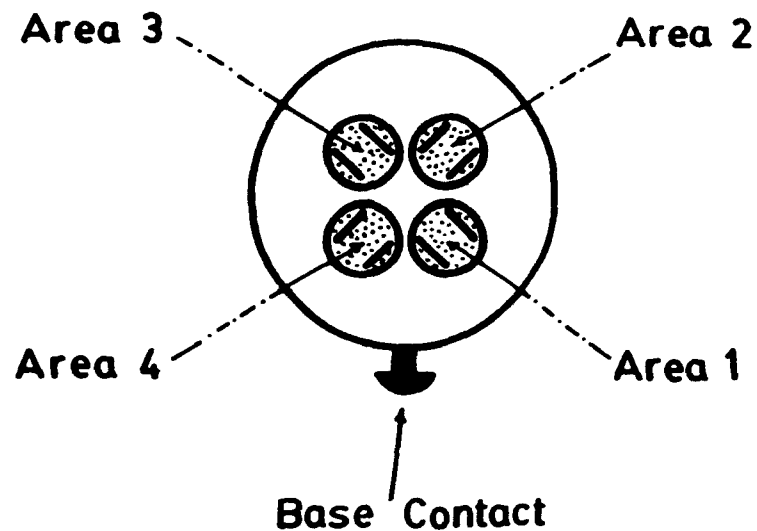
4 D c potential between Cd target and sample, averaged over 10 sputtering periods

5 Setting of gas inlet valve in arbitrary units

6 Evaporation current 40 A

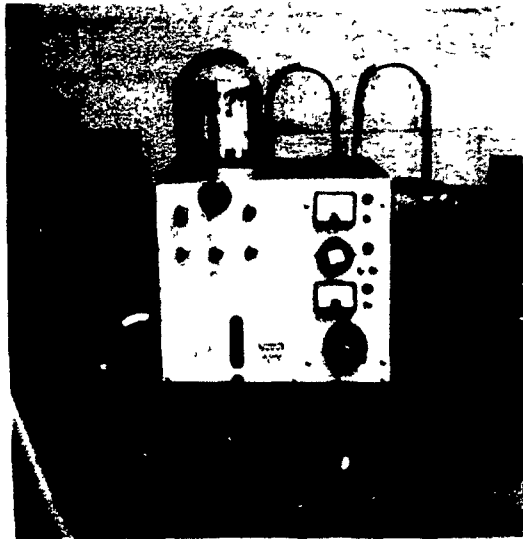


(a)

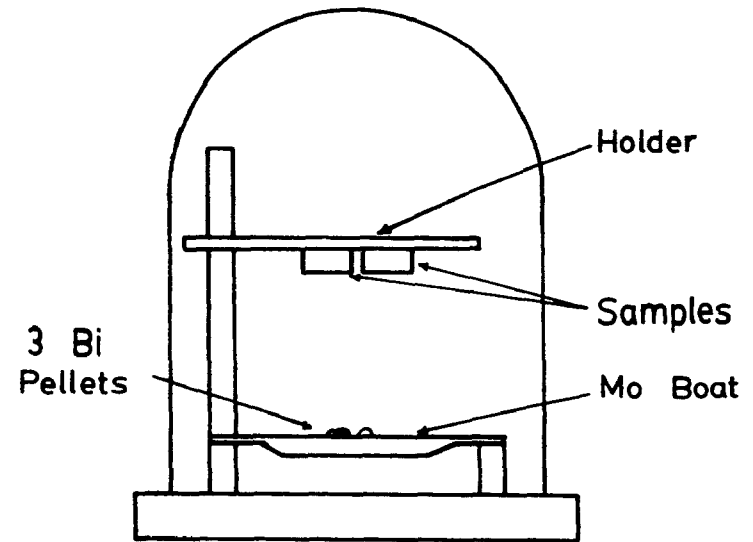


(b)

Fig.4.1 Schematic diagram of the structure of the aluminum stud Se-CdO sample used in this study showing (a) the different cell layers and (b) the numbering scheme of the four cells in the sample.

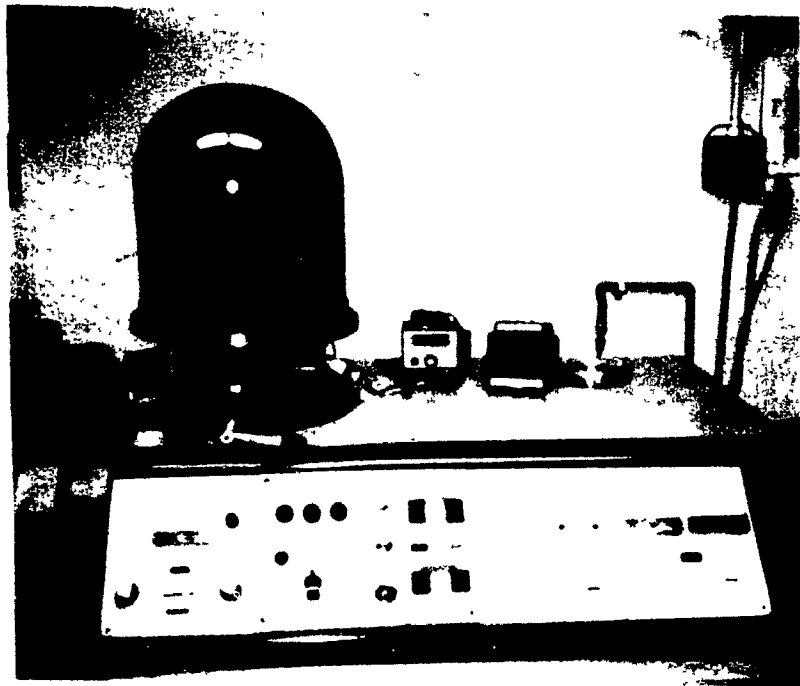


(a)

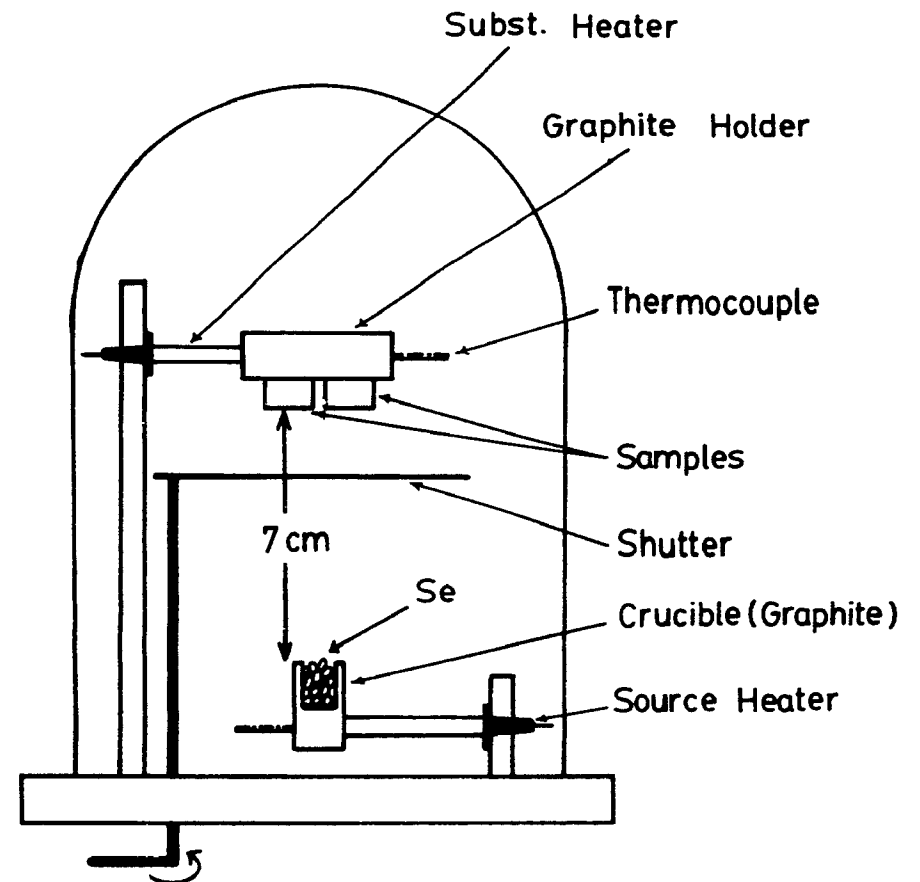


(b)

Fig.4.2 (a) Photograph of Edwards vacuum system (model 6E4, 6-inch bell jar) used for bismuth and Wood's alloy evaporations.
(b) Schematic diagram of the arrangement used inside the bell jar for bismuth evaporation.

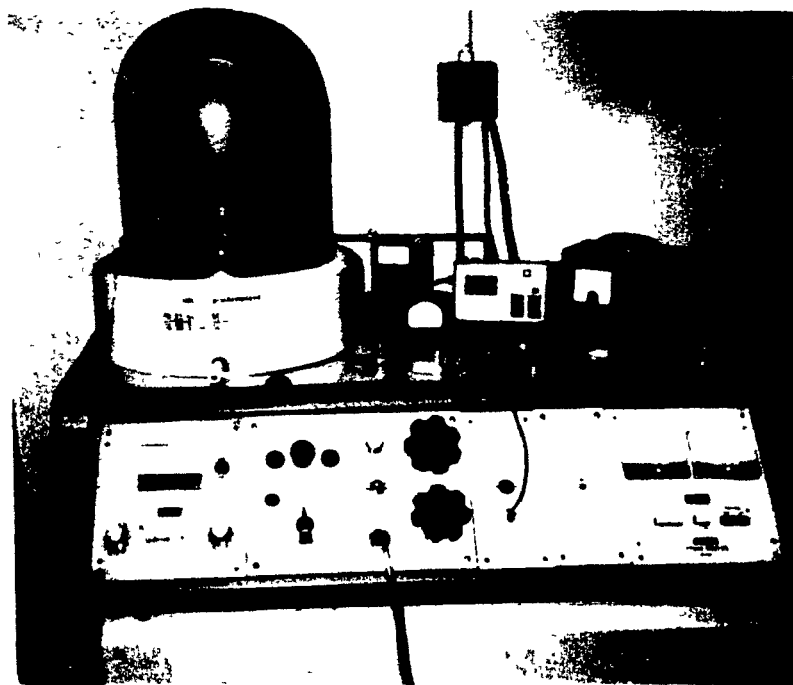


(a)

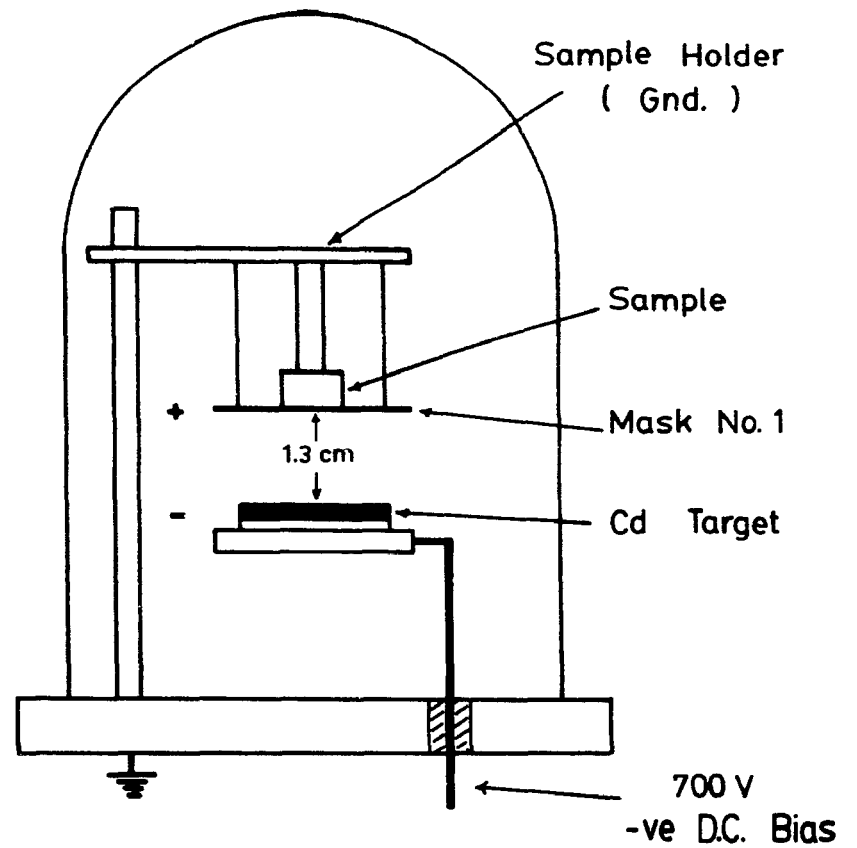


(b)

Fig.4.3 (a) Photograph of Edwards vacuum system (model E12E3, 12-inch bell jar) used for selenium evaporation.
 (b) Schematic diagram of the arrangement used inside the chamber.



(a)



(b)

Fig.4.4 (a) Photograph of second Edwards vacuum system (model E12E3, 12-inch bell jar) used for CdO d.c. sputtering.
(b) A schematic diagram of the arrangement used inside the chamber.

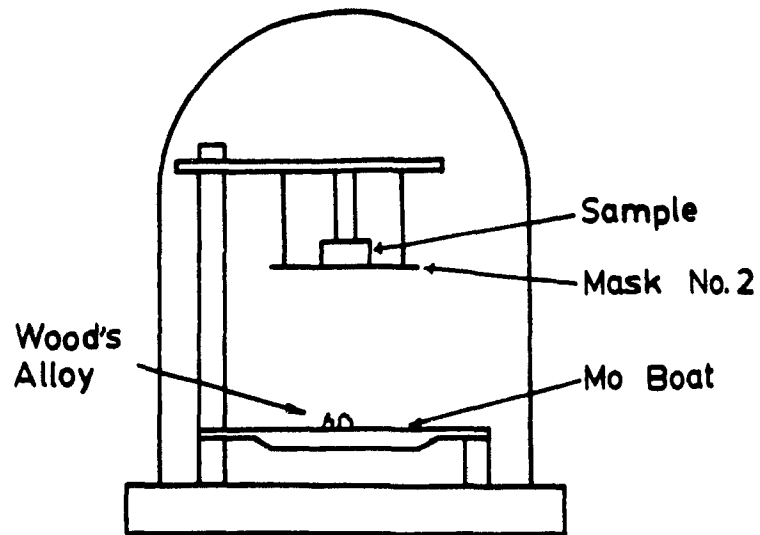


Fig.4.5 Schematic diagram of arrangement inside vacuum system (Edwards model 6E4) used for Wood's alloy evaporation.

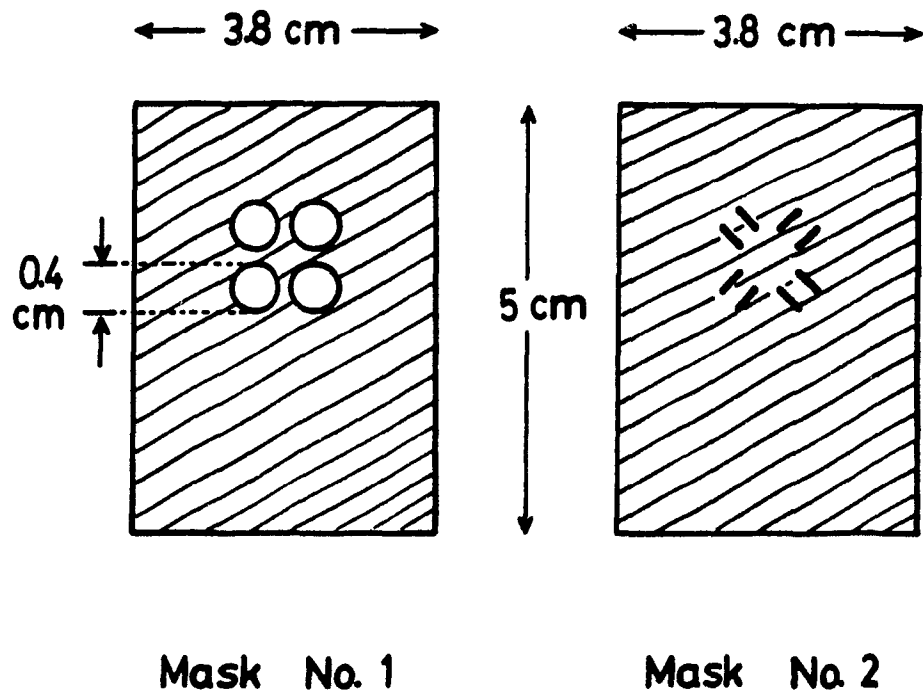


Fig.4.6 Diagram of shadow masks used in deposition - mask number 1 for CdO and mask number 2 for contact stripes.

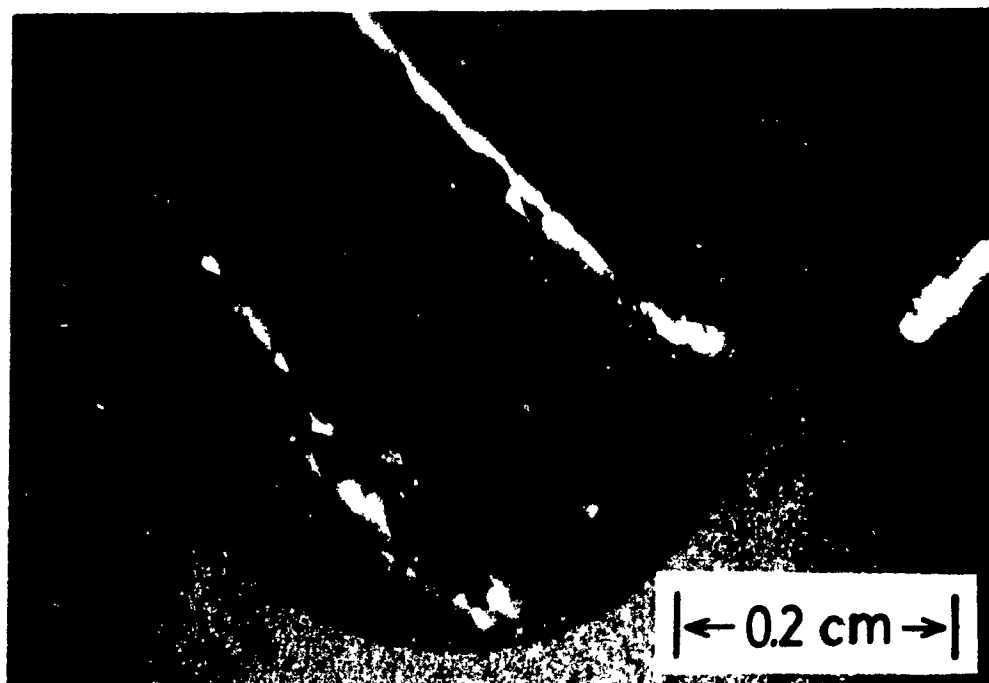


Fig.4.7 View looking down on a single Se-CdO cell.

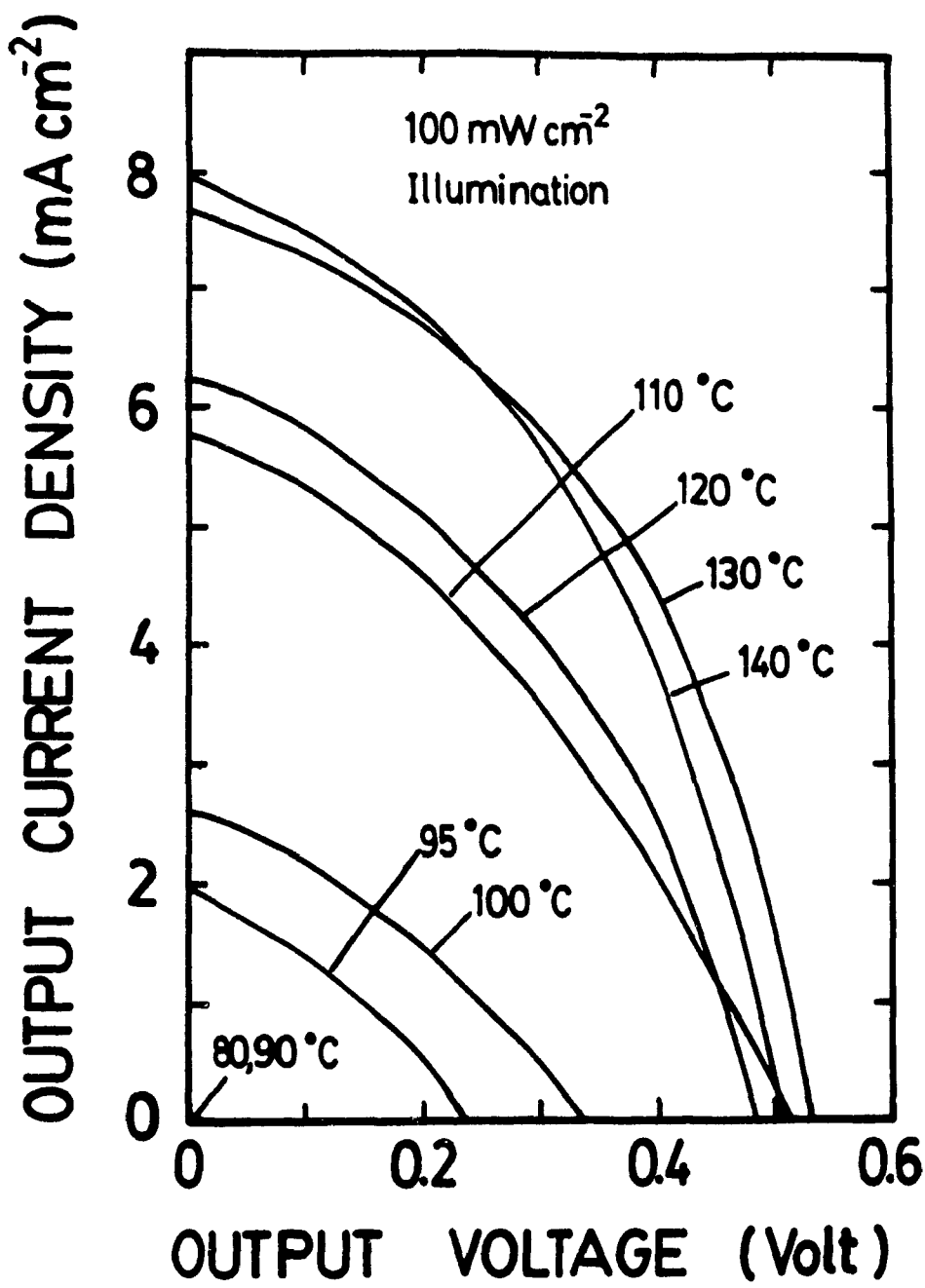


Fig.4.8 Representative curves of illuminated j-V characteristics of cells fabricated at eight different substrate temperatures (simulated AM1 illumination).

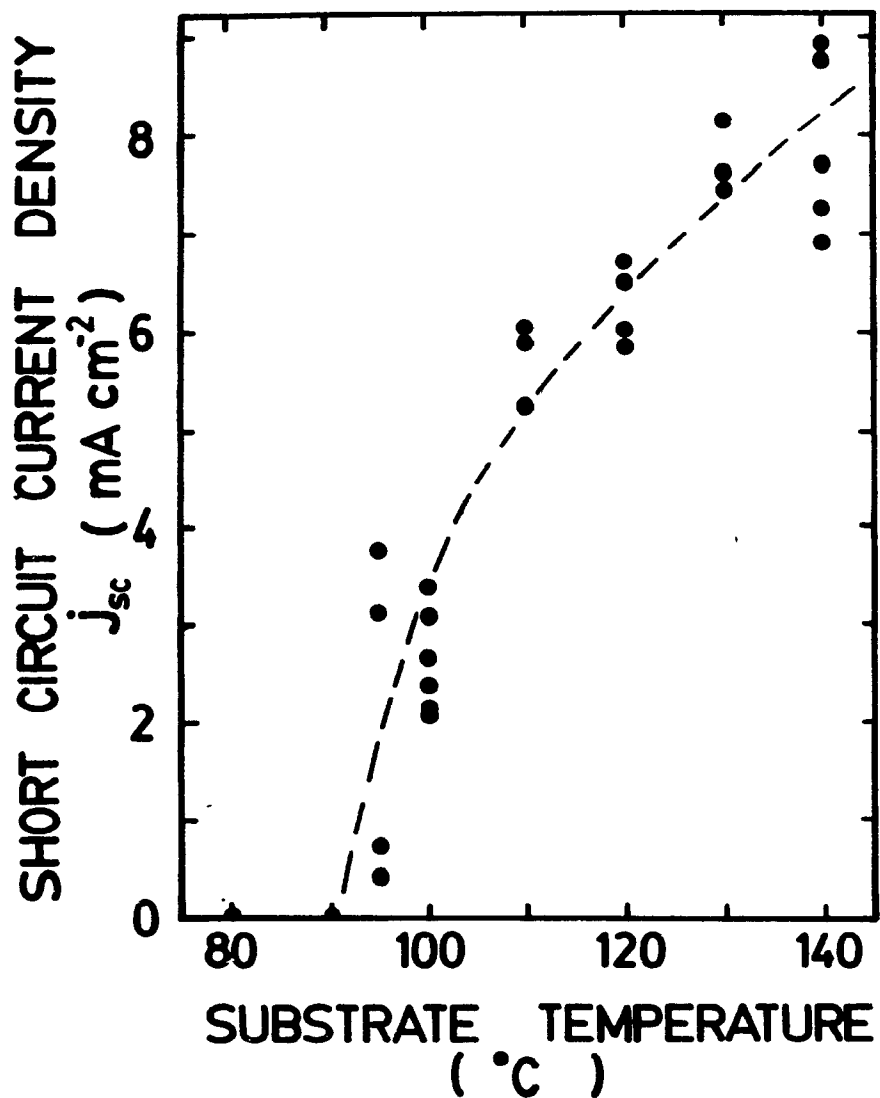


Fig.4.9 Short circuit current density of cells fabricated at different substrate temperatures. The dashed line is intended to show the trend of the results.

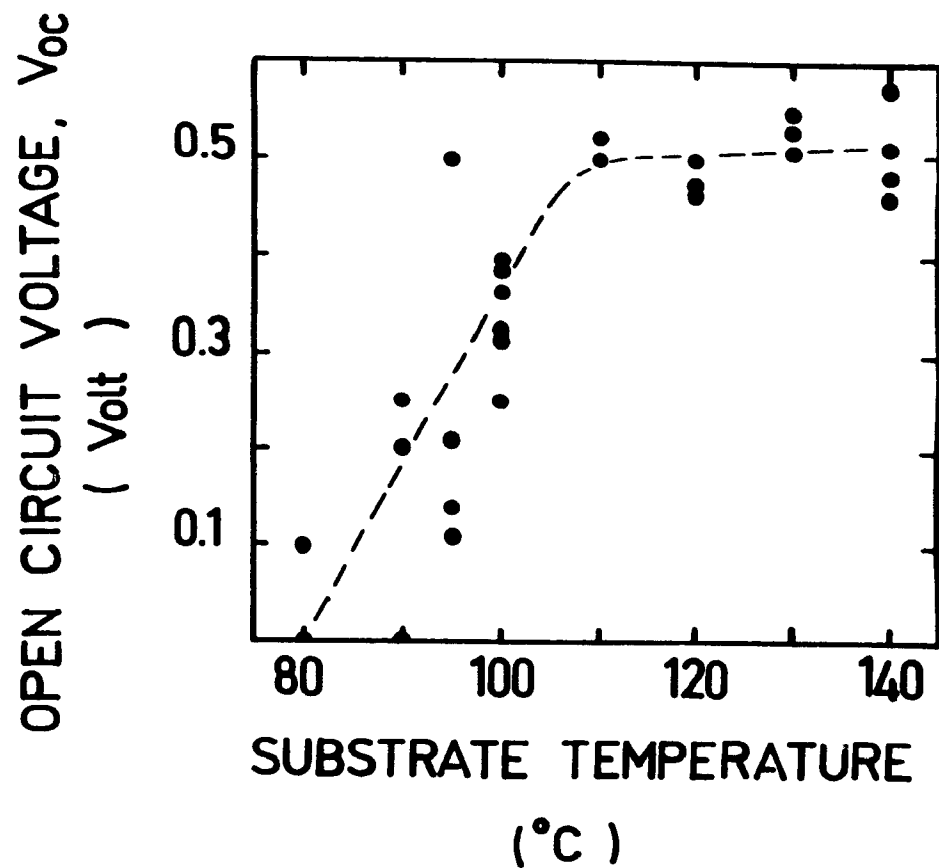


Fig.4.10 Open circuit voltage of cells fabricated at different substrate temperatures. The dashed line is intended to show the trend of the results.

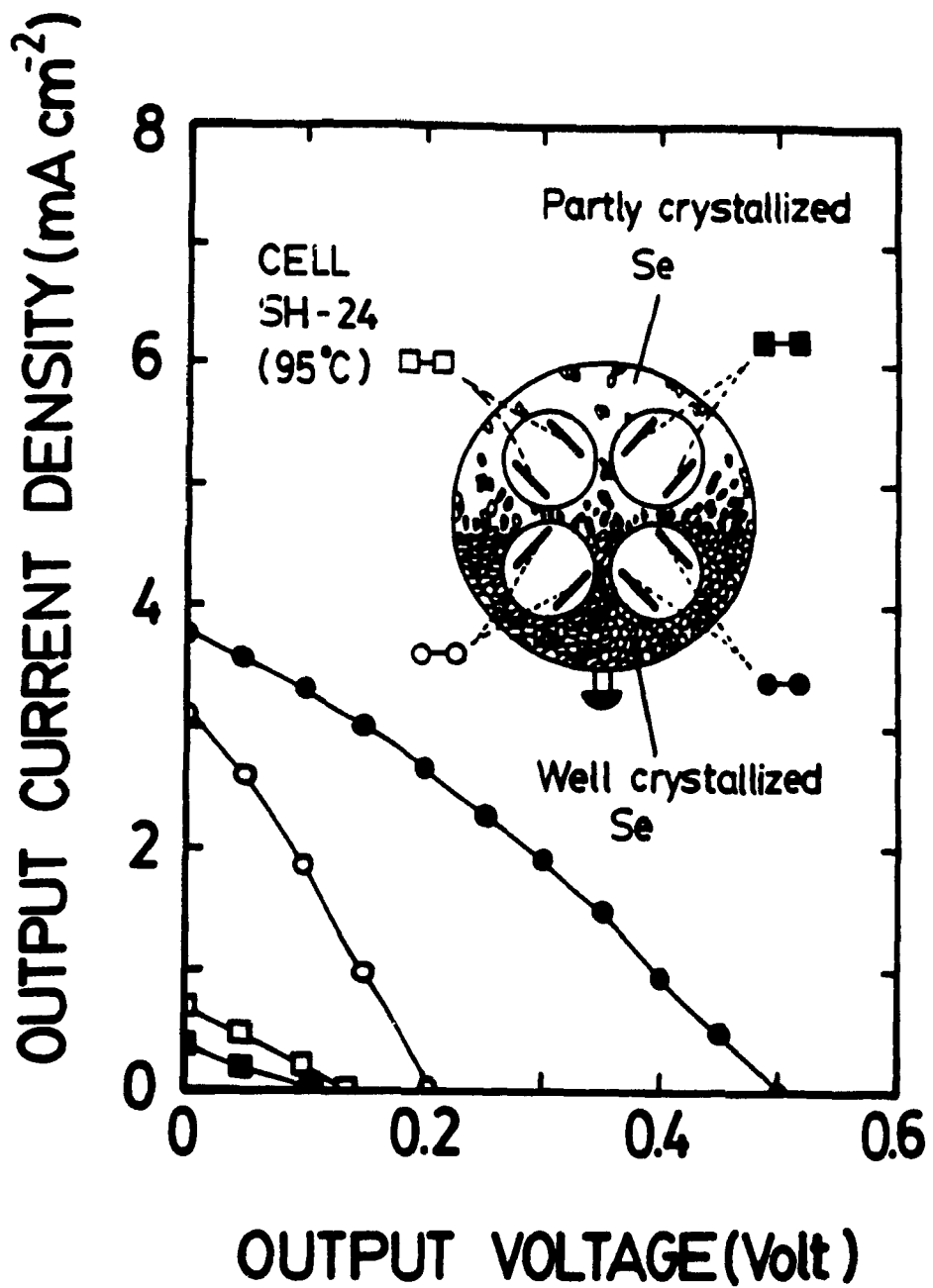


Fig.4.11 Illuminated j-V characteristics of sample SH-24 fabricated at a substrate temperature of 95°C, where a variation in the crystallization across the selenium surface was apparent (simulated AM1 illumination).

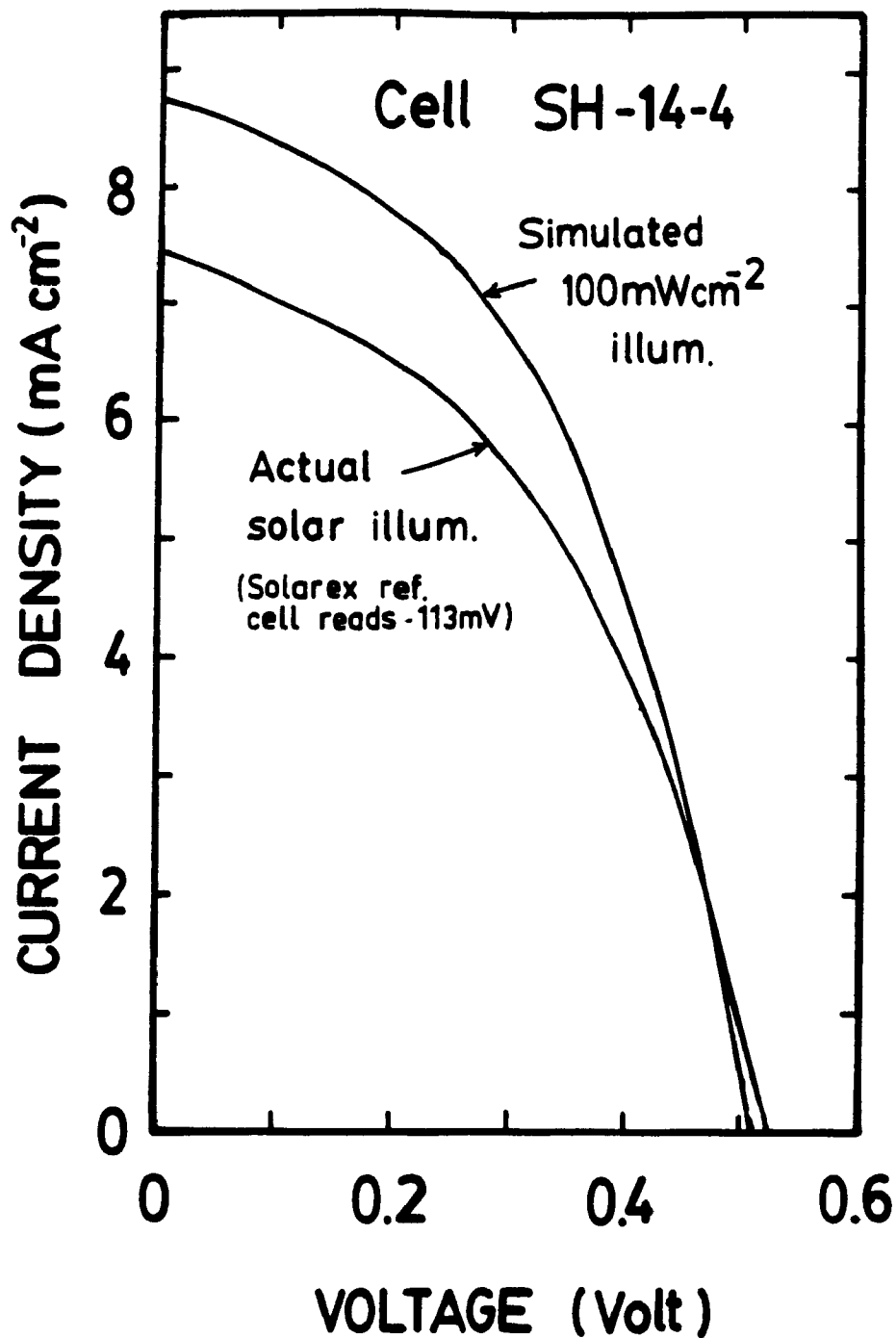


Fig.4.12 Illuminated j-V characteristics of cell SH-14-4 measured under actual solar illumination (October 5, 1987, 1:20pm in Montreal) and under simulated AM1 illumination. A Solarex commercial cell calibrated to yield 124.4mV under AM1 registered 113mV during the solar illumination.

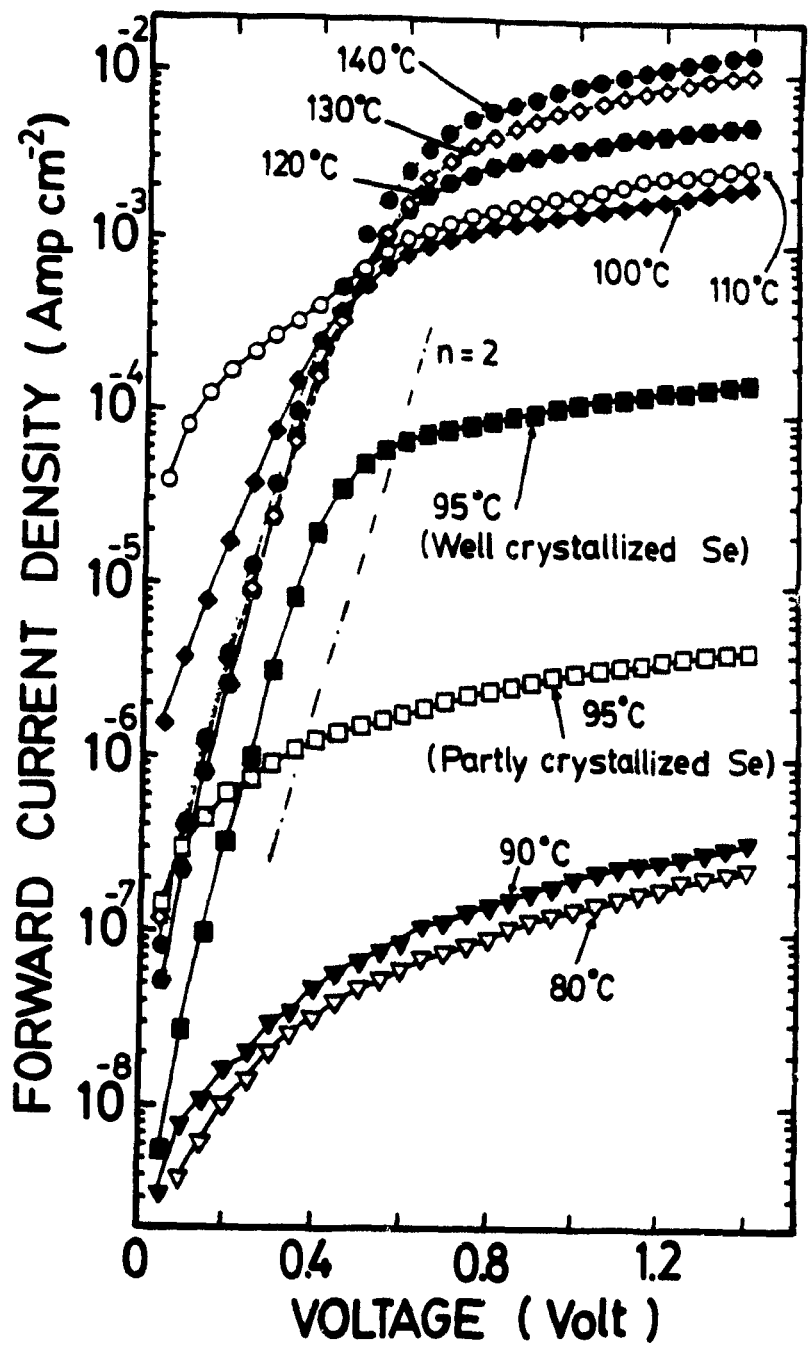


Fig.4.13 Dark forward j-V characteristics of cells fabricated at eight different substrate temperatures. The initial slopes of the characteristics are to be compared with that of the line corresponding to n=2, where n is the ideality factor of the diode equation (see Appendix).

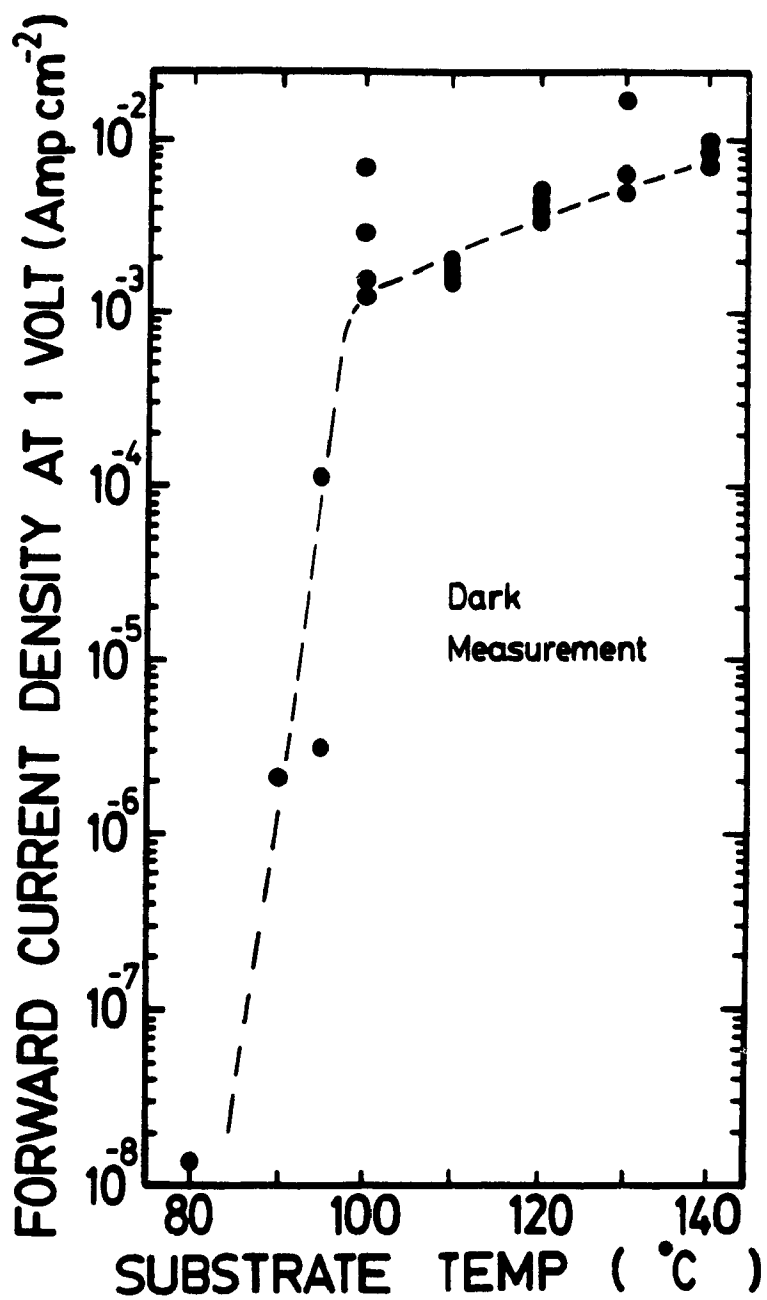


Fig.4.14 Plot of dark forward current density at 1 volt of cells against substrate temperature. The dashed line is intended to show the trend of the results.

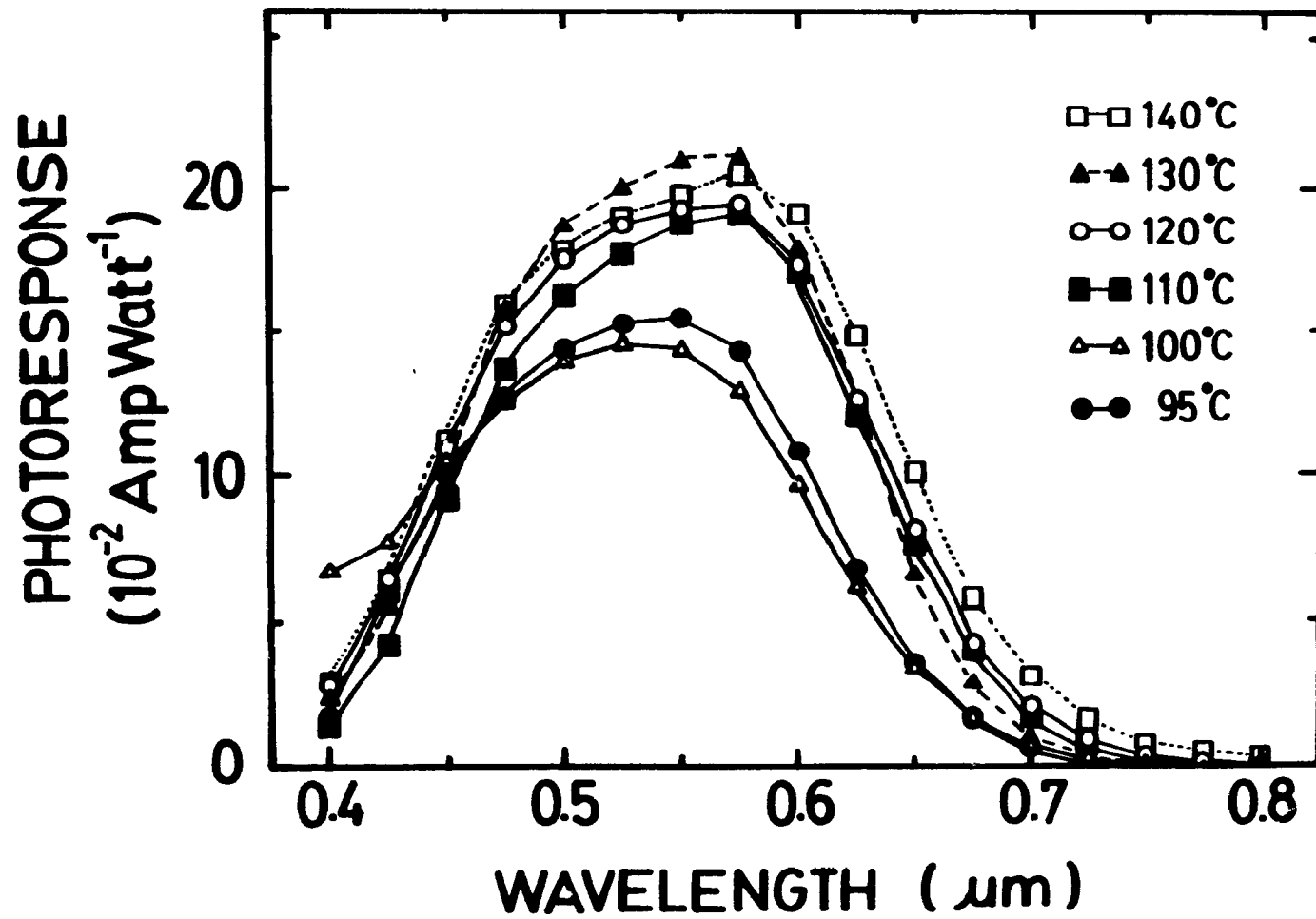


Fig.4.15 Photoresponse of cells fabricated at six different substrate temperatures between 95 and 140°C.

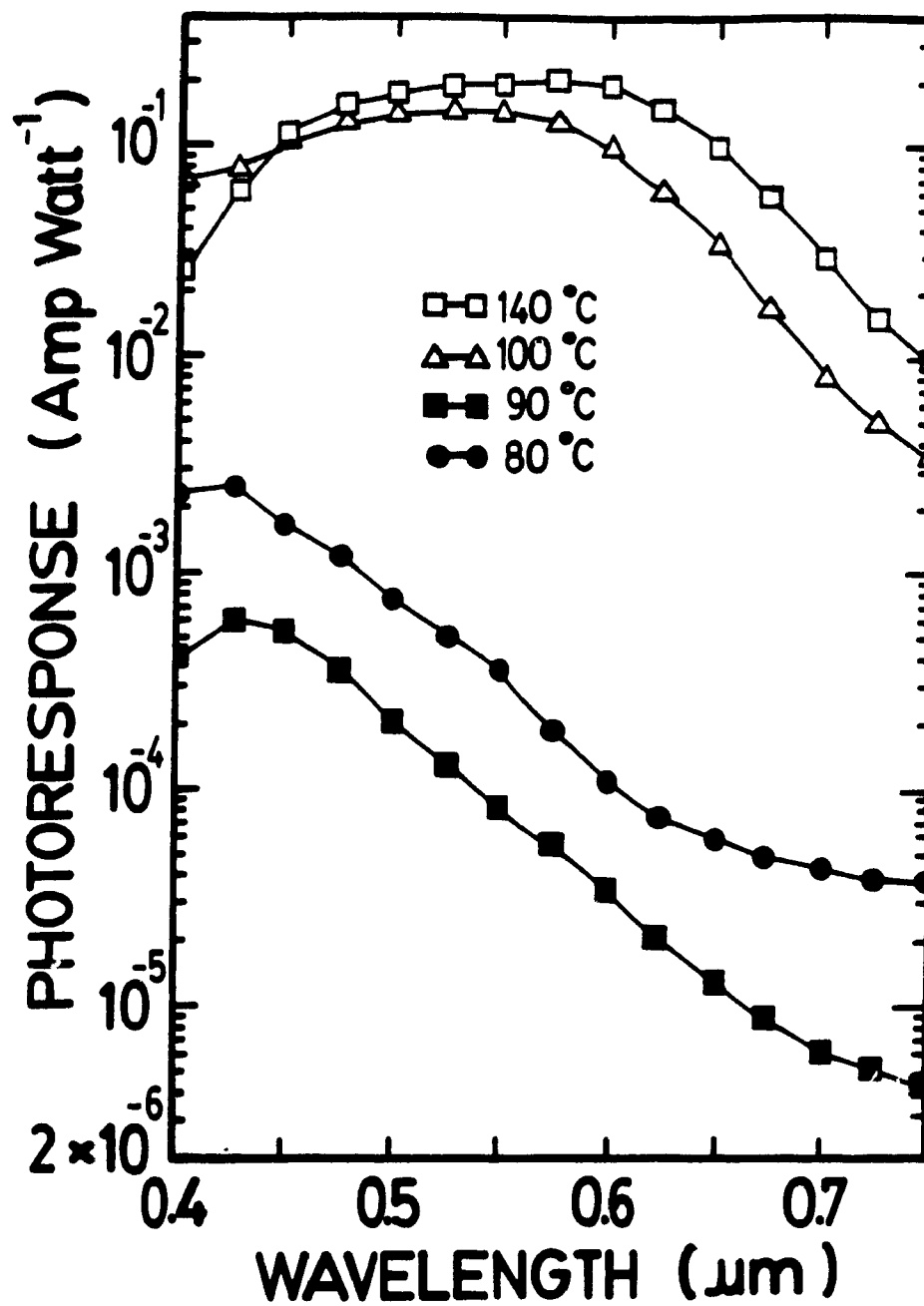


Fig.4.16 A comparison between the photoresponse of cells fabricated at the substrate temperatures 80, 90, 100 and 140°C.

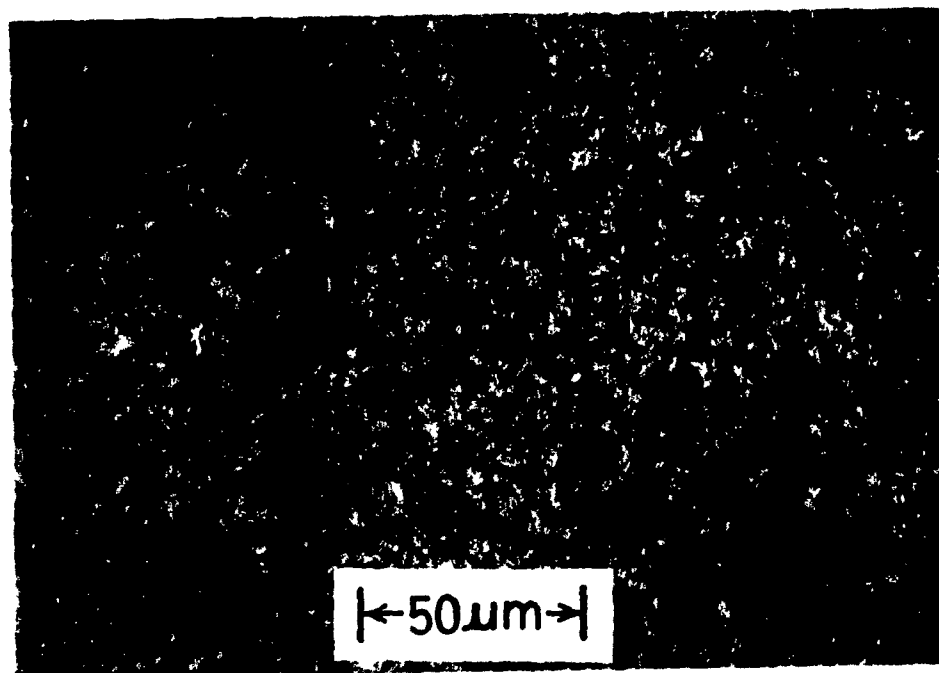
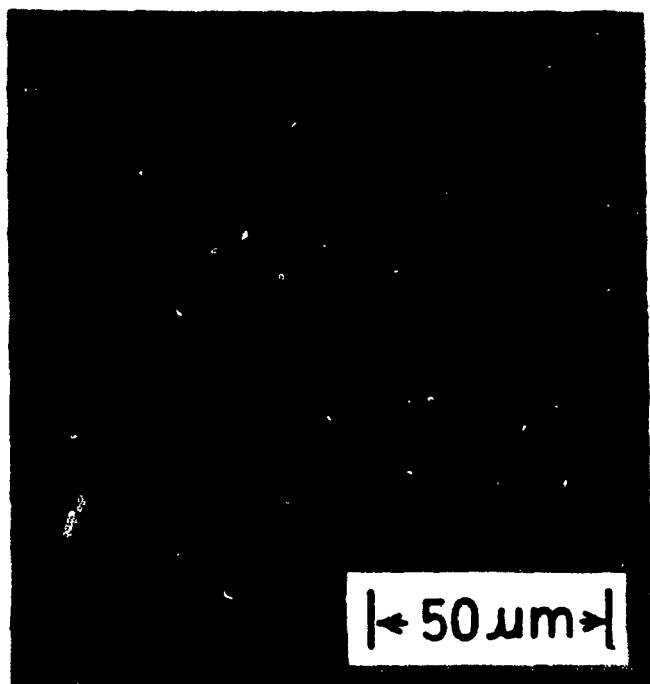
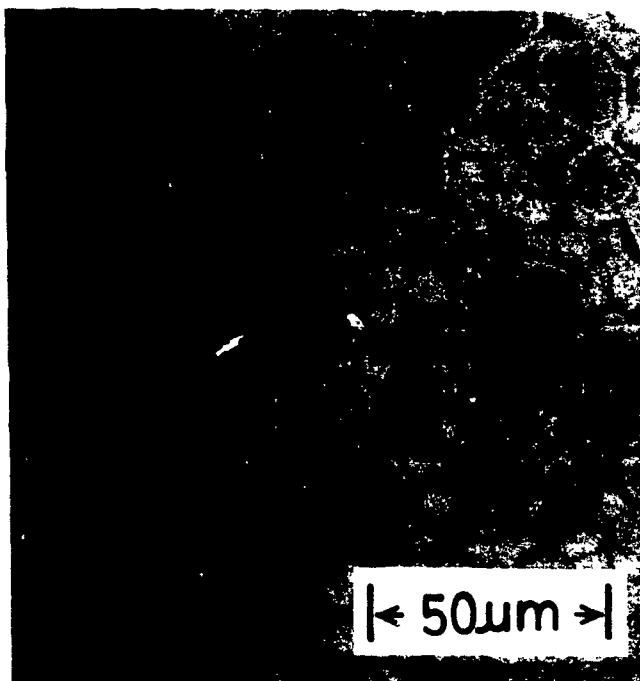


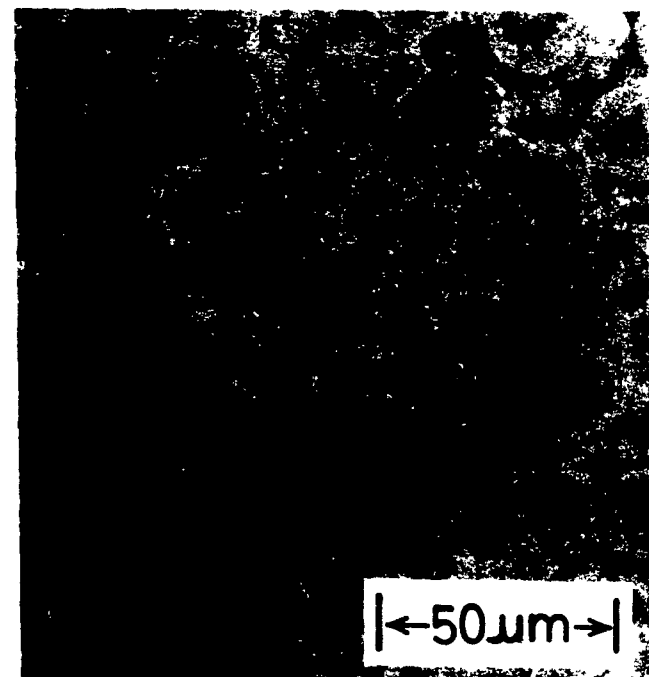
Fig.4.17 Surface view of a selenium film deposited at a substrate temperature of 120°C.



(a)



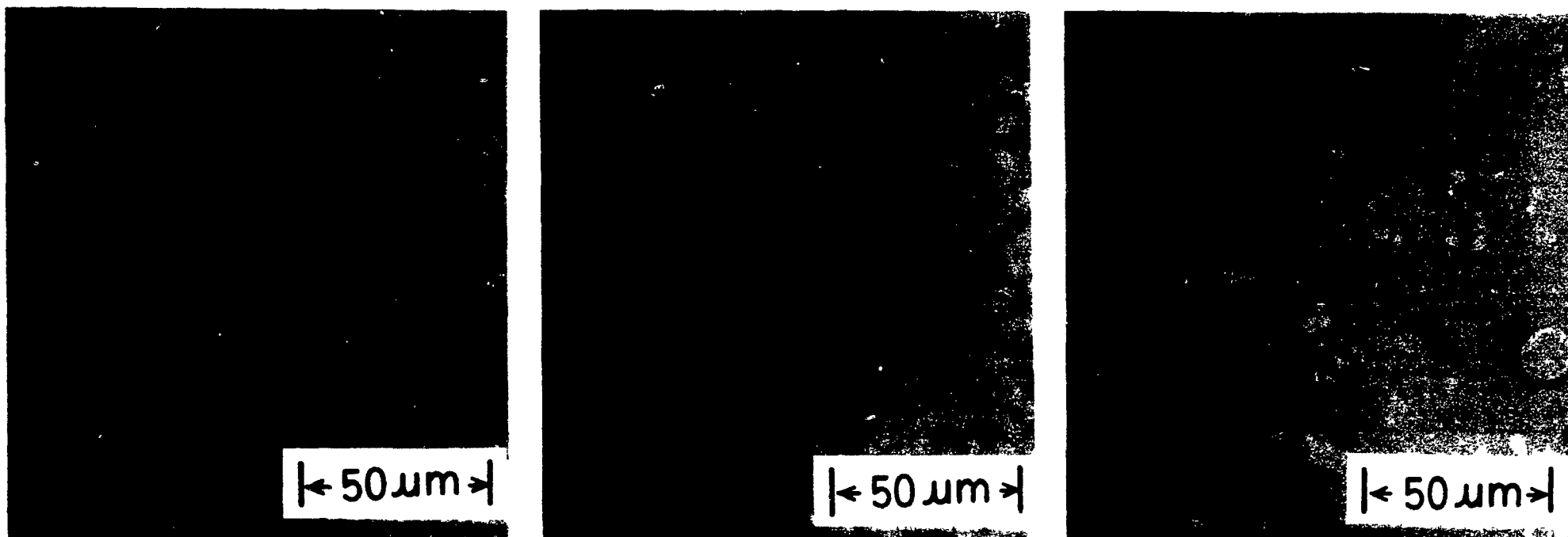
(b)



(c)

Fig.4.18 Surface view of three regions of a selenium film deposited at a substrate temperature of 100°C.

- (a) Region made up of mostly smaller grains.
- (b) Region where both smaller and larger grains cover comparable areas
- (c) Region dominated by mostly larger grains.



(a)

(b)

(c)

Fig.4.19 Surface view of three regions of a selenium film deposited at a substrate temperature of 95°C.
(a) Region showing high degree of crystallization.
(b) Region of partial crystallization.
(c) Region of little crystallization.

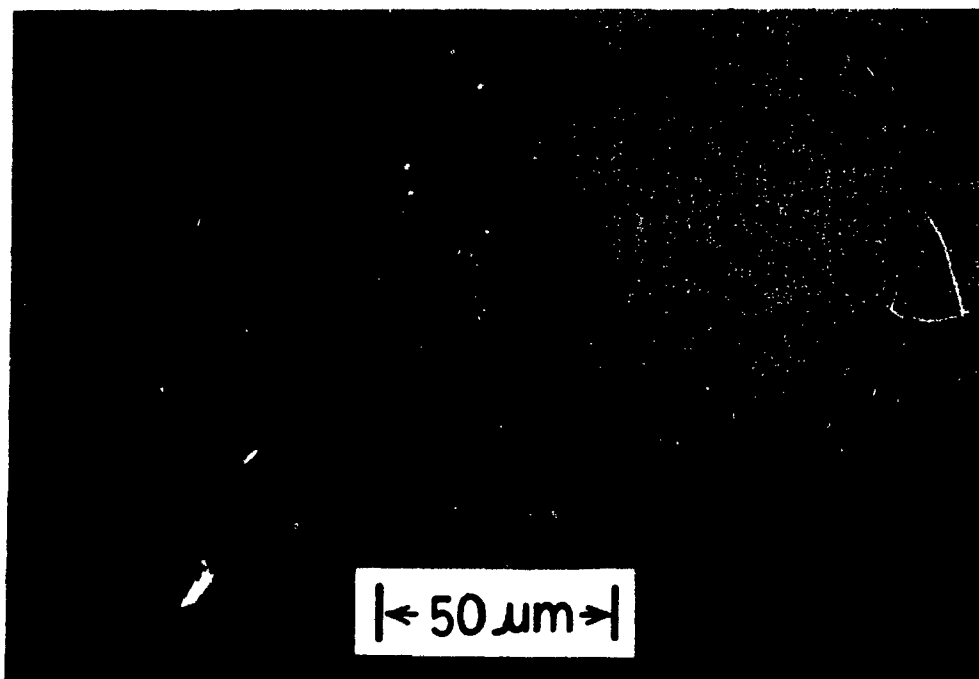


Fig.4.20 Surface view of a selenium film deposited at a substrate temperature of 90°C, showing very little crystallization.

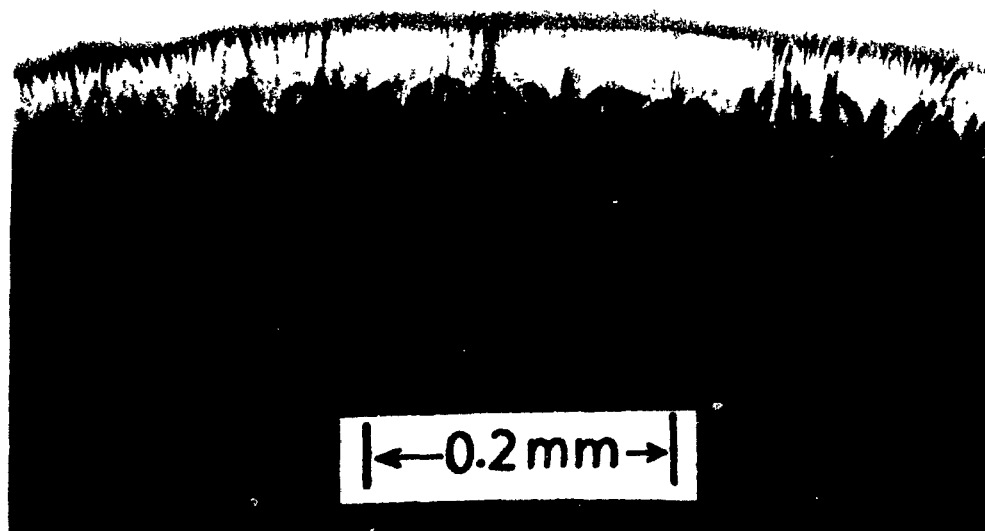
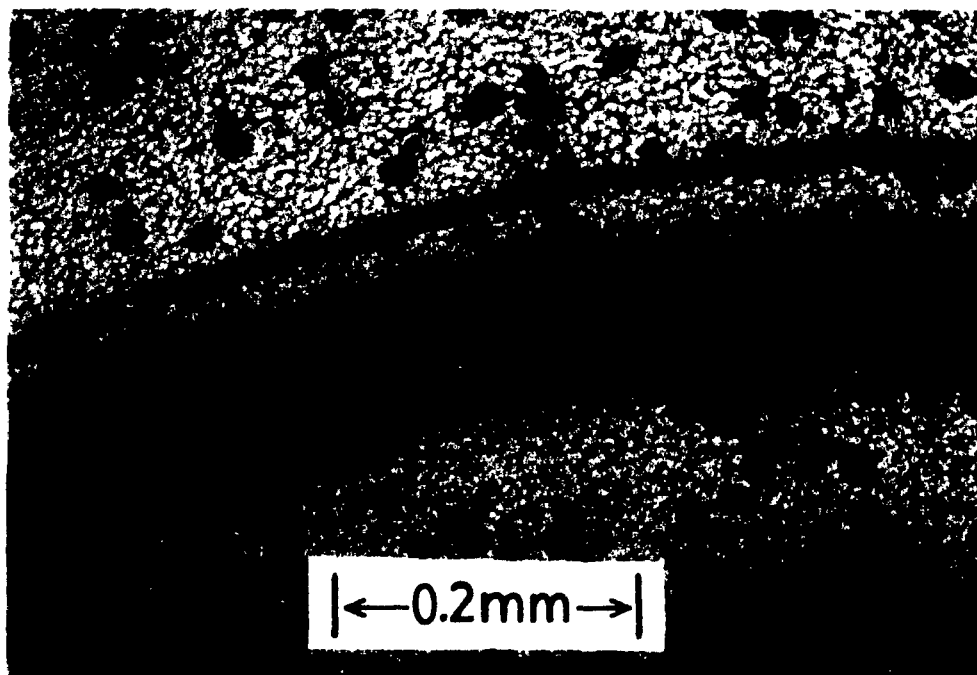


Fig.4.21 A comparison between two selenium films after CdO sputtering under similar conditions.
(a) A well crystallized selenium (100°C)
(b) An amorphous selenium film (80°C).

Chapter 5

PRELIMINARY STUDIES ON R.F. SPUTTERED Se-CdO CELLS

5.1 INTRODUCTION

As indicated in chapter 1, the deposition of the CdO layer in the Se-CdO cells can also be accomplished by r.f. magnetron sputtering, in contrast to the d.c. reactive sputtering method, described in chapter 4. In principle, r.f. sputtering from an oxide target in an argon ambient, should yield a fixed film stoichiometry, since no reaction between cadmium and oxygen is apparently involved at first thought. Furthermore, with lower sputtering pressures inherent in r.f. magnetron systems, the deposited CdO film would be expected to be of both greater purity and density.

Cells were therefore prepared using this deposition technique and accordingly in this chapter the fabrication and results of such cells are described. Since the fabrication of the Se-CdO cells involved many parameters in the deposition of the selenium and CdO layers, the present work with r.f. sputtering must be considered as only a first step in utilizing this technique.

In order to obtain better control of the sputtering conditions, CdO depositions were first carried out on glass slide substrates and then on selenium in cell structures. In the case of the glass samples, the parameters varied were sputtering power and sputtering pressure. Table 5.1 gives the details of their fabrication. In the case of the cells, the r.f. sputtering parameters examined were sputtering pressure and deposition time. No power variation results for the cells are presented, since only limited experiments were done with changing this

parameter. It should also be mentioned that attempts were not made to vary the composition of the CdO target so as to obtain different film properties. The fabrication conditions of the r.f. sputtered cells are given in Tables 5.2(a) and (b).

5.2 SAMPLE PREPARATION

In this section, the fabrication of the glass slide samples as well as the Se-CdO cells by the r.f. sputtering technique is presented. A description of the preparation of the CdO powder targets employed, is also given.

(a) R.f. Sputtering Apparatus

In this study, the deposition of the CdO films was carried out in a Varian r.f. planar magnetron sputtering system having a 12-inch diameter bell jar and an M4 diffusion pump. The system employed a U.S.Gun II sputtering source with a 5-cm diameter, water cooled, target assembly. The source also contained a built-in, ring-shaped, permanent magnet situated below the target mounting plate. A d.c. converter and r.f. generator unit (U.S.Inc. model RF-500MB) supplied the source with r.f. power at 13.56 MHz, through a matching network. The peak output capability of the power supply was rated at 500 watts. Fig.5.1 shows a photograph of this system.

(b) CdO Powder Target Preparation

In contrast to the metallic cadmium target used in the d.c. reactive sputtering method (chapter 4), a cadmium oxide powder target was employed for the r.f. sputtering case. A total of three experimental targets were prepared whereby the CdO powder material was mechanically compressed into a more condensed state so as to improve the uniformity and reproducibility of the

deposited CdO films. Fig.5.2 shows a schematic of the target material in its 5-cm aluminum tray.

In fabricating the first target, denoted by target A, the CdO powder was poured into the aluminum tray using a spatula and hand-pressed gently with a flat weight, so as to produce a level target surface. For target B, the CdO in the aluminum tray was compressed at a much higher pressure (about 3 tons per square inch) using a mechanical stainless steel press. In the case of target C, the CdO powder was first machine-pressed in the absence of the aluminum tray and then sintered in air at 900°C for about 1 hour. After cooling down, the CdO disk now slightly smaller in size, was placed in the aluminum tray ready for use. An attempt was also made to bond the CdO disk to a circular aluminum plate using silver epoxy resin but this was not successful. It should be noted here that, after sintering, the CdO appeared somewhat darker in colour, which could have been due to a change in its stoichiometry.

In depositing the films on glass substrates, target A was used for samples Z-1 to Z-9 and Z-17 to Z-28 (Table 5.1), while target C was employed for samples Z-29 to Z-47. In the case of the Se-CdO cells, target B was utilized for all the devices. In general, targets were sputter-cleaned (etched) to establish an equilibrium surface layer before any actual depositions were made.

(c) CdO Depositions on Glass Substrates

The r.f. sputtering of CdO on glass substrates was done in the following fashion. After placing the target in position within the chamber, the glass substrate was pre-cleaned with propanol so as to remove any oil-based contaminants from its surface and was then mounted a few centimeters above the target on a special holder (see Fig.5.3). With the apparatus set in place, the vacuum chamber was

pumped down to a pressure of about 2×10^{-6} Torr and the r.f. generator switched on. Following an indication on the console that the power supply was ready, high purity argon was introduced into the chamber, via an inlet valve, which was adjusted to maintain the desired pressure. The r.f. excitation was then initiated at the required power setting, instantaneously producing a plasma discharge (of purple-magenta colour) between the source and the substrate. The sputtering was carried out for a period of 30 minutes after which the excitation was turned off. The argon gas and high vacuum valves were then closed, air was let into the chamber and the samples removed.

It is noted here that during the deposition of glass-substrate samples Z-1 to Z-9 and Z-17 to Z-28, the sputtering for 30 minutes was done in a continuous fashion, while in the case of samples Z-29 to Z-47, the sputtering process was carried out intermittently. In this case, 3-minute sputtering periods separated by 5-minute intervals (keeping the sample in the argon ambient) were repeated for a total deposition time of 30 minutes.

(d) CdO Deposition in Cells

The CdO deposition in the r.f. sputtered cells was done in much the same fashion as described above for the glass-substrate samples. However, continuous sputtering was used for all of the cells. A special stainless steel holder, shown in Fig.5.4, was employed to support the aluminum stud substrate in each case using mask number 1 (Fig.4.6, chapter 4) to define the four CdO areas (cells) on the selenium layer. Table 5.2 (b) gives the CdO deposition conditions for all the devices made.

(e) Other Cell Fabrication Details

The structure of the r.f. sputtered cells was the same as that described in chapter 4. The preparation of the aluminum stud substrate was the same. The bismuth evaporation was also unchanged, except that a Cooke vacuum system model CV301FR was used for most of the depositions (see Table 5.2(a)). In the case of the selenium evaporation however, the graphite source crucible used for cells in chapter 4 was replaced with either a molybdenum boat (Fig.5.5(a)) or a stainless steel crucible (Fig.5.5(b)). The latter was used for samples Z-74 to Z-77, while the molybdenum boat was employed for samples Z-78 to Z-82 (see Table 5.2(a)). Furthermore, in the case of samples Z-78, Z-79 and Z-82, the selenium was deposited at a much higher rate, with the substrate maintained at an elevated temperature (Table 5.2(a)), such that the deposited film was initially amorphous. The selenium film was allowed to crystallize for a period of about 10 minutes before decreasing the substrate temperature. This was mainly done to obtain thicker selenium films with shorter evaporation times.

5.3 EXPERIMENTAL RESULTS

In this section, results are first presented on CdO films deposited on glass substrates and then on the Se-CdO cells.

(a) CdO Films Deposited on Glass

(i) Effect of sputtering pressure

The effect of sputtering pressure on the thickness and resistivity of the CdO films is shown in Figs.5.6 and 5.7 respectively. In Fig.5.6, it is seen that for samples Z-38 to Z-47 prepared with the sintered target C (solid symbols), the

thickness of the CdO film first increased and then decreased with increasing sputtering pressure, exhibiting a maximum at around 2 to 10 mTorr. For the other two sets of samples Z-6 to Z-9 (electrode separation 5cm) and Z-23 to Z-28 (separation 4cm) prepared with the hand-pressed target A (open symbols), the trend seems to be somewhat similar but rather suppressed. In Fig.5.7, where film resistivity is plotted against sputtering pressure, the general trend is seen to be a monotonic increase of CdO resistivity with increasing sputtering pressure. In these results, target preparation did not seem to show a strong effect.

(ii) Effect of sputtering power

Results of CdO films sputtered at different power settings are shown in Figs.5.8 and 5.9. In Fig.5.8, a plot of CdO film thickness against power setting is shown. Here it is seen that the film thickness in general increased linearly with increasing sputtering power. In the case of samples prepared with the sintered target C (solid symbols), the slope of the increase is noted to be much greater than that for the samples fabricated with the hand-pressed target A (open symbols). In Fig.5.9, a plot of CdO resistivity against power level is shown. It can be seen here that, with increasing sputtering power from about 10 to 40 watts, a rather sharp drop in film resistivity was exhibited. Beyond 40 watts however, the lower film resistivity was essentially unchanged at least up to 100 watts. The average resistivity in this region for the films deposited with target C was about twice that of the films sputtered with target A.

(b) R.f. Sputtered Se-CdO Cells

(i) Uniformity of CdO depositions

Experiments were carried out to verify the reproducibility of results from one run to the next under the same nominal fabrication conditions. Accordingly, Se-

CdO sample Z-82 was prepared with four CdO areas successively deposited on a common selenium substrate using the same nominal sputtering parameters. The illustrated characteristics of these four cells are shown in Fig.5.10. It is seen that the first deposited cell yielded the largest j_{sc} and V_{oc} values of all four cells. The subsequent depositions showed lower j_{sc} values but essentially no systematic change in the second, third and fourth depositions. However, V_{oc} generally decreased from run to run.

Arising from this result, six CdO areas were successively deposited on a glass substrate (not shown) under the same conditions (40 W, 30 min., 7 mTorr and 5 cm). All six areas showed about the same transparency with a third order red interference colour, indicating essentially no change in thickness from area to area. Upon measuring the resistance of each of the areas, using two probes about 1 cm apart, it was found however, that the resistance monotonically decreased by about one order of magnitude from the first to the sixth deposition. This run-to-run resistance decrease, however, was not investigated further at this stage but must be considered when changes in fabrication parameters are examined.

Since in the case of sample Z-82, the change between the first and second depositions was not large, it was not taken into account in the experiments to be described in the next section, concerning sputtering pressure and deposition time, where there were only two successive depositions made per stud sample.

(ii) Effect of sputtering pressure

Representative characteristics, measured under an illumination of 100 $mWcm^{-2}$, of two sets of samples prepared at different sputtering pressures, are shown in Figs.5.11(a) and (b). It is seen, in both figures, that while j_{sc} showed no clear trend, the open circuit vol' at lower pressure was much reduced

compared to that at higher pressure. This is better seen in Fig.5.12, where a plot of j_{sc} and V_{oc} against sputtering pressure is shown. Here it is seen that j_{sc} seems to show an initial decrease with pressure between 1 and 2 mTorr, followed by an increase to a maximum j_{sc} value of about 4 mAcm^{-2} at 65 mTorr, beyond which a sharp fall in j_{sc} was observed. In the case of V_{oc} however, the general trend seems to be an increase in open circuit voltage with increasing sputtering pressure.

Figs.5.13(a) and (b) show representative dark j - V characteristics of the same two sets of samples described above. Here it is observed that at lower pressure, the lines are markedly curved with current density values much larger than those observed in the d.c. reactively sputtered cell (sample SH-14), shown for comparison by the dashed lines in both figures. Furthermore, current at a given voltage generally decreased with sputtering pressure, particularly at lower voltage.

Fig.5.14 shows plots against pressure of the three quantities: inter-stripe resistance R_{st} , CdO film thickness t , and their product $R_{st} \cdot t$. Here it is seen that R_{st} showed an increase of about one order of magnitude with increasing sputtering pressure between 1 and 110 mTorr. The film thickness t , however, was seen to increase up to a maximum between pressures of about 2 and 10 mTorr and then to decrease at higher pressure, much like the trend observed for the glass samples in Fig.5.6. It is interesting to note here that the thickness of the CdO film peaks in about the same range of 2 to 10 mTorr for both the glass samples and the Se-CdO cells (Figs.5.6 and 5.14) even though the deposition conditions were somewhat different. Despite the maximum in film thickness observed with sputtering pressure, the product $R_{st} \cdot t$, which is proportional to the electrical resistivity of the CdO film, exhibited a monotonic increase with increasing sputtering pressure. This may be compared with the much larger increase of resistivity seen in the glass substrate samples over the same pressure range (Fig.5.7).

(iii) *Effect of deposition time*

In Fig.5.15, four representative curves of illuminated characteristics for cells fabricated with different sputtering times, are shown. As indicated in the figure, cell performance increased with increasing sputtering time from 15 to 60 minutes. However, for the 120-minute deposition run, j_{sc} for the cells was reduced. These results are shown more clearly in Fig.5.16, where a plot of both j_{sc} and V_{oc} against sputtering pressure is given. It is seen here that while V_{oc} increases with increasing deposition time and appears to saturate, j_{sc} increases to a maximum and then falls off.

Fig.5.17 shows the variation with sputtering time of the inter-stripe resistance R_{st} , CdO film thickness t , their product $R_{st}.t$ and the dark forward resistance R_d (from dark j-V curve at 1 volt). It is seen that with increasing sputtering time, the CdO film thickness increased monotonically as expected. However, while both R_{st} and $R_{st}.t$ initially decreased, a slight increase was observed for the larger deposition time of 120 minutes. The trend observed for R_d was less obvious, although it suggests a general decrease with deposition time.

(iv) *Accidental change of cell characteristics*

During dark current-voltage measurements on cell Z-81-2, when 0.7 volts was applied in the reverse direction, a sudden decrease of current was observed. On remeasuring the dark and illuminated j-V characteristics, it was clear that a dramatic change in the device had taken place. Fig.5.18 shows the illuminated j-V curves both before and after this event (solid lines). It is seen that, while j_{sc} was increased by some 50%, V_{oc} was more than doubled. Fig.5.19 shows the dark characteristics of this cell before and after the change (solid lines). Here it is noted that the current before the change was large and typical of cells with low

shunt resistance. After the change however, the dark j - V characteristic showed lower current at smaller voltage much like normal cells with an ideality factor of about $n=2$.

5.4 DISCUSSION

Results obtained on both glass-substrate and Se-CdO samples prepared by the r.f. sputtering method are now discussed.

(a) *Uniformity of CdO Depositions*

It was seen earlier in the successively deposited CdO films that, despite keeping the external fabrication parameters constant, the characteristics of the films on glass and in cells changed from run to run. The decrease of resistance observed in the glass samples, may have been caused by either a change in the stoichiometry of the target surface with sputtering time or to progressive target heating. The latter effect is considered the more likely. While the target was water-cooled, as mentioned in section 5.2(a), it is still possible for the surface temperature to rise with continuous use over a period of time. This would increase the deposition rate of the CdO and render the deposited film oxygen-deficient and hence more conducting, if cadmium and oxygen atoms were sputtered separately. In the case of the cells in sample Z-81, the decrease in V_{oc} with order of deposition could arise from the lower resistance CdO sputtered at a higher rate, penetrating thinner regions or weak spots in the selenium.

(b) *Effect of Sputtering Pressure*

Despite sputtering from a fixed composition CdO target in a non-reactive ambient of argon, it was seen that with increasing sputtering pressure, both the

resistivity of the glass-substrate CdO films and the $R_{st,t}$ product in the Se-CdO cells increased significantly. This surprising result is somewhat similar to the effect found in d.c. reactive sputtering, where at higher pressure, the lower deposition rate provided a longer time for the reaction between cadmium and oxygen to take place, resulting in higher resistivity, stoichiometric CdO films. Thus, the question is raised whether in r.f. sputtering from a nominal CdO target, atoms of cadmium and oxygen are released separately, as already alluded to in (a) above. If so, then the deposition rate would also play a role in influencing the stoichiometry of the deposited CdO film.

An alternative explanation for the apparent increase in resistivity with pressure is an increase in film porosity, but this would also mean a substantial increase of CdO film thickness, which was not observed. The general increase of V_{oc} with sputtering pressure is consistent with the decrease of dark current at lower voltage, resulting from increased shunt resistance, which in turn could arise from the increase of CdO resistivity with pressure.

Comparison of the dark j-V characteristics between d.c. reactively sputtered and r.f. magnetron sputtered cells, shows the latter to be more curved and to yield more current at a given voltage. In terms of the simple circuit model of the Appendix, the differences would seem to imply lower shunt and lower series resistances for the r.f. sputtered cells. If this trend is confirmed in future work, it would appear that the CdO is more conducting and hence more oxygen-deficient with r.f. sputtering. This could explain the lower R_s values (see Appendix) observed but not directly the reduced R_{sh} values. The latter may suggest that in r.f. sputtering, greater penetration of the CdO film via pin holes or localized weak spots in the selenium occurs.

The variation of film thickness with pressure suggests an optimum operating

range of 2 to 10 mTorr , where the deposition rate is greatest. The reduced thickness at lower pressure is believed to be due to less efficient ion collection by the cathode, while at higher pressure, the fall in thickness is attributed to a reduced mean free path of the sputtered atoms, resulting in a lower deposition rate [29].

(c) Effect of Deposition Time

The trends observed for both j_{sc} and V_{oc} with deposition time were similar to those observed in cells prepared by d.c. reactive sputtering [5]. The initial rise in j_{sc} with time is attributed to increased thickness of the CdO film, resulting in decreased series resistance in the cells. On the other hand, the decrease of j_{sc} at the longer deposition time is no doubt due to reduced film transparency resulting from the greater CdO thickness. The monotonic increase of V_{oc} with time is probably due to an increase of shunt resistance with increasing film thickness.

In principle, increasing sputtering time should increase film thickness but should not affect its stoichiometry. Hence, the apparent initial decrease in the product $R_{st.t}$ and subsequent slight increase with time is not understood. However, as mentioned earlier, this may be an effect introduced by target heating whereby with continued sputtering, the resistivity of the deposited film is decreased. It is also possible that at longer deposition times, the subsequent rise in resistivity is due to increased substrate heating arising from continued electron and ion bombardment. This rise in temperature could affect the crystallinity of the selenium surface layer and hence its conductivity.

(d) Effect of Sputtering Power

In depositing the CdO films on glass substrates, it was seen that, in general, the film thickness increased linearly with increasing sputtering power. This effect is

understandable, since sputtering power is proportional to the current flow (of the argon ions) between the sample and the cathode, if the cathode potential is constant. Thus, the higher the sputtering power, the larger the number of ions striking the target surface and hence the larger the deposition rate, which in turn leads to a thicker CdO film. By comparing the films in sets of samples deposited with the two different targets A and C, it was seen that the thicknesses of films deposited with the sintered target C were about three times greater than those of samples prepared with the hand-pressed target A. This greater deposition rate is not surprising, since for the sintered denser target C, a greater sputtering yield would be expected. Accordingly, as is commonly accepted, sintered targets are to be preferred for efficient film deposition.

The electrical resistivity of the CdO films deposited at different power levels showed a rather unexpected strong initial decrease with increasing sputtering power from 10 to 40 watts. Beyond this range however, the resistivity seemed more or less independent of power level. This decrease in resistivity implies that at higher sputtering power, the stoichiometry of the sputtered film was decreased. This could arise from the increase of deposition rate with power, as indicated in Fig.5.8. The stoichiometry decrease could be explained if again it is assumed that the cadmium and oxygen atoms are sputtered separately from the target. In this case, time is required for the atom to recombine at the substrate. Hence as the deposition rate is increased, there is insufficient time for the recombination to take place completely and the resulting CdO is oxygen deficient and therefore more conducting.

(f) Device Performance Change

The change in the characteristics of cell Z-81-2, shown in Figs.5.18 and 5.19 as a result of the application of a reverse voltage, can qualitatively be explained

by an increase in shunt resistance, resulting possibly from the "burning out" of a localized short circuit across the active junction. An attempt was therefore made to fit the curves of Figs.5.18 and 5.19 using the simple equivalent circuit model of the Appendix. The dashed and dotted lines in Fig.5.18 represent such fits, where the parameters involved are stated for the two illuminated curves. The values of j_{ph} and n in equation A.2 were taken to be 2.5 mAcm^{-2} and 2 respectively. It is noted that the obtained area shunt resistance (R_{sh}) values increased from 80 ohm cm^2 before the event to infinity after it. However, the values of j_0 and R_s needed for the fitting were different from one curve to the other. The parameters for the fitted curve A in Fig.5.18 before the event were also found to fit approximately the corresponding dark j-V curve in Fig.5.19. However the parameters for the curve B after the event did not at all fit the experimental dark j-V curve very well in Fig.5.19. This part of the disagreement is attributed to the simplicity of the equivalent circuit model used.

Table 5.1
R.f. Sputtered CdO films on Glass Substrates

Sample ¹	Sputtering Conditions ²				Film Characteristics		
	Power ³ (watt)	Press. ⁴ (mTorr)	Time (min)	Sep. ⁵ (cm)	Thick. ⁶ (μm)	Resistivity ⁷ (10^{-4} ohm cm)	Order, Colour ⁸
Z-1	10	5	30	5	0.05	18700.0	thin yellow ⁹
Z-2	20	5	30	5	0.10	3600.0	1 st yellow
Z-3	40	5	30	5	0.25	3.1	3 rd green
Z-4	80	5	30	5	0.60	4.0	5 th green
Z-5	100	5	30	5	0.70	3.2	5 th red
Z-6	40	0.5	30	5	0.14	3.2	2 nd green
Z-7	40	1	30	5	0.22	3.6	2 nd yellow
Z-8	40	10	30	5	0.16	42.0	1 st red
Z-9	40	45	30	5	0.02	63.0	thin yellow ⁹
Z-17	10	1	30	4	0.07	131.0	1 st yellow
Z-18	20	1	30	4	0.15	6.5	2 nd blue
Z-19	30	1	30	4	0.21	2.3	3 rd green
Z-20	40	1	30	4	0.35	2.6	3 rd red
Z-21	60	1	30	4	0.35	2.4	3 rd red
Z-22	70	1	30	4	0.42	3.1	4 th green
Z-23	40	0.5	30	4	0.35	3.7	3 rd red
Z-24	40	0.75	30	4	0.40	3.3	3 rd red
Z-25	40	1	30	4	0.35	2.9	3 rd red
Z-26	40	5	30	4	0.375	3.2	3 rd red
Z-27	40	10	30	4	0.375	12.0	3 rd green
Z-28	40	50	30	4	0.16	28.0	2 nd blue
Z-29	10	1	10x3	3	0.255	861.0	3 rd green
Z-30	20	1	10x3	3	0.44	45.4	4 th green
Z-31	30	1	10x3	3	0.663	10.4	-
Z-32	40	1	10x3	3	0.87	5.8	-
Z-33	50	1	10x3	3	1.09	5.0	-
Z-34	60	1	10x3	3	1.11	7.8	-
Z-35	70	1	10x3	3	1.24	6.5	-
Z-36	80	1	10x3	3	1.55	8.1	-
Z-37	80	1	10x3	3	1.4	5.8	-
Z-38	60	1	10x3	3	0.78	7.8	-
Z-39	60	1.5	10x3	3	0.98	5.7	-
Z-40	60	2	10x3	3	1.3	3.0	-
Z-41	60	5	10x3	3	1.5	5.8	-
Z-42	60	0.7	10x3	3	0.56	15.0	5 th green
Z-43	60	1	10x3	3	0.92	8.0	-
Z-44	60	2	10x3	3	1.45	12.1	-
Z-45	60	7	10x3	3	1.34	10.9	-
Z-46	60	10	10x3	3	1.48	9.5	-
Z-47	60	100	10x3	3	0.22	1164.0	2 nd yellow

1. Samples Z-10 to Z-16 were used to study variation of deposition time and electrode separation but are not shown.
2. Samples Z-1 to Z-9 and Z-17 to Z-28 were sputtered from the hand-compressed target A. Samples Z-29 to Z-47 were prepared with the machine-compressed and sintered target C (see Target Preparation, section 5.2).
3. R.F. power setting as indicated on system console.

4. Pressure of the argon gas inside the chamber.
5. Separation between sample and target.
6. Film thickness as measured by the Dektak instrument.
7. Film resistivity as measured using the four point probe method described in chapter 1.
8. Order and colour (arising from interference) of the central region of the sample.

Table 5.2(a)
Bismuth and Selenium Deposition Conditions
of r.f. Sputtered Se-CdO Cells

Sample	Bismuth Evaporation					Selenium Evaporation					Remarks	
	Pell.	Time (min)	Sep. (cm)	Currt. (amp)	Syst. ¹	Time (min)	Sep. ² (cm)	Subst. ³ Temp. (°C)	Currt. ⁴ (amp)	Source ⁵ Temp. (°C)		Thick. (μm)
Z-74	5	2	8	60	Coo	60	8	140	-	250	20	
Z-75	5	2	8	60	Coo	60	8	140	-	250	20	
Z-76	5	2	8	60	Coo	60	8	140	-	250	20	
Z-77	5	2	8	60	Coo	90	9	140	-	240	12	
Z-78	3	3	6	40	Edw	5	8	150	4.0	-	40	"Flash-like" selenium evaporation.
Z-79	3	3	6	40	Edw	5	8	150	4.0	-	40	"Flash-like" Se evaporation.
Z-80	4	5	8	50	Coo	10	8	140	2.2	-	30	
Z-81	4	5	8	50	Coo	10	8	140	2.2	-	30	
Z-82	3	5	6	40	Edw	5	8	150	4.0	-	35	"Flash-like" Se evaporation.

1 Edw: Edwards vacuum system model 6E4,
 Coo. Cooke vacuum system model CV301FR

2. Separation between source and substrate

3 Temperature of the substrate during evaporation.

4. Primary current of transformer with secondary side connected to molybdenum boat. Primary-to-secondary windings ratio 22:1. Mo boat used for samples Z-78 to Z-82

5 Temperature of stainless steel crucible during selenium evaporation, used for samples Z-74 to Z-77.

Table 5.2(b)
R.f. Sputtering Conditions of Se-CdO Cells

Sample	Cell ⁶	CdO r.f. Sputtering ⁹					Thick. ¹¹ (μm)	Remarks
		Power ⁷ (watt)	Press. ⁸ (mTorr)	Time (min)	Order	Colour ¹⁰		
Z-74	1,2	20	5	30	2 nd	blue	0.19	Good cell performance.
	3,4	20	5	60	2 nd	red	0.28	
Z-75	1,2	20	5	15	1 st	red	0.14	Reasonable cells. Fairly good cells.
	3,4	20	5	120	4 th	green	0.425	
Z-76	1,2	100	5	15	3 rd	red	0.42	Fairly good cells. Reasonable cells.
	3,4	80	5	15	3 rd	green	0.33	
Z-77	1,2	60	5	15	2 nd	yellow	0.24	Poor cells poss. due to Se film
	3,4	40	5	15	2 nd	blue	0.19	
Z-78	3,4	40	1	30	2 nd	green	0.2	Relatively poor cells.
	1,2	40	2	30	3 rd	red	0.42	
Z-79	3,4	40	7	30	3 rd	red	0.42	Fairly good cells.
	1,2	40	65	30	2 nd	yellow	0.23	
Z-80	3,4	40	1.2	30	2 nd	green	0.2	Relatively poor cells.
	1,2	40	2	30	3 rd	yellow	0.35	
Z-81	1,2	40	7	30	3 rd	red	0.42	Shunt effect (2). Reduced j_{sc}
	3,4	40	110	30	2 nd	yellow	0.24	
Z-82	4,1,2,3	40	7	30	3 rd	red	0.46	Uniformity exp.

6. See Sample Preparation chapter 4 for relative cell positions on aluminum rod. Cells listed in order of deposition.

7. R.F. power setting indicated on system console.

8. Pressure of argon gas inside the chamber.

9. Substrate-to-target separation 2.5 cm. Machine-pressed target B used.

10. Order and colour determined from interference.

11. Film thickness as derived from interference.



Fig.5.1 Photograph of the Varian r.f. magnetron sputtering system employed for CdO deposition.

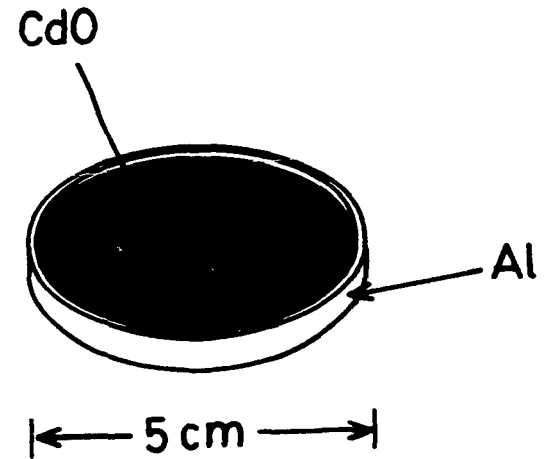


Fig.5.2 Schematic diagram of the CdO target used for r.f. sputtering.

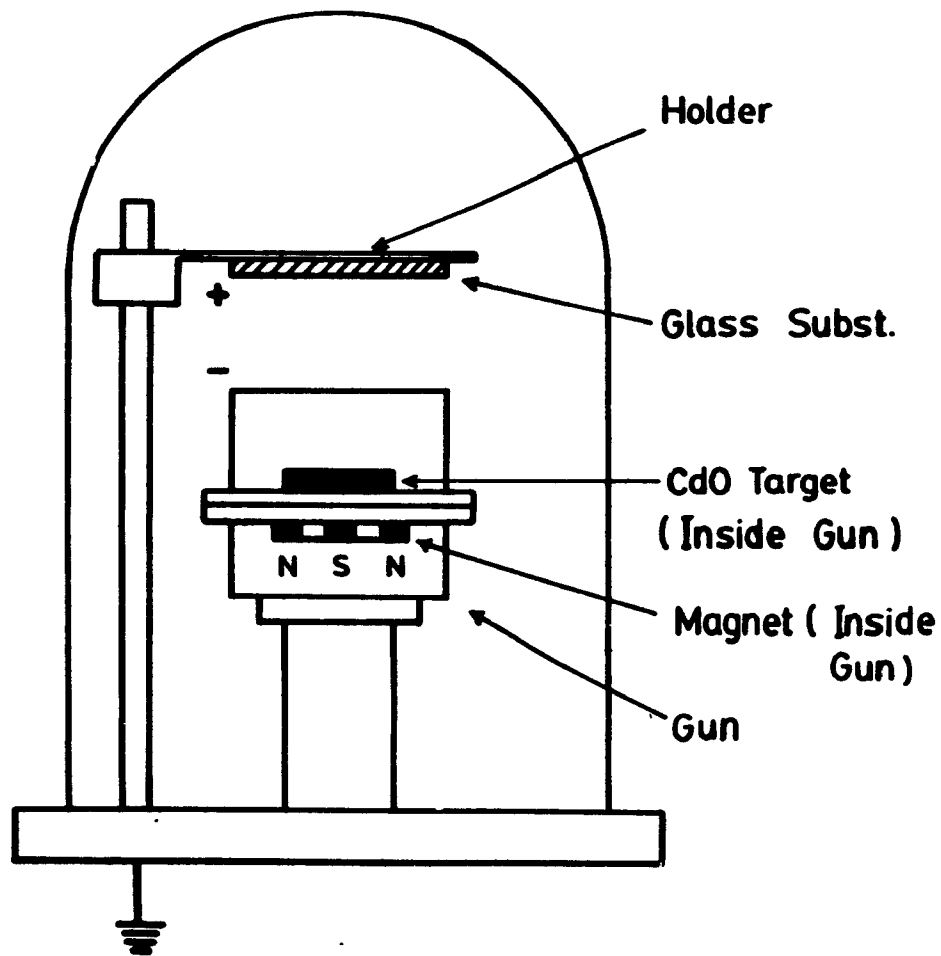


Fig.5.3 Schematic diagram of the arrangement inside the vacuum chamber of the r.f. sputtering system.

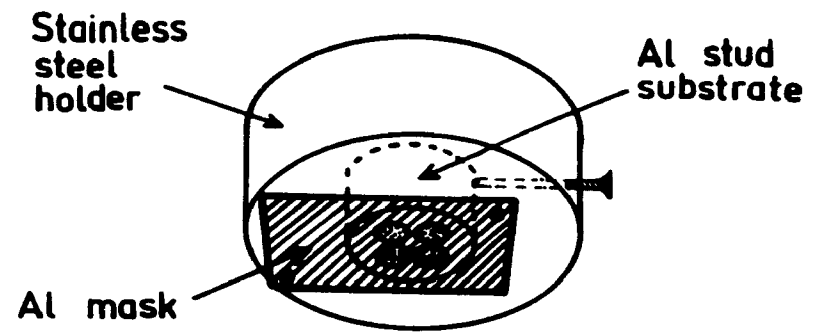
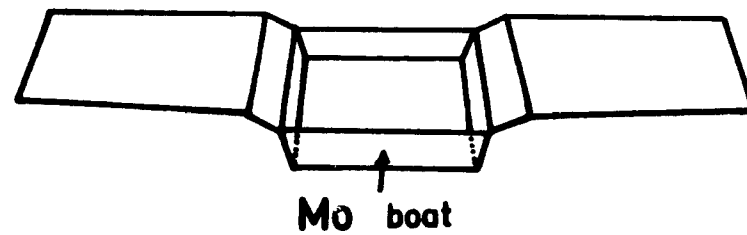
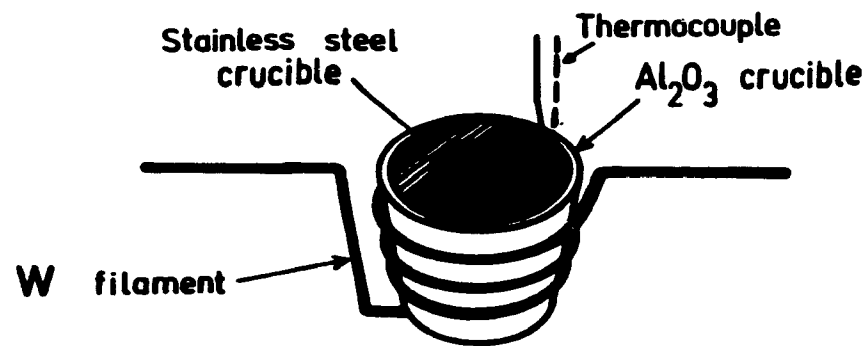


Fig.5.4 Schematic diagram of the stainless steel stud holder used in r.f. sputtering.



(a)



(b)

Fig.5.5 Schematic diagrams of (a) the molybdenum boat and (b) the stainless steel crucible used for the selenium evaporation.

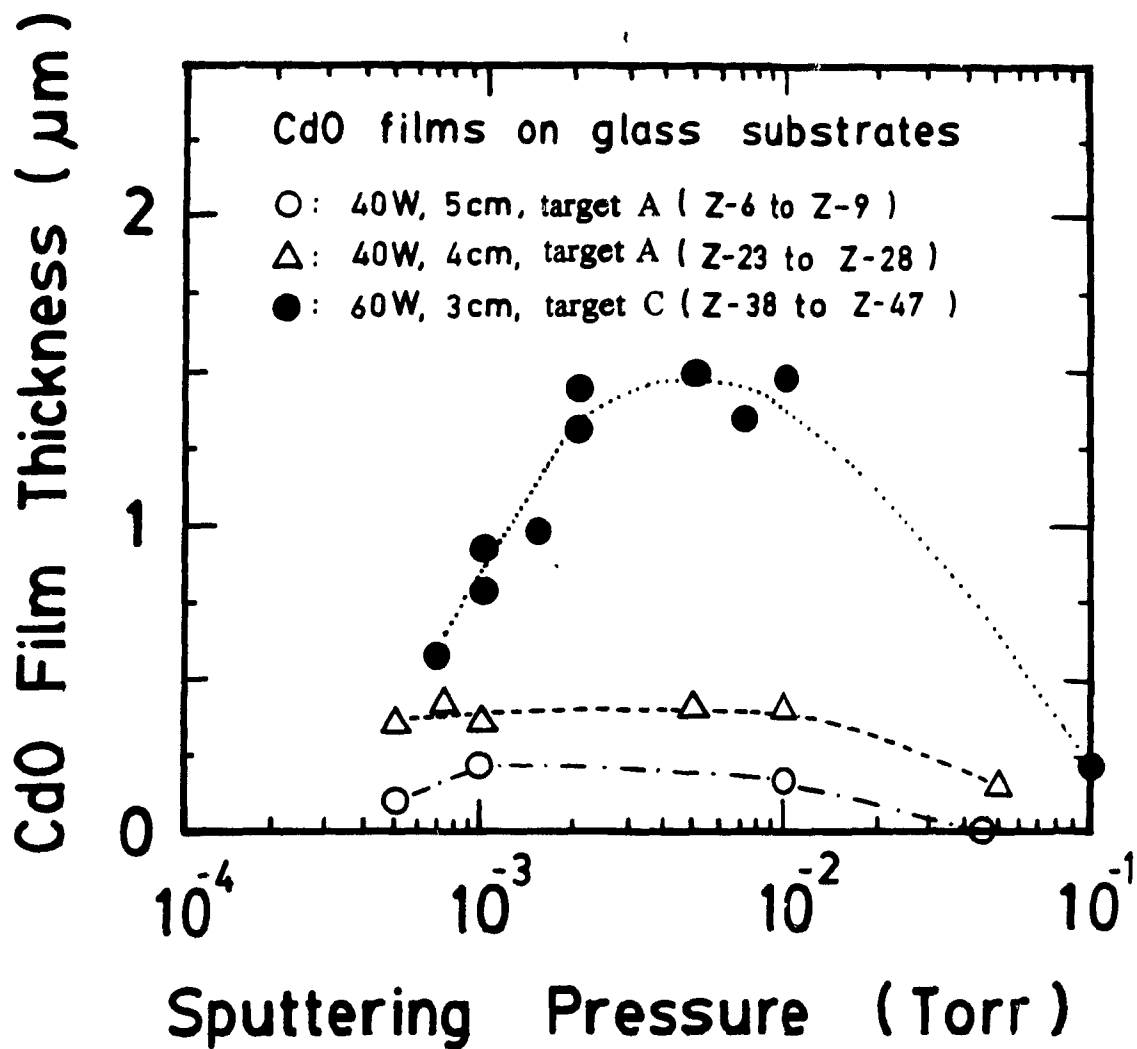


Fig.5.6 Plot of CdO thickness against sputtering pressure for films deposited on glass substrates under different conditions.

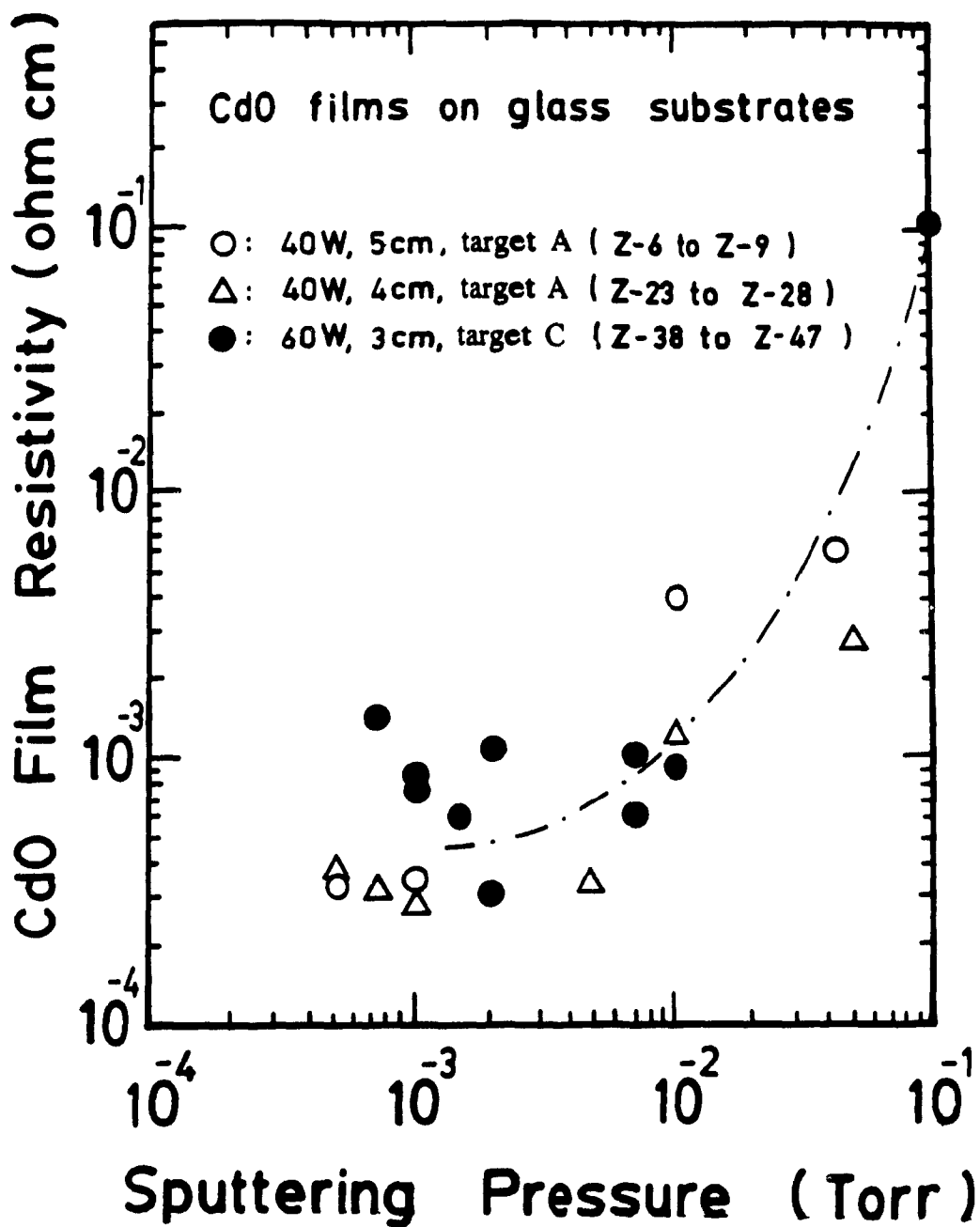


Fig.5.7 Plot of CdO resistivity against sputtering pressure for films deposited on glass substrates.

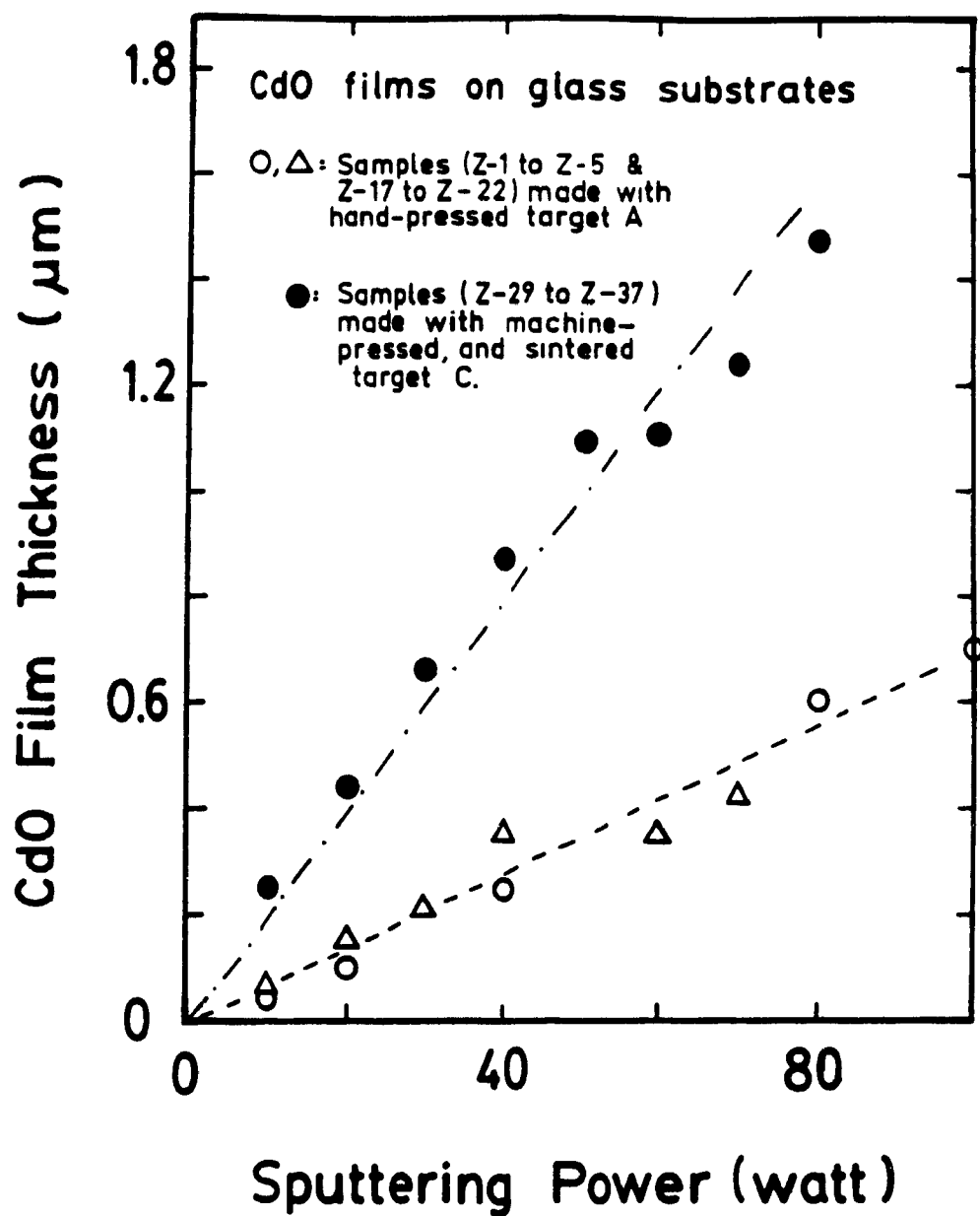


Fig.5.8 Plot of CdO thickness against sputtering power for films deposited on glass substrates using targets prepared in two different ways.

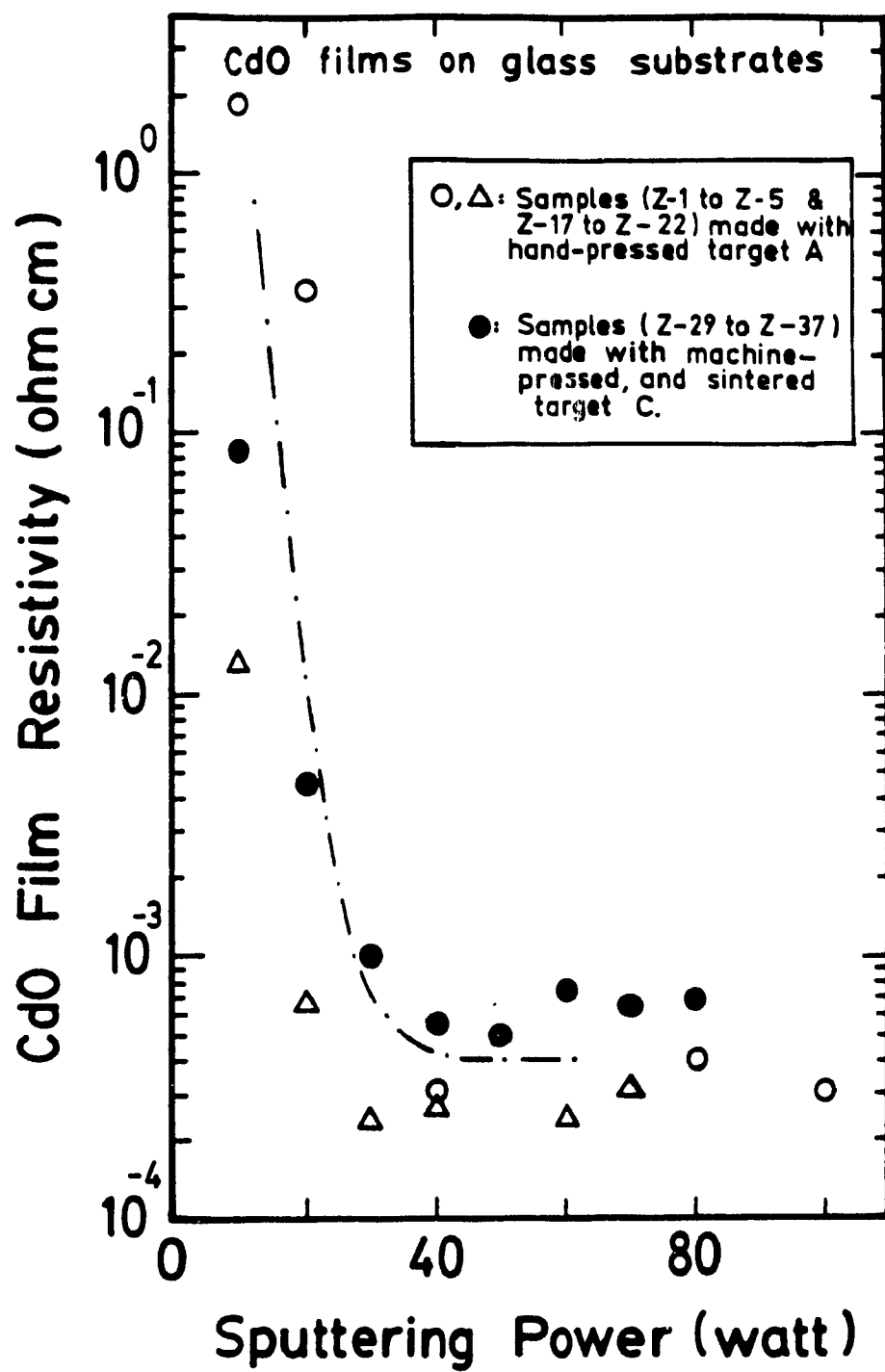


Fig.5.9 Plot of CdO resistivity against sputtering power for films deposited on glass substrates.

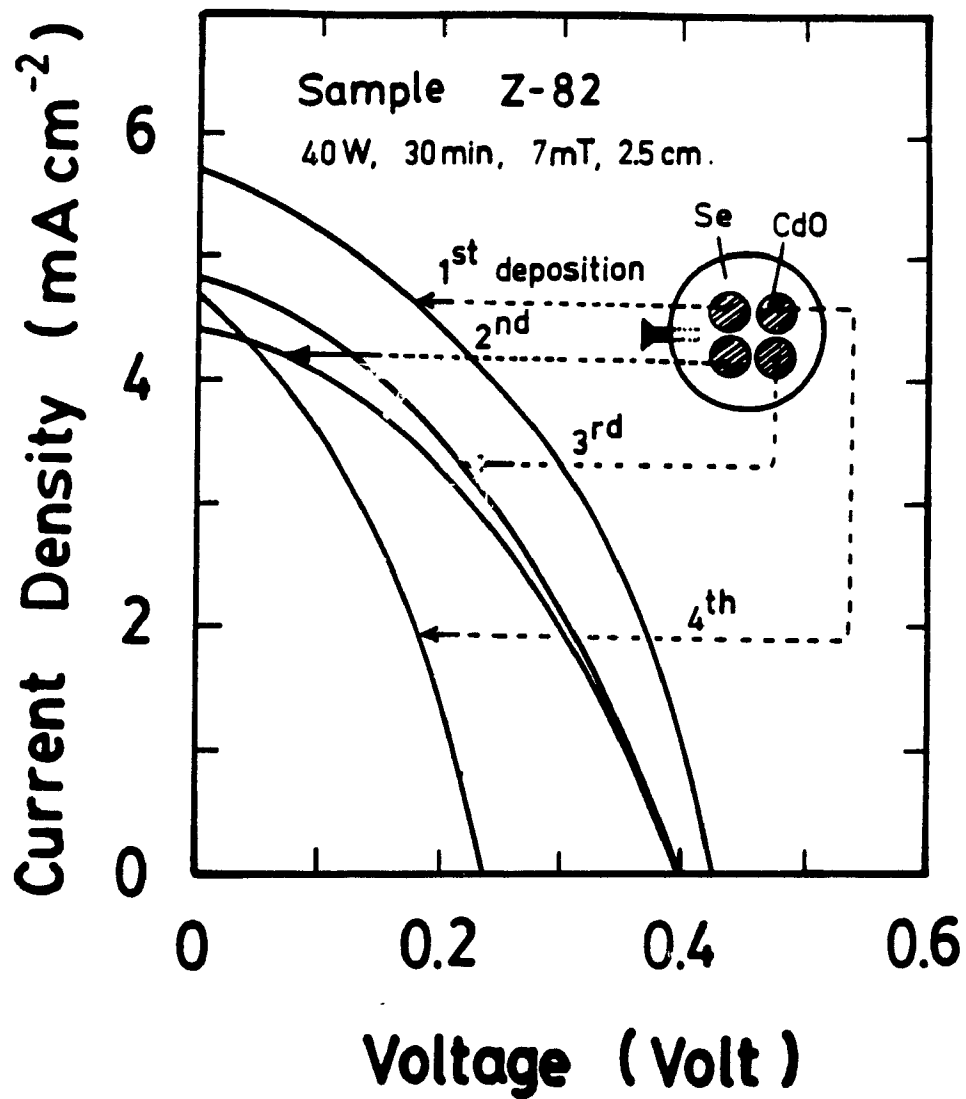
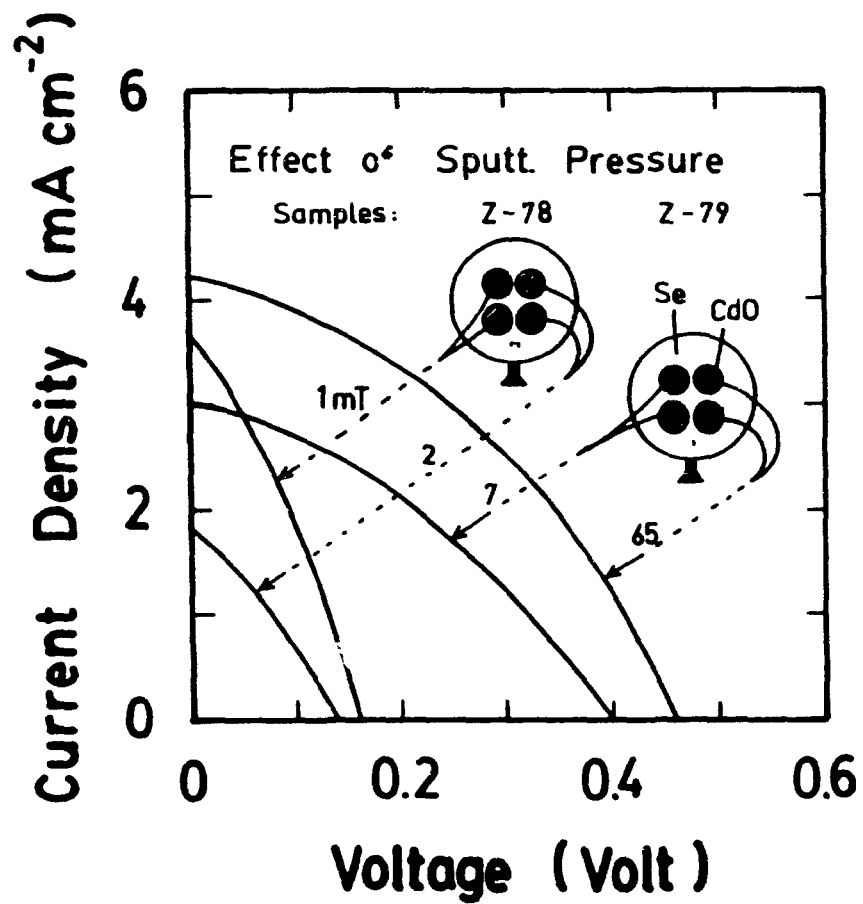
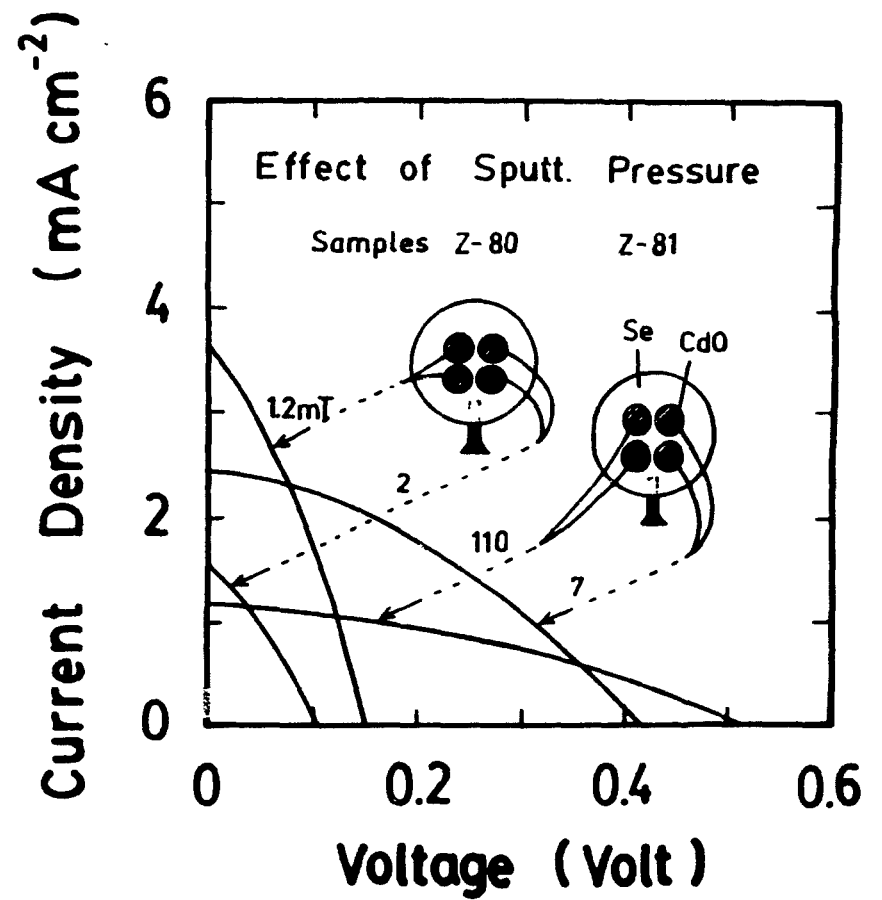


Fig.5.10 Illuminated j-V characteristics of cells deposited sequentially but under the same nominal sputtering conditions.



(a)



(b)

Fig.5.11 Illuminated average j-V characteristics of pairs of cells deposited at different sputtering pressures.
(a) pressures 1, 2, 7 and 65 mTorr,
(b) pressures 1.2, 2, 7 and 110 mTorr.

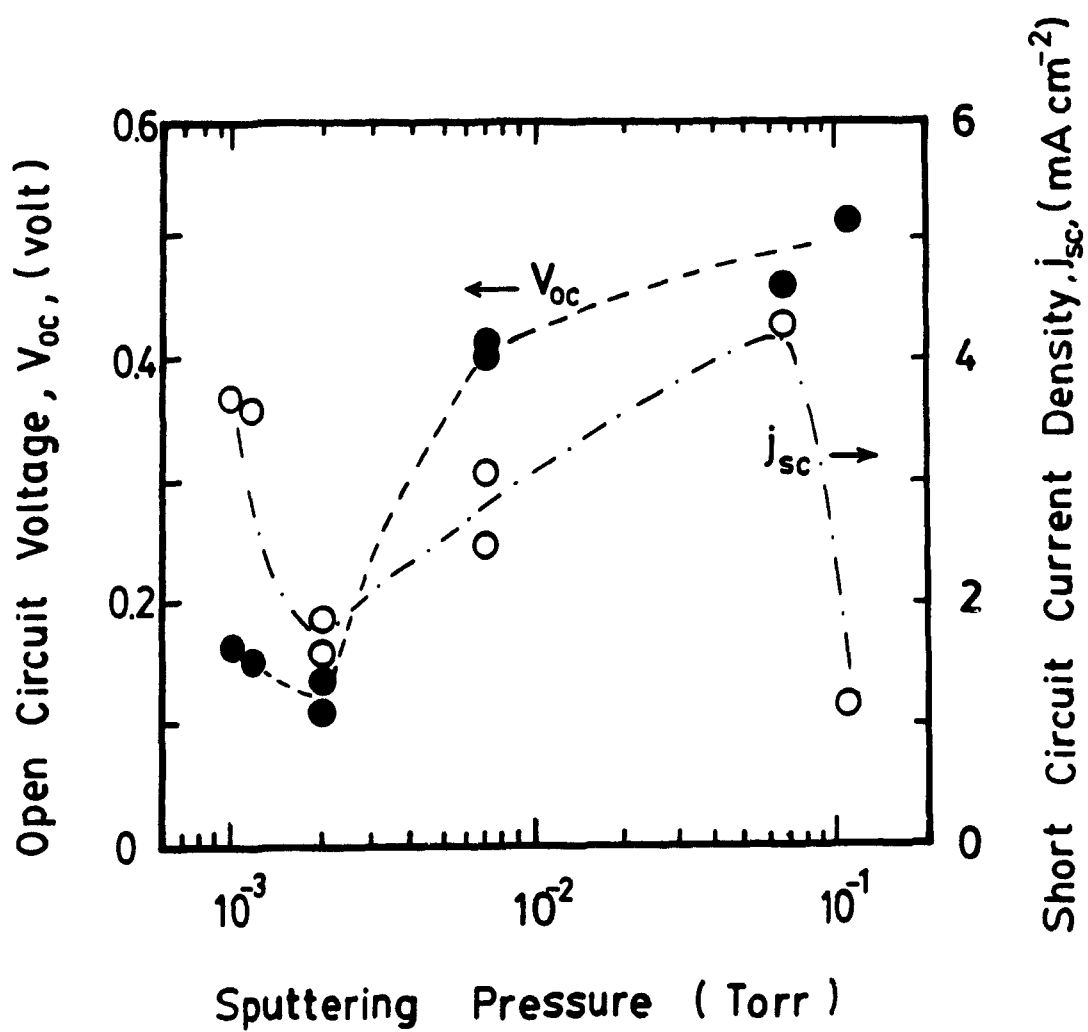
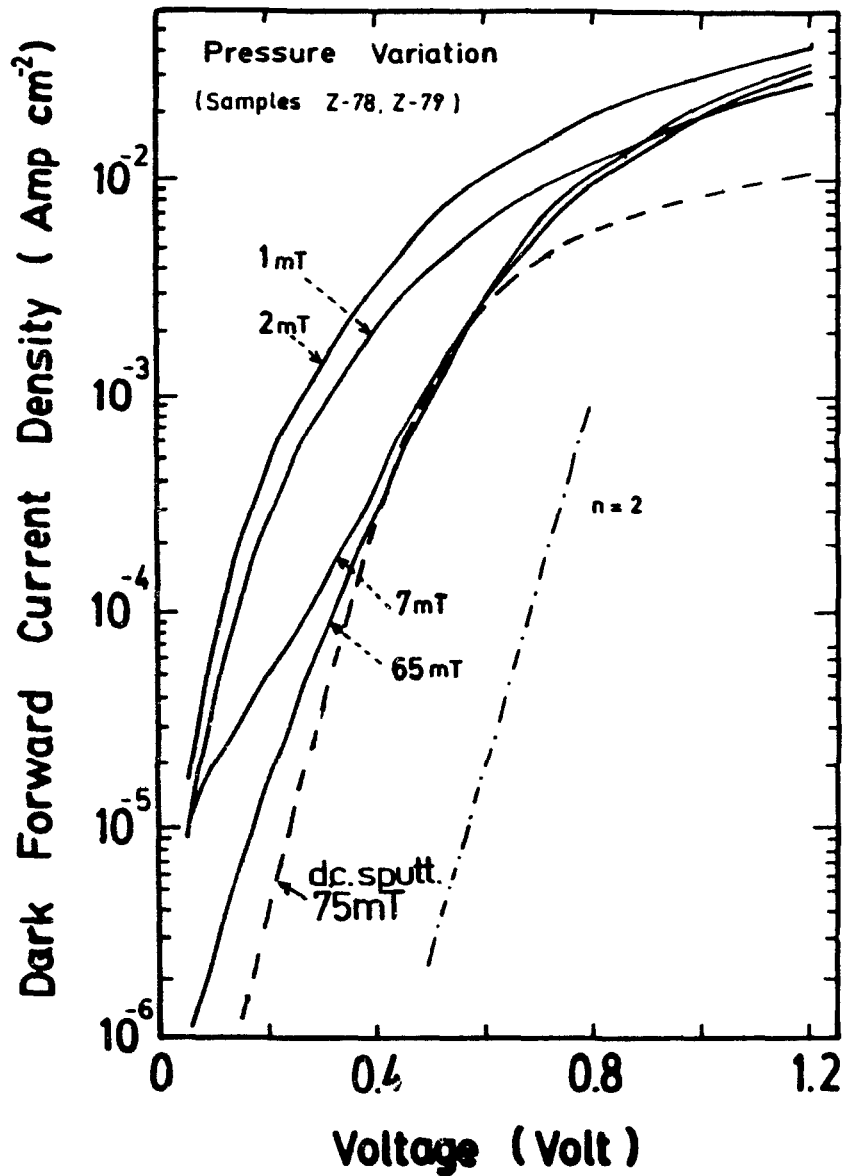
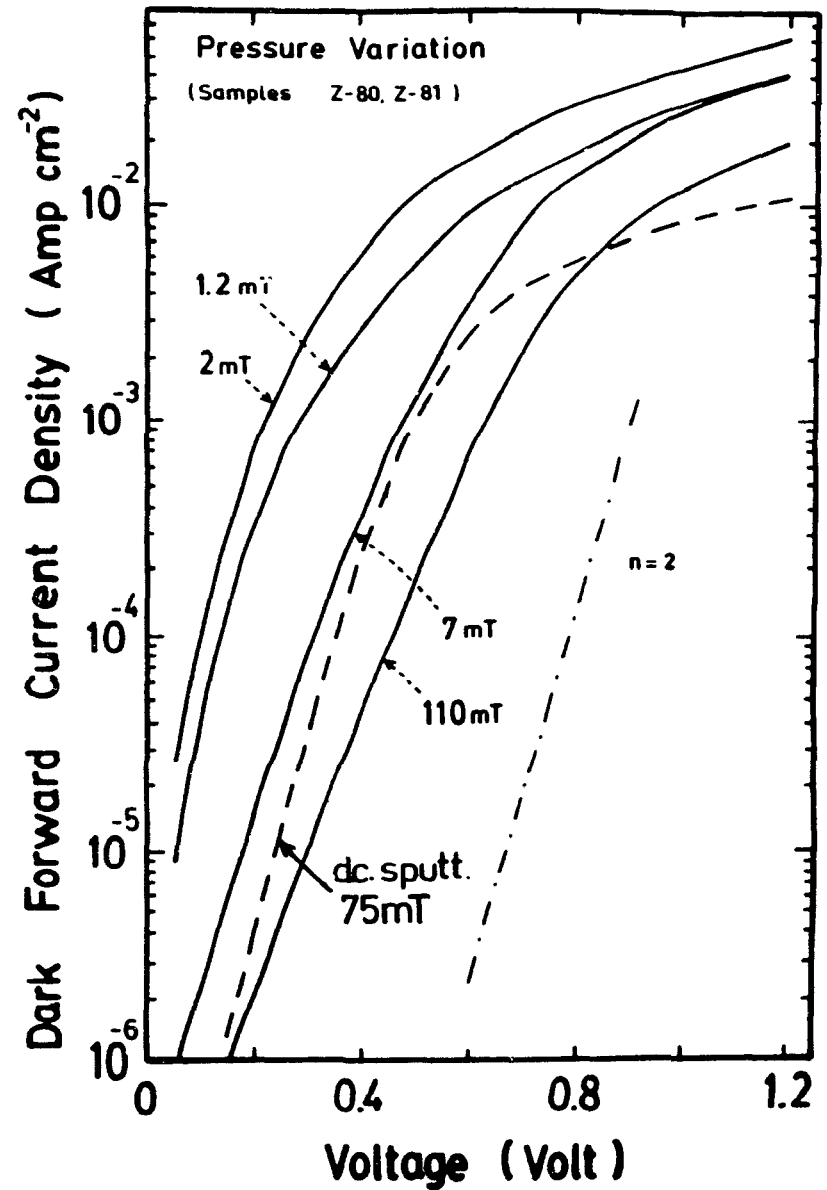


Fig.5.12 Plot of j_{sc} and V_{oc} for cells against sputtering pressure.



(a)



(b)

Fig.5.13 Dark forward average j-V characteristics of pairs of cells deposited at different sputtering pressures.

(a) pressures 1, 2, 7 and 65 mTorr,

(b) pressures 1.2, 2, 7 and 110 mTorr

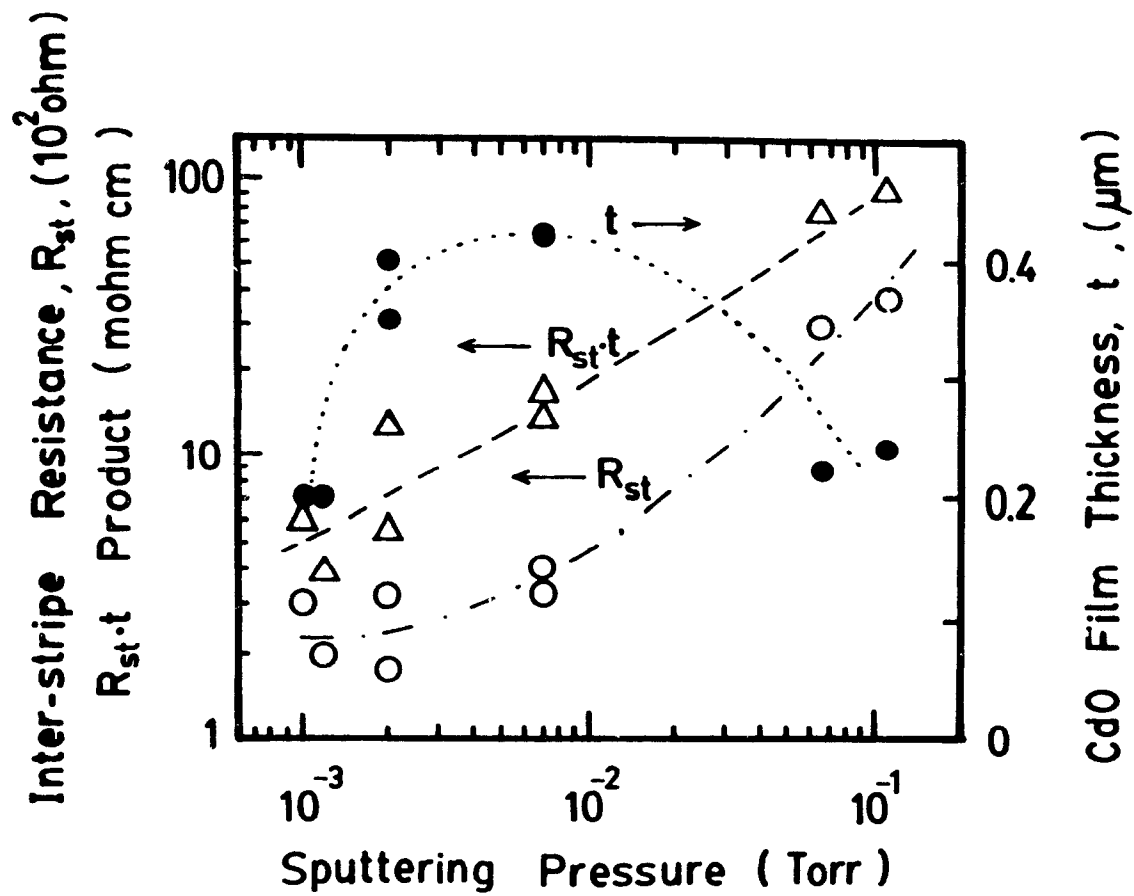


Fig.5.14 Plot against pressure of the quantities: inter-stripe resistance R_{st} , CdO thickness t and their product $R_{st} \cdot t$ for cells fabricated at different sputtering pressures.

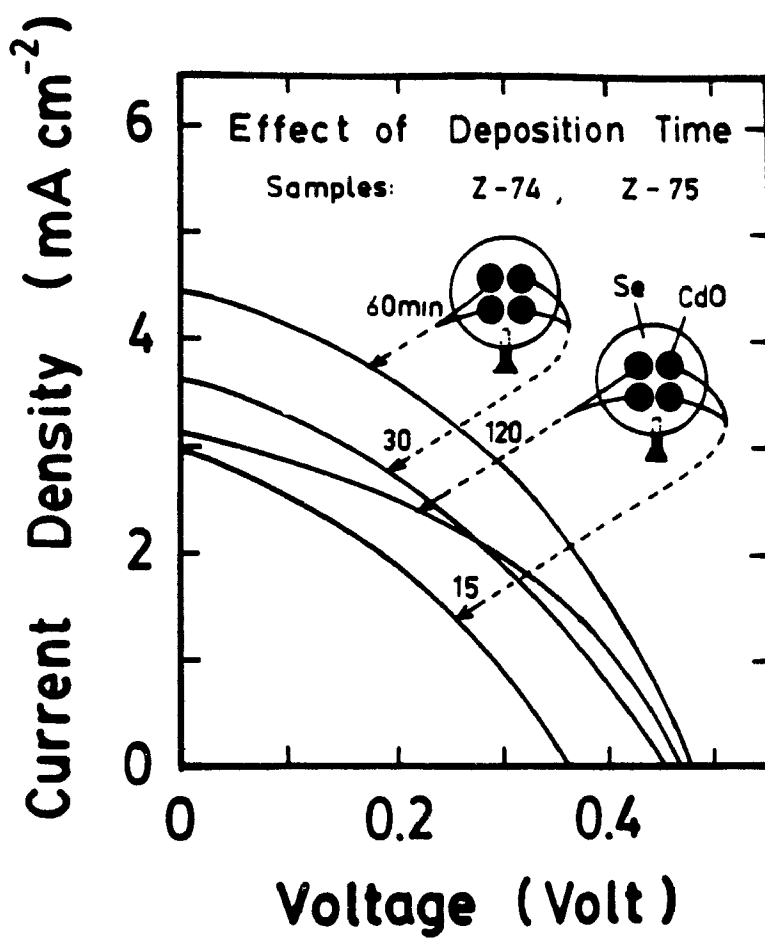


Fig.5.15 Illuminated j-V curves of cells in which the CdO was deposited for different times by r.f. sputtering.

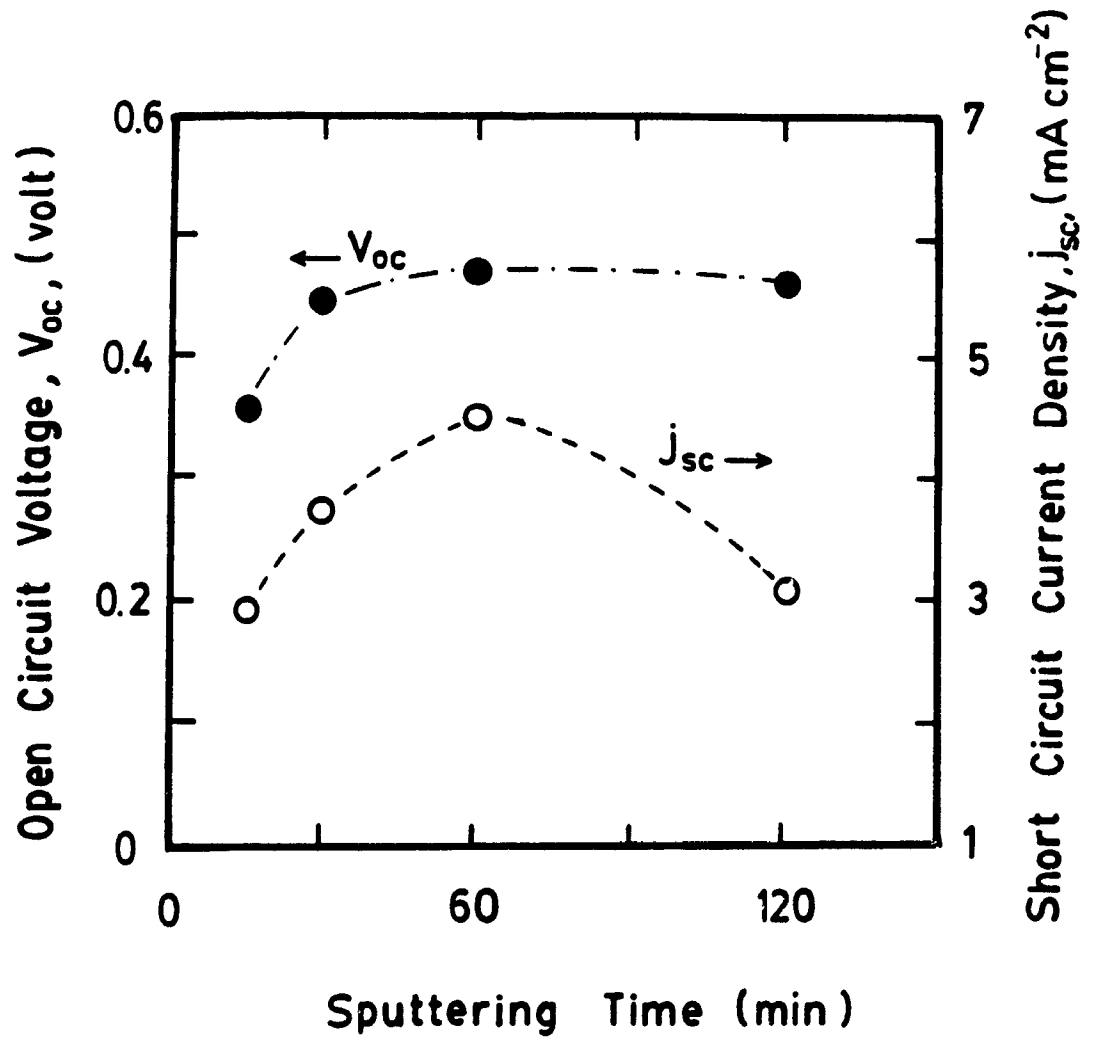


Fig.5.16 Plot of j_{sc} and V_{oc} of cells against sputtering time.

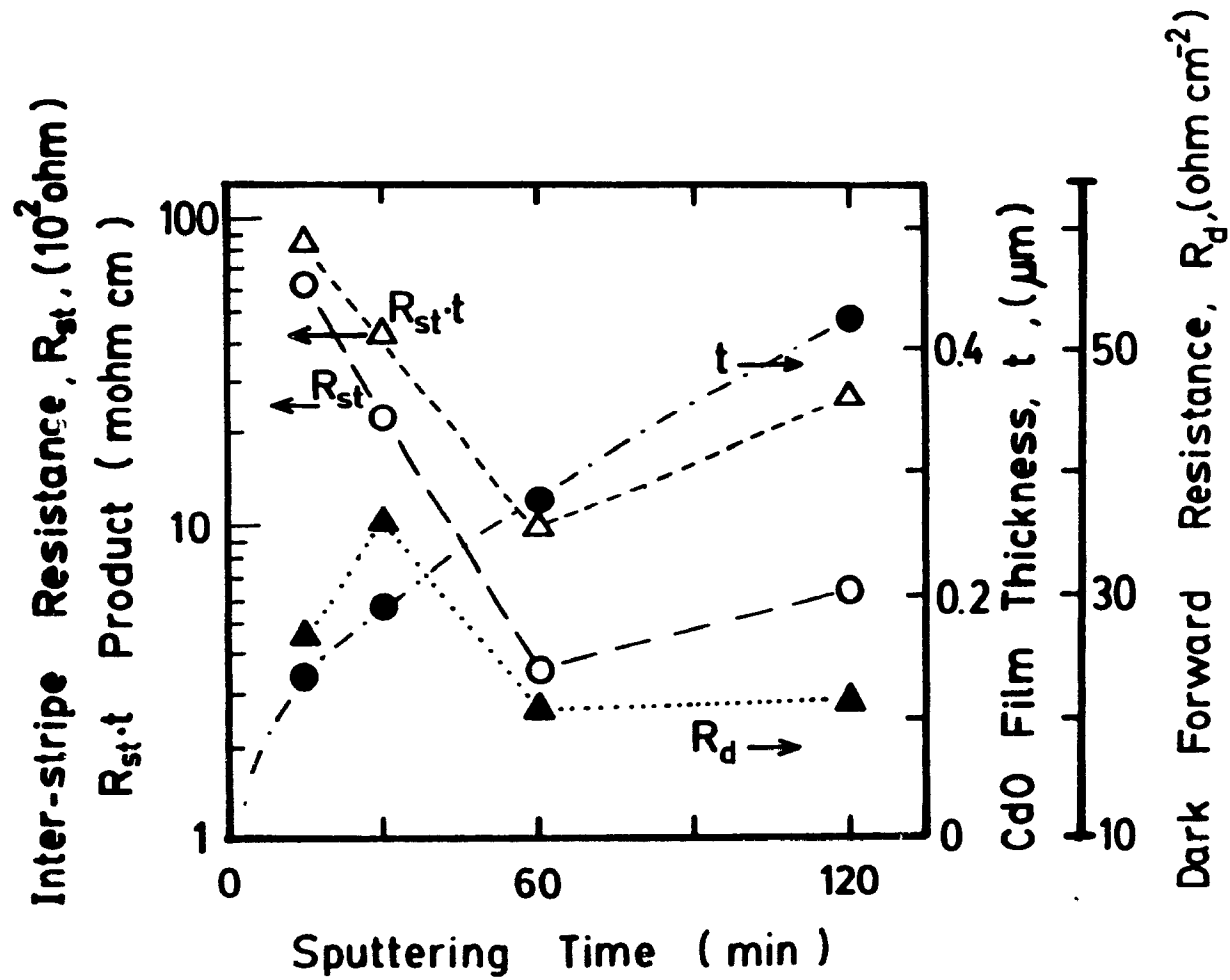


Fig.5.17 Plot against deposition time of the quantities: inter-stripe resistance R_{st} , CdO thickness t , their product $R_{st} \cdot t$ and the dark forward resistance R_d at 1 volt, for cells fabricated with different sputtering times.

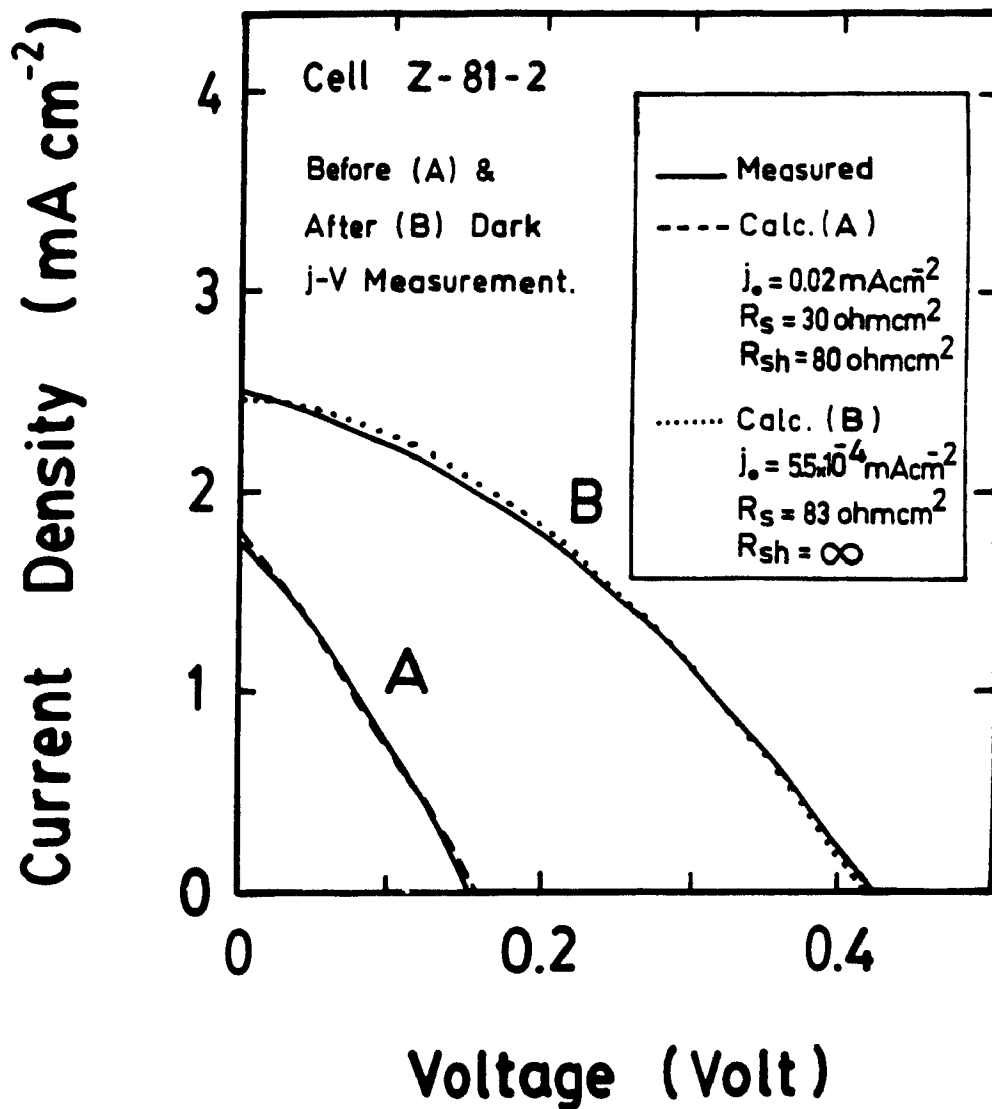


Fig.5.18 Illuminated j-V characteristics of cell Z-81-2 before and after the reverse voltage application. The solid lines represent the experimental results, while the dashed and dotted lines indicate the curves calculated using equation A.1 (see Appendix).

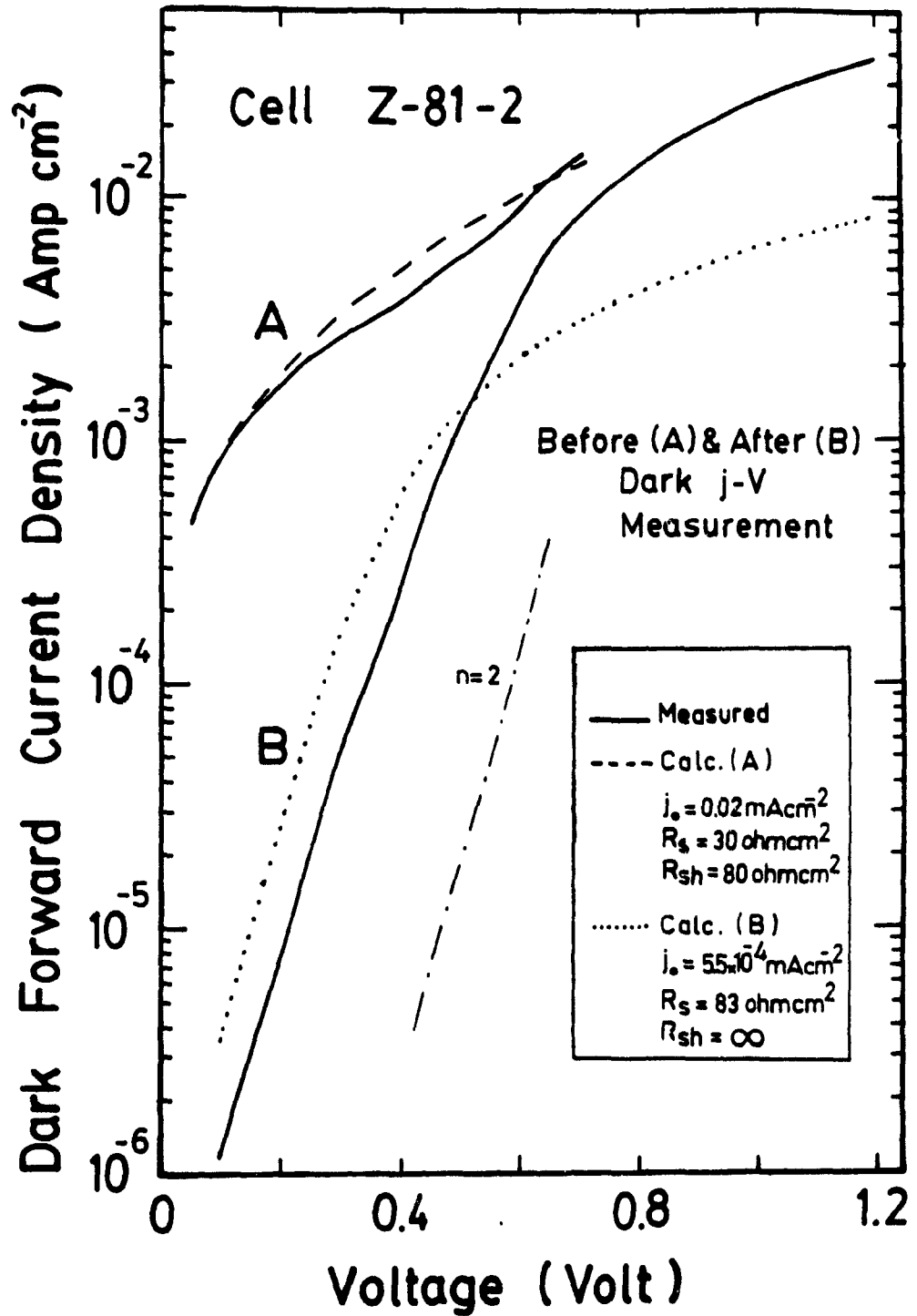


Fig.5.19 Dark forward j-V characteristics of cell Z-81-2 before and after the reverse voltage application. The solid lines represent the experimental results, while the dashed and dotted lines indicate the curves calculated using equation A.2 (see Appendix).

Chapter 6

EXPLORATORY Se-CdO PHOTOVOLTAIC PANELS

6.1 INTRODUCTION

The Se-CdO cell, as indicated in chapter 1, would appear to have potential for powering small consumer electronics products, such as calculators and watches. These products are frequently used under artificial indoor lighting, whose wavelength spectrum is just about the same as that for the photoresponse of the Se-CdO cell.

Since the electronics of a modern pocket calculator requires about 1.5 volts for effective functioning and the Se-CdO cell yields an open circuit voltage of only about 0.5 volt (under high illumination levels), it is evident that a number of these cells must be electrically connected in series in order to supply the voltage level required. Therefore, the structure of the research cells studied in chapters 4 and 5 were not suitable, since in these devices the four cells were deposited on a common aluminum substrate and hence they could not be electrically connected in series.

Accordingly, in this chapter, experiments are described to fabricate small panels, in which the cells were deposited on an insulating substrate and then connected in series. It should be emphasized here that this work is very preliminary and represents a study to demonstrate simply the feasibility of such structures. The panels fabricated were therefore far from optimal but yielded enough results to point the way towards better techniques.

In order to make a working panel, several technological problems had to be

overcome. Some of these were difficulties in depositing crystalline selenium films onto the glass substrate, due to weak adhesion, low sticking of the selenium to the substrate and non-uniformity in characteristics from cell-to-cell across the panel. There were also difficulties in first isolating the cells on the panel from one another and then connecting them satisfactorily in series. The methods used to surmount these difficulties were simply first-time solutions and therefore, as already mentioned, the panels fabricated were under-optimized devices.

Basically two types of panel structure were attempted. In one structure, apart from the substrate, the deposition of the cell layers was done in the conventional way - that is with a film sequence of bismuth, selenium and then CdO (window layer). This structure is referred to as the normal structure and is illustrated schematically in Fig.6.1(a). In another cell structure, referred to as the inverted structure, the sequence was CdO (window layer), selenium and then bismuth, with illumination through a transparent substrate, as illustrated in Fig.6.1(b). The fabrication and results are first presented for the normal structures and then for the inverted devices. The fabrication conditions are given in Table 6.1 for eighteen normal panels and in Table 6.3 for four inverted panels.

6.2 PREPARATION OF NORMAL PANELS

As indicated in Table 6.1, eighteen normal structures were fabricated and, in this section, their preparation is now described. In these structures, seven different configurations were used, which are illustrated in Figs.6.2 and 6.3. The three configurations A, B and C in Fig.6.2 will be described in greater detail, since they yielded better panels than the other configurations. The deposition processes for the panel cells were essentially the same as those used for the aluminum stud cells and therefore only those processes that were done differently will be

described here.

One of the differences in the fabrication procedures involved the set of four masks, shown in Fig.6.4, used in preparing the panel cells. These masks were employed in defining the areas of deposition on the substrate for the various materials, as indicated in the figure. The fabrication steps are described below.

(a) Substrate Preparation

Since in a panel for a pocket calculator, the cells, as already mentioned, must be electrically connected in series to obtain the required voltage (about 1.5 volt), it was necessary to use an electrically insulating substrate, in contrast to the conducting substrate used in the aluminum stud research cells. A microscope glass slide was found to be a convenient choice for the panel substrate, even though its transparency was not needed for these normal structures (see Fig.6.1(a)). The glass slide was prepared for the depositions in the following way (Fig.6.5(a) and (b)). It was first immersed in acetone for about 2 to 3 minutes to remove organic contaminants. Then one side of the glass slide was mechanically roughened by hand using Emery paper (grit #600). This was done on a flat plate to ensure abrasive uniformity, for a period of about 10 minutes until the glass was just translucent. The roughening of the glass was necessary to ensure adhesion of the deposited materials.

In order to minimize the spreading of glass dust into the atmosphere, as well as to increase the abrasive action, water (de-ionized) was used to wet the sand paper during the roughening process. Following this step, the glass slide was rinsed thoroughly with de-ionized water and then dried with soft tissues (Kimwipe brand). The glass slide was then ready for the first deposition step, involving the bismuth layer.

(b) Bismuth Deposition

In this step, mask number 4, shown in Fig.6.4(b), was used to define eight bismuth areas on the substrate. Immediately after roughening the glass slide, it was mounted in a vacuum coating system (usually Edwards model 6E4, see Table 6.1) with the mask adjacent to the roughend side. Then bismuth was deposited on that side of the substrate, as described earlier for the stud cells in chapter 4, with the conditions indicated in Table 6.1 for the eighteen panels (see Fig.6.5(c)). The bismuth evaporation step was repeated for those panels having configurations A and B with the same mask shifted in position in order to elongate the bismuth areas.

(c) Selenium Deposition

Following the bismuth coating, the deposition of the selenium was carried out by evaporation (see Fig.6.5(d)), in essentially the same fashion as that for the aluminum stud cells, as described in chapter 4. However, the graphite substrate holder used for the research cells was replaced with a larger steel block holder, shown in Fig.6.6, to support the larger panel substrates. The original graphite source crucible was also replaced with either a molybdenum boat or stainless steel crucible, shown earlier in Fig.5.5(a) and (b) respectively. The selenium evaporation parameters are given for the panels in Table 6.1.

In the case of panels with configuration A, the same mask number 4 used for the bismuth layer, was again employed for the selenium deposition. For panels with configurations B and C however, the selenium was deposited with mask number 5 which, it may be noted, had larger apertures than mask number 4.

(d) CdO Deposition

Following the selenium deposition, the CdO areas were sputtered using the same residual air technique, employed for the aluminum stud research cells, described earlier in chapter 4. The sputtering parameters were also nominally the same with 30 minutes of sputtering time, 20mA of sputtering current and a pressure of 75 mTorr. However, the mounting holder of the substrates was different because of the larger dimensions of the panel structures. This holder (Fig.6.7) consisted of an 8-cm diameter cylindrical stainless steel block attached to a similar but longer aluminum block. The latter was intended to dissipate the heat away from the substrate during sputtering.

For panels with configuration A, mask number 3 was used to define the CdO areas, while for panels with configurations B and C, mask number 5 was employed again but displaced with respect to the selenium areas, as shown in Fig.6.2. Since this same mask was also used to define the selenium areas, it was important to clean the mask thoroughly to remove any residual selenium before using it in CdO sputtering.

It should be explained here that the lateral overlap of the CdO with the selenium, depicted in Fig.6.2, for configurations B and C, occurred naturally. It is due to the fact that deposited areas by sputtering are always larger than those obtained by evaporation using the same mask.

(e) Wood's Alloy Deposition and Interconnects

After the cells in the panels were sputtered, Wood's alloy contacts were evaporated onto the CdO and bismuth layers of each cell as small dots (see Fig.6.5(f)) to form the front and back contacts respectively. The evaporation was done in the same manner as was described previously in chapter 4, except mask

number 6 was used, shown in Fig.6.4. For panels with configuration C, the third dot on each cell was obtained by a second Wood's alloy evaporation.

The series connection of most of the cells was accomplished by soldering a thin strand of copper wire from the Wood's metal contact(s) on the CdO of one cell to the single contact on the bismuth area of the next cell. Wood's metal solder was used entirely in this operation.

(f) Panels With Configurations D, E, F and G

Preparational details for panels made with configurations D, E, F and G (Fig. 6.3) will not be presented, since they yielded poorer performance compared with cells having the configurations A, B and C. Nevertheless, some features of the former configurations are worth pointing out. In configuration D, a metal stripe (Wood's alloy or aluminum) was deposited on the CdO to collect the current instead of the dot contacts. In configuration E, the stripe contact was also used to interconnect the cells in the panel, whereas in configuration F, the cell-to-cell interconnection was done by side-shifting the bismuth, selenium and CdO areas successively such that the CdO of one cell overlapped with the bismuth of the neighbouring cell. These contact geometries would seem to offer more efficient current collection than the dot contacts and wire interconnects normally used. Attempts were also made to isolate cells on a panel by post-fabrication scribing (configuration G) instead of using masks. The techniques used in configurations D, E, F and G were unsuccessful but their further development should not be ruled out in future work.

(g) Photolithographic Experiments

Attempts were made to utilize photolithography, employing chemical etchants, in isolating the cells on the glass slides, instead of using metal masks.

These attempts were not successful due to difficulties in finding the proper selective etchants for the CdO, selenium and bismuth materials involved. Therefore, further details of this work are not described. Nevertheless, it is useful to record in Table 6.2 the etchants used along with their effect on the different cell materials.

6.3 EXPERIMENTAL RESULTS ON NORMAL PANELS

Measurements were made on most of the panels given in Table 6.1. The panels were primarily characterized in terms of their illuminated current density - voltage curves as a measure of their performance. However, results of just six Se-CdO panels, which were of special interest, are presented in this section.

(a) *Performance of Panel Cells*

Among the six samples, panel Z-68 gave the best overall output, whose illuminated characteristics are shown in Fig.6.8(a) and (b). The figure shows curves for all eight cells of this panel under an illumination of 100 mWcm^{-2} . It is seen that the open circuit voltage showed little variation from cell to cell, with an average value of about 0.42 volt. However, the short circuit current density seemed to exhibit a somewhat greater variation from cell to cell, with values ranging from 2.25 up to 3.0 mAcm^{-2} . It can also be seen that the cells located near the center of the panel yielded lower short circuit currents than those cells on either side. The illuminated characteristics of one cell of panel Z-68 (cell number 2) are given in Fig.6.9, where a schematic cross section of the cell is also shown. Here it is seen that the front surface contact A produced a short circuit current about twice that of contact B, which was located at the edge of the cell, where there was no underlying bismuth. The characteristic of contact B thus seems to suggest higher

series resistance than contact A. By contrast, the open circuit voltages of the two contacts were not significantly different.

(b) Overall Panel Performance

Figure 6.10 shows the illuminated characteristics, measured under an illumination of about 20 mWcm^{-2} , of Se-CdO panel Z-68 and a commercial panel (of unknown material but assumed to be amorphous silicon). The commercial panel consisted of four series-connected cells with a total area of about 3.6 cm^2 , while the total area of the 8-cell Se-CdO panel Z-68 was around 4.8 cm^2 . It can be seen that, although the short circuit current of panel Z-68 was about one third that of the commercial panel, its open circuit voltage was only about 15% less.

Fig.6.11 shows a commercial pocket calculator with its original solar panel (whose characteristics are shown in Fig.6.10) replaced with the Se-CdO panel Z-68. The calculator with the Se-CdO panel was found to operate satisfactorily, despite its lower performance compared with that of the original panel. The colour variation from the center to the edge of panel Z-68, seen clearly in the photograph of Fig.6.11, represents a thickness variation in the CdO film.

(c) Glass Substrate Cells versus Aluminum Stud Cells

Figure 6.12 shows a comparison of the illuminated characteristics of glass substrate panel cells with a single characteristic of an aluminum stud cell of the type treated in chapter 4. The figure shows the curves for one of the best aluminum stud cells (cell SH-14-4) together with one of the best and one of the poorest glass substrate cells (Z-51-4 and Z-57-7 respectively). The dashed line represents an average curve for the glass substrate cells. It is seen that the cell Z-51-4 showed a short circuit current density of about half that of the aluminum stud cell; the fill factor was also not as large but the open circuit voltage was only

slightly less than that of the research cell. To be noted also is the large range of performance variation among the glass substrate panel cells.

(d) Uniformity of CdO Film

As already seen in Fig.6.11, the CdO film exhibited a thickness variation from the center of the panel towards its edges. This variation is believed to be due to the geometry of the sputtering arrangement. An attempt was therefore made to achieve a more uniform CdO film thickness by sputtering a lesser number of cells at a given time. Panel Z-59 was therefore fabricated by first depositing only four cells on the left hand side of the substrate, with the other four selenium areas screened out; then the process was repeated immediately for the second four cells on the right hand side. The illuminated characteristics of both the first four and the second four cells are shown in Figs.6.13(a) and (b) respectively. It is seen that the cells produced by the second CdO deposition exhibited somewhat poorer performance than those produced by the first, even though the sputtering parameters were nominally the same for both runs.

Arising from this result, an experiment was carried out whereby three groups of CdO areas were deposited successively on glass. The time interval between the first and second depositions was about 15 minutes, while that between the second and third depositions was around 3 hours. Fig.6.14 shows a photograph of the substrate after the three depositions. As can be seen, both the first and third deposited areas appeared much lighter in colour than the those deposited in the second run. In measuring the resistance of each of the areas, using two probes about 1 cm apart, it was found that the average resistance of the first and third deposits was about 425 and 625 ohms respectively, while that for the darker areas, produced in the second deposition, was only about 68 ohms.

(e) Uniformity of Selenium Film

In Fig. 6.15, the illuminated characteristics of six cells of panel Z-58 are shown. The figure also shows the relative position of these cells with respect to the stainless steel source crucible used during the selenium evaporation. Here, it is seen that the performance of each cell improved with increase of distance of the cell position along the panel from the center line of the crucible opening. However, at the extreme left hand edge of the glass substrate, "black" selenium was found to be deposited. This form of selenium, from previous work[30], appears to be detrimental to good cell performance and hence, complete cells were not made in this region. The thickness of the selenium film was found to decrease monotonically with distance along the substrate in going from area 5 to area 1 in Fig.6.15.

(f) Effect of Cell Short Circuit

The effect of a short circuit between the front and back metal contacts of a cell in a panel is shown in Figs.6.16 and 6.17. In panel Z-60 the Wood's alloy dots were seen clearly to have penetrated completely through the CdO and selenium layers to the bismuth layer, as viewed from the glass substrate side.

Fig.6.16 shows the illuminated characteristics of the eight cells of panel Z-60, where it is seen that the overall performance of the cells was much reduced. The dark current density - voltage characteristic of cell Z-60-5, shown in Fig.6.17, was clearly linear and non-rectifying. Thus, despite the short circuits, the illuminated characteristics of the cells, while small, were still measurable.

6.4 PREPARATION OF INVERTED PANELS

Four panels of the inverted structure type (Fig.6.1(b)) were prepared, with their fabrication conditions given in Table 6.3. The configurations of these four panels are shown in Fig.6.18. The preparation of panels Z-52, Z-70 and Z-72, with the configurations H, I and J respectively, will only be described in this section. Panel Z-54 will not be described, since its configuration K is almost identical to configuration H and no results are presented on it, in any case.

The panels were fabricated in a similar manner to that used for the normal structure panels except that an inverse sequence of deposition was employed. The first deposition was for the window material (CdO or cadmium), followed by the selenium layer, a metal contact film (Wood's metal, bismuth or platinum) and then Wood's alloy contacts. Masks 3, 5 and 6 (shown in Fig.6.4) were used in these steps.

(a) *Substrate Preparation*

In choosing a substrate for the inverted panels, it is clear that a transparent material must be employed, since the light must pass through the substrate to be incident on the CdO layer, which is deposited first. Hence microscope slides were again used as the substrates for these inverted structures.

In preparing the substrates for the panels of configurations I and J (panels Z-70 and Z-72 respectively), the glass slide was given the same abrasive treatment as that used for the normal structure panels described earlier. However, for panel Z-52 of configuration H, the slide was used as supplied, that is with a smooth polished surface.

(b) Window Material Deposition

Two different materials, CdO and cadmium, were employed for the window layer in these inverted panels. Panels Z-52 and Z-70 (configs. H and I) were fabricated with a CdO window layer, while panel Z-72 (config. J) utilized a thin cadmium film instead.

For panels Z-52 and Z-70, the deposition of the CdO layer was carried out in an identical fashion to that used for the normal panels. In the case of panel Z-52, the CdO was deposited over the entire substrate area with no mask used. However for panel Z-70, mask number 5 was employed. Furthermore, in this panel, a cadmium-rich CdO layer was deposited at the end of the sputtering run, in an attempt to improve the sticking of the selenium film to this layer (see Table 6.3).

In the case of panel Z-72, the deposition of the thin cadmium film was done by evaporation (see again Table 6.3) using the Cooke vacuum system (model CV301FR). These cadmium areas, defined using mask number 5, were deposited with an evaporation time short enough to produce a film sufficiently thin so that light could pass through it and reach the active region in the selenium.

(c) Selenium Deposition

In fabricating the inverted panels, the deposition of the selenium was the most difficult. In many evaporation attempts (not shown in Table 6.3) the selenium was evaporated with the substrate present but no actual deposit was seen on the CdO.

Despite this apparent difficulty, the selenium film was successfully deposited on the CdO (with no mask used) in panel Z-52 but the improved sticking is not understood in this case, especially since a smooth glass substrate was used. In this

particular panel, the substrate holder clamp screened the selenium away from a small strip of CdO on which the contacts were made (config. H in Fig.6.18).

In the case of the other two inverted panels, Z-70 and Z-72, the selenium was satisfactorily deposited, possibly because the exposed surface layers on the substrates were cadmium-rich CdO and cadmium respectively. The deposition for panel Z-70 was done using mask number 5, which was shifted in position with respect to the CdO areas to allow for the contacts, as shown in configuration I in Fig.6.18. In the case of panel Z-72, the deposition of the selenium was done somewhat differently. Here the evaporation was carried out at a higher rate with the substrate maintained at a temperature of about 120°C. This resulted initially in an amorphous selenium film, which was then allowed to crystallize at 120°C for a period of about 15 to 20 minutes under vacuum. This process was only done to see how it would compare with the in situ crystallization process normally used during deposition.

(d) Metal Contact Deposition

In the inverted panels, three alternative metals were used as the contact to the selenium, namely Wood's alloy, bismuth or platinum. Wood's alloy was a convenient choice because of its low melting point, bismuth was used as the back contact material in the stud cells and platinum has a high electronic work function.

In panel Z-52, Wood's alloy was evaporated onto the selenium in the form of a wide stripe across the panel (see config. H in Fig.6.18) as described earlier. For panel Z-70 (config. I), bismuth was evaporated onto the selenium using mask number 3. Here the evaporation was again done as outlined for the aluminum stud cell except that the Cooke vacuum system was used (see Table 6.3). In panel Z-72 (config. J), platinum was deposited by evaporation, using mask number 3, in an

Edwards E306A coating system. Here it was necessary to evaporate the platinum in a rapid "flash evaporation-like" manner to avoid alloying from taking place between the platinum strands and the tungsten filament.

(e) *Wood's Alloy Contacts and Interconnects*

Using mask number 6, Wood's alloy dot contacts were deposited by evaporation on all the panels. In each panel, the cells were soldered separately (using thin copper strands) for electrical measurements. Since in panel Z-52, no masks were used to define cells, two areas were isolated as separate devices using scribing action, which was done prior to soldering.

6.5 EXPERIMENTAL RESULTS ON INVERTED PANELS

In this section, test results are presented on the inverted panels Z-52, Z-70 and Z-72. Measurement of illuminated as well as dark characteristics of cells in these panels was made to evaluate their performance. It should be noted again however, that these results are preliminary and by no means reflect the full potential of the inverted structures.

(a) *Glass-CdO-Se-Bi Inverted Panels*

In Fig.6.19, the illuminated characteristics of the two cells of panel Z-52 are shown. It is seen that, despite non-optimal fabrication conditions, the two cells did yield measurable values of open circuit voltage and short circuit current density, amounting to about 0.22 volt and 1.25 mAcm^{-2} respectively.

The illuminated and dark characteristics of cells of panel Z-70 are shown in Fig.6.20 and 6.21 respectively. The inset in both figures shows a cross sectional view of a single cell of the panel. It is seen in Fig.6.20, that the characteristics,

under an illumination of 100 mWcm^{-2} , for all eight cells showed rather low photovoltaic output in terms of both V_{oc} and j_{sc} . The dark characteristic of cell number 6 of this panel is shown in Fig.6.21. Here, it is seen that the dark current density at a forward bias voltage of 1 volt of around 0.2 mAcm^{-2} is rather small compared to values observed in aluminum stud cells. Furthermore, the rectification ratio at higher voltages, beyond about 0.5 volt is also seen to be small. It is interesting to note that, at voltages below about 0.5 volt, the "reverse" current was found to exceed the "forward" current. This observation might suggest the occurrence of quantum mechanical tunnelling in this voltage range.

(b) Glass-Cd-Se-Pt Inverted Panel

In Fig.6.22, curves for the eight cells of panel Z-72, under an illumination of 100 mWcm^{-2} , are shown. Here it is seen that this non-conventional Cd-Se-Pt structure produced an output larger than those of the two inverted panels using CdO. It is also seen that, in this panel, the performance of the cells generally decreased with cell position in going away from the center of the panel. The dark characteristics of cells 1 and 4 of this panel are given in Fig.6.23. Here, it is observed that in cell number 4, at 1.0 volt, the forward current and rectification ratio were greater than those in cell number 1. The lower forward dark current in cell 1 at 1.0 volt suggests higher series resistance than in cell 4. This is consistent with the lower illuminated j_{sc} value of cell 1, shown in Fig.6.22.

6.6 DISCUSSION

In this section a discussion of the results on the panels is given, together with possible explanations of the effects observed. The discussion will first focus on the normal structures and then on the inverted ones.

(a) *Normal Structures*

Since the development of the Se-CdO panels, described in this chapter, was still in its early stages, an antireflection coating and an efficient current collecting metal grid were not incorporated into the fabrications of the cells. The reason for this was to keep the structures as simple as possible and to minimize the number of fabrication parameters.

One of the better panels made was the normal structure Z-68, which produced sufficient power to operate a commercial calculator, even under low illumination levels, which is an encouraging outcome at this stage. Furthermore, even though the panel cells were not optimized, the performance of one of the better glass cells was only about half that of one of the best aluminum stud cells. The lower performance of the panel cells is not surprising, since the optimized conditions for the aluminum stud cells may not apply to cells deposited on glass.

In view of this and the fact that panel Z-68 had a performance of only about one third that of the original calculator panel, it would seem that a Se-CdO panel can indeed be fabricated with a performance about equal to that of the commercial panel. In fabricating these panels, a number of configurations were employed, of which the three configurations A, B and C were described in some detail. Of these, configuration C is preferred from a technological point of view, since short circuits through the selenium film were more readily detectable by virtue of having the two contacts. From a performance viewpoint however, configurations A and B are preferred due to their larger bismuth areas.

The results on panel Z-58, and to a lesser extent on panel Z-68, show that cell performance increased with decrease of selenium thickness, arising from cell position - that is the distance of an individual cell along the substrate from the

source projection point. It is suspected that this effect is not due to a smaller film thickness *per se* but to a lower deposition rate. In this case, the better performance could arise from larger selenium grains. However, this was not able to be verified during microscopic observation of the cells.

In the results of cell Z-59, where two groups of CdO areas were deposited in successive runs, and in the experiment where CdO areas were deposited successively on a glass substrate, it was clear that the second deposition in both cases was affected by the immediately previous one. However, in the case of the glass slide experiment, when the depositions were separated by a period of about three hours, instead of fifteen minutes, the memory of the first deposition was essentially lost. This memory effect is believed to be associated with the target. One possibility is that its surface oxidation condition from one run to the next is affected, but another, more likely cause is excessive heating. Thus, what may happen is that, because of insufficient cooling, the target temperature rises during the first sputtering run and this higher temperature results in a faster deposition during the second run [19]. Arising from this high deposition rate, the CdO film is deficient in oxygen and is consequently less transparent, as is observed experimentally.

In panel Z-60, the observed short circuits through the selenium film were caused possibly by hot clusters of Wood's alloy arising from rapid evaporation. Despite the fact that the Wood's alloy dots actually penetrated right through the selenium film reaching the bismuth layer, the cells in the panel still yielded a small but measurable output. It is interesting to note that the slopes of both the dark and illuminated j-V characteristics of cell 5 of this panel yielded the same resistance value of about 80 ohms, which, in fact, can be regarded as the sum of the shunt and series resistances of the cell through the Wood's alloy short circuit.

The series interconnections of the cells in panels with configurations A, B and C were accomplished using thin copper wires and Wood's alloy solder. While this is a somewhat crude method, it was employed here only because of its simplicity. However, in configurations E and F, other means of interconnection were attempted, and although these were not initially successful, they are still viable alternatives to direct soldering.

(b) Inverted Structures

So far as is known, the inverted Se-CdO photovoltaic structures fabricated in the present work represent the first time that such a device has been reported. Less work was done on inverted panels than on the normal structures, largely due to fabrication difficulties. However, the inverted structure does offer some possible advantages over the normal one. Firstly, the layers are deposited in the order of decreasing melting point, so that it is possible to have the CdO maintained above the melting point of selenium (217°C) during its deposition. A second advantage is that the transparent substrate can also act as a protective cover for the cell. The substrate, with a lower refractive index than CdO, can also decrease somewhat the overall reflectance loss, and the inverted cells did indeed appear to be slightly darker than the normal cells.

Despite these potential benefits, the inverted structures yielded a lower performance than the normal structures. This was due in part, in the case of the three inverted panels where CdO was used, to series resistance arising from the absence of current collecting stripes on the CdO. In case of panel Z-72, where cadmium was used instead of CdO, the performance was better, presumably due to the higher conductance of this layer. It is possible in this panel that CdSe might have formed between the selenium and the cadmium.

In the case of panel Z-70, the improved sticking between the selenium film and the CdO layer may have been due to the fact that cadmium-rich CdO was used as an interfacial layer between the two. In panel Z-72, where the window layer was only metallic cadmium, there was no sticking problem what-so-ever and hence this tends to support the above conclusion. The cadmium-rich CdO panel Z-70 was also unique in exhibiting a dark "reverse" current in excess of its "forward" current at lower voltages, which is characteristic of quantum mechanical tunnelling. Possibly, in this case, cadmium diffused into the selenium, causing it to have a very high acceptor concentration near the junction. However, the fact that panel Z-72 did not show such tunnelling effects could be due to the shorter deposition time for the selenium or to the back contact of platinum used instead of bismuth.

The decrease of cell performance with distance away from the center of the substrate in panel Z-72 appears, from the dark characteristics, to be due to both high series and low shunt resistance in cell 1 compared with cell 4 for example. The illuminated characteristics indicate mainly higher series resistance in the outer cells. While the low shunt resistance could be due to small localized short circuits in the selenium, no visible evidence of this was apparent.

Table 6.1
Fabrication of Normal Structure Panels (Glass-Bi-Se-CdO)

Panel	Config. ¹	Bismuth Evap. ²				Selenium Evap.						CdO Sputt. ⁸		Wood's Alloy Evap. ¹⁰			Remarks
		Pell. (min)	Time (min)	Rept. ³	Syst.	Time (min)	Sep. ⁴ (cm)	Subst. Temp. ⁵ (°C)	Curri. ⁶ (amp)	Source Temp. ⁷ (°C)	Thick. (µm)	Order	Colour ⁹	Time (min)	Sep. (cm)	Rept.	
Z-51	A	4	7	2	Edw	45	7	140	-	240	30	3 rd	green	5	7	1	Five relatively good cells. No 4 best Se-CdO cell on glass.
Z-55	G	3	7	1	Edw	60	8	140	-	240	8	3 rd	red	5	7	1	Cell performance somewhat poor, scribing used for area isolation
Z-56	G	4	10	1	Edw	60	9	140	-	240	20	4 th	green	7	6	1	Performance rather low, isolation by scribing.
Z-57	C	4	10	1	Edw	55	8	140	-	250	-	3 rd	green	5	6	2	Poor cell performance, used for etching experiments.
Z-58	A	4	7	2	Edw	100	8	140	-	250	35	4 th	red	5	6	1	Cells showed effect of Se deposition on performance.
Z-59	A	5	5	2	Edw	30	7	140	2.4	-	20	5 th	green	5	6	1	CdO deposition done twice, four areas at a time
Z-60	B	3	5	2	Edw	35	10	150	2.4	-	40	-	-	5	6	1	Short circuits in cells Wood's alloy evap current 40A.
Z-61	B	3	5	2	Edw	25	8	140	2.6	-	20	3 rd	green	7	7	1	Relatively poor performance
Z-62	E	2	7	2	Edw	30	9	140	2.2	-	20	3 rd	green	7	7	1	Poor performance, cell to-cell interconnects by Wood's alloy stripes.
Z-63	E	2	6	2	Edw	50	9	140	2.2	-	35	4 th	red	5	6	1	Performance was low, cell interconnects by Wood's alloy stripes
Z-64	E	2	6	2	Edw	35	9	140	2.2	-	30	4 th	green	5	9	1	Performance rather poor, interconnects using Wood's alloy stripes
Z-65	F	2	5	1	Edw	40	8	150	2.4	-	35	4 th	red	-	-	-	Low performance, cell to-cell interconnects by CdO-Bi overlaps.
Z-66	F	2	5	1	Edw	50	8	150	2.4	-	30	3 rd	red	-	-	-	Poor performance, cell interconnects by CdO-Bi overlaps
Z-67	E	2	5	2	Edw	30	9	140	2.2	-	10	3 rd	red	-	-	-	Panel abandoned.
Z-68	C	2	5	1	Coo	40	10	140	2.2	-	>20	3 rd	red	5	10	2	Fairly good overall panel performance, used to operate calculator.
Z-69	D	2	5	1	Coo	50	10	140	2.2	-	20	4 th	blue	5	10	3	Poor performance.
Z-71	C	3	5	1	Coo	50	10	140	2.2	-	25	4 th	green	-	-	-	Wood's alloy stripes used, rather resistive
Z-73	D	3	5	1	Coo	50	10	140	2.2	-	15	4 th	green	-	-	-	Aluminum stripes used, fairly resistive.

1 Panel configurations are shown in Figs 6.2 and 6.3.
Effective cell area: config. A 0.30 cm², config. B - F 0.6 cm², config. G about 1 cm²

2 Boat current 40A in Edwards vacuum system model 6B4 (Edw) and 50A in Cooke vacuum system model CV301FR (Coo). Source-to-sample separation 7 cm

3 Number of times the evaporation was carried out

4 Separation between source and substrate

5 Temperature of the substrate during evaporation

6 Primary current of transformer with secondary side connected to molybdenum boat Primary-to-secondary windings ratio 22:1 Mo boat used for panels Z-59 to Z-69, Z-71 and Z-73

7 Temperature of stainless steel crucible during selenium evaporation, used for panels Z-51, Z-55 to Z-58

8 Sputtering parameters pressure 75 mTorr, current 20 mA, time 10x3 min, Ar flow rate 15 sccm⁻¹, substrate-to-target separation 1.3 cm and target d.c. potential -400 V

9 Order and colour determined from interference

10 Evaporation current 35A unless indicated

Table 6.2
Summary of Chemical Etching Results

<i>Solution</i>	<i>Materials Treated</i>				
	<i>Bi</i>	<i>Se</i>	<i>CdO</i>	<i>Resist</i> ¹	<i>Glass</i> ²
H ₂ SO ₄	●	○	●	●	○
HNO ₃ (hot)	●	●	●	●	○
HCl	●	○	●	●	○
Buffered HF	○	○	●	○	●
HF	○	○	●	○	●
HNO ₃ + HCl	●	○	●	●	○
HNO ₃ + H ₂ SO ₄ (hot)	●	●	●	●	○
CH ₃ COOH	○	○	n/a	n/a	○
NH ₄ OH	○	○	●	○	○
CS ₂	○	○	n/a	n/a	○
CS ₂ + HCl	○	○	n/a	n/a	○
CHCl ₃	○	○	○	n/a	○
Acetone	○	○	○	●	○
Trichloroethylene	○	○	○	●	○

Legend

- | | |
|---------------------------|--|
| ● Etching action, | 1. Shipley negative photoresist. |
| ○ No etching observed, | 2. Fisher Scientific microscope glass slide. |
| n/a Results not examined. | |

Table 6.3
Fabrication of Inverted Structure Panels (Glass-CdO/Cd-Se-Metal)

Panel	Config. ¹	Window Layer Deposition on Glass			Selenium Evaporation						Metal Contact Evaporation ⁸				Remarks	
		Matr.	Tech. ²	Order, Colour ³	Time (min)	Sep. ⁴ (cm)	Subst. ⁵ Temp. (°C)	Curr. ⁶ (amp)	Source ⁷ Temp. (°C)	Thick. (µm)	Matr.	Time (min)	Sep. (cm)	Curr. (amp)		Syst. ⁹
Z-52	H	CdO	Sputt.	3 rd green	60	7	140	-	245	15	Wood's alloy	5	6	35	Edw	First functional inverted structure, satisfactory adhesion, two areas isolated by scribing.
Z-54	K	CdO	Sputt.	3 rd green	60	7	140	-	240	12	B1	5	7	40	Edw	Performance rather low, isolation by scribing, used for etching experiments.
Z-70	I	CdO	Sputt.	3 rd green	50	10	140	2.1	-	15	B1	5	8	50	Coo	Cd-rich CdO deposited at end of sputtering run
Z-72	J	Cd	Evap.	-	5	9	120	3.4	-	15	Pt	0.5	4	100	Edw2	Selenium deposition carried out at a higher rate, best overall inverted panel

1. Panel configurations shown in Fig 6.18.
Effective cell areas for config. H, K, I and J
0.35, 1, 0.6 and 0.46 cm² respectively

2. CdO sputtering parameters: pressure 75 mTorr, current 20 mA, time 100 min., Ar flow rate 15 ml.min.⁻¹, substrate-to-target separation 1.5 cm and target d.c. potential - 600 V.
Cd evaporation parameters: molybdenum boat current 45A, substrate-to-source separation 10 cm and time 5 min. (in Cooke vacuum system model CV301FR).

3. Interference order and colour

4. Separation between source and substrate

5. Temperature of the substrate during evaporation

6. Primary current of transformer with secondary connected to Mo boat. Primary-to-secondary windings ratio 22:1. Mo boat used for panels Z-70 and Z-72.

7. Temperature of stainless steel crucible during selenium evaporation, used for panels Z-52 and Z-54.

8. This step was followed also by a Wood's alloy evaporation for solder contacts.

9. Edw, Coo and Edw2 denote Edwards model 6E4, Cooke model CV301FR and Edwards model E306A vacuum systems respectively.

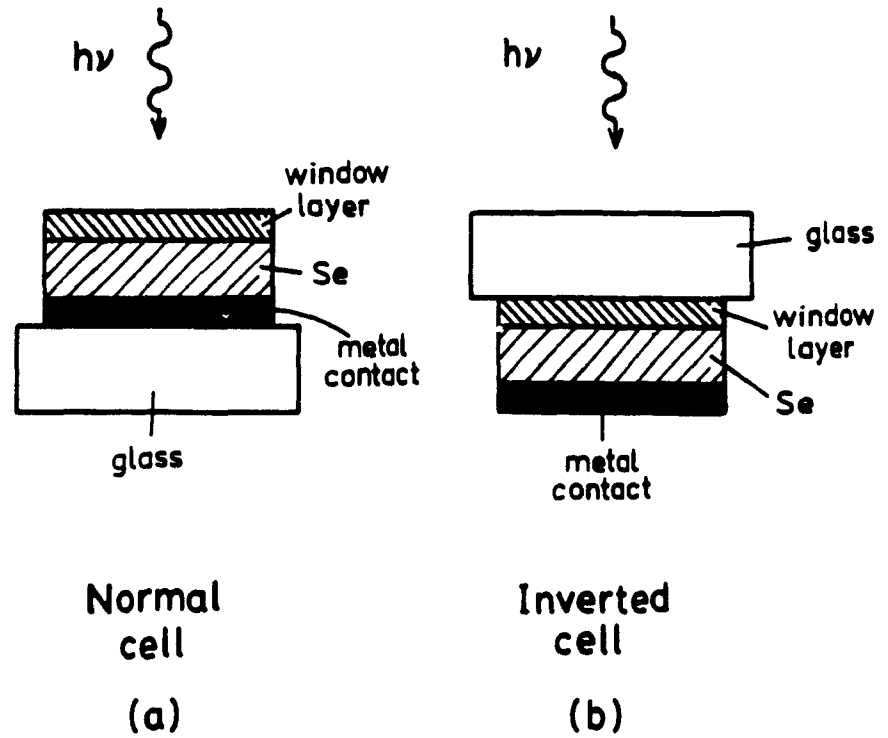


Fig.6.1 Schematic diagrams of (a) a typical normal structure for a photovoltaic cell and (b) an inverted type structure.

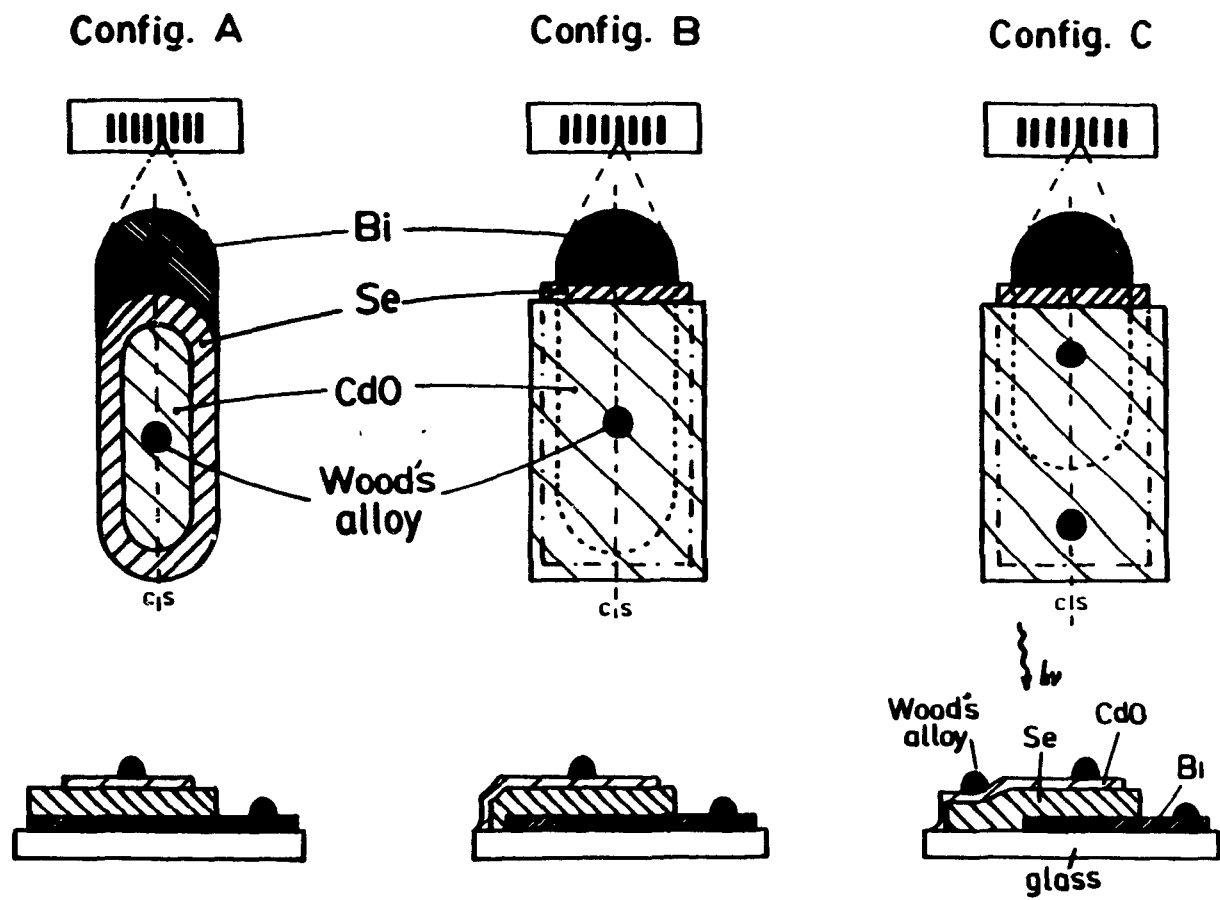


Fig.6.2 Schematic diagram of the normal panel configurations A, B and C.

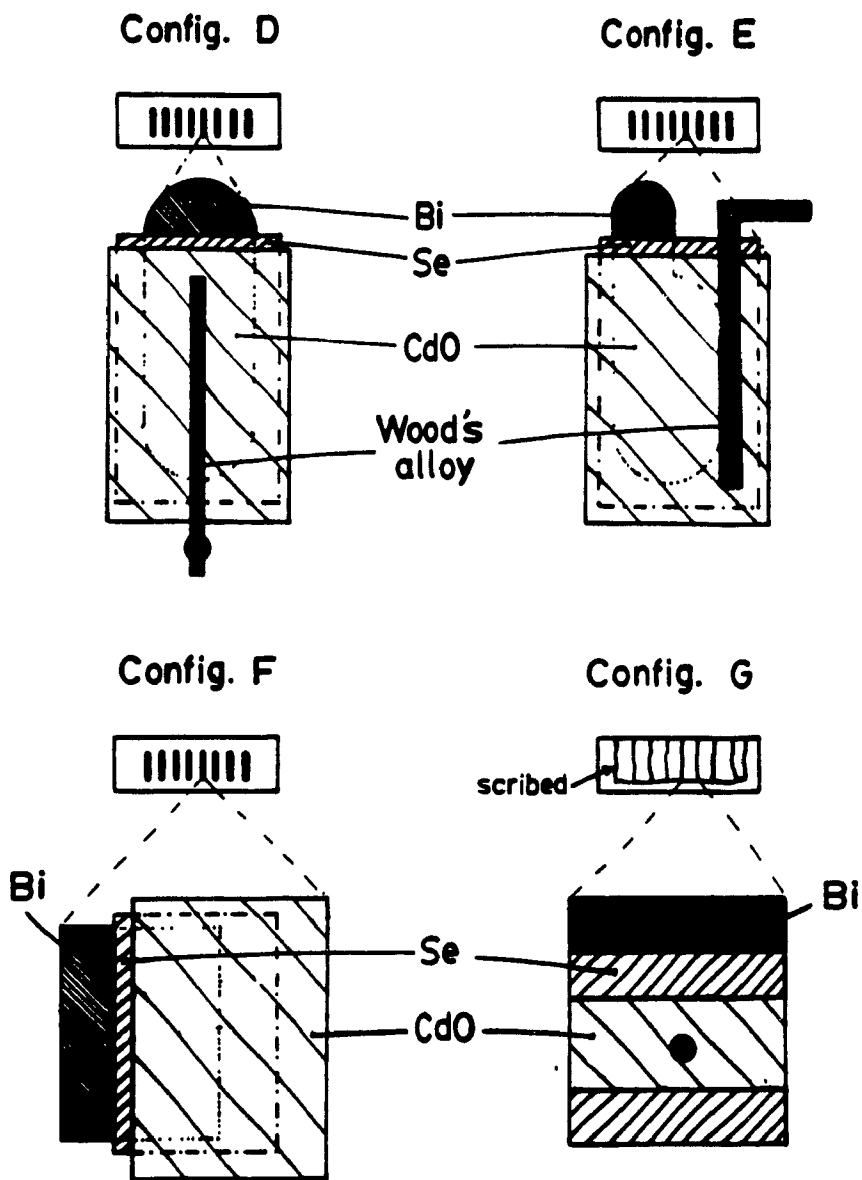


Fig.6.3 Schematic diagram of the normal panel configurations D, E, F and G.

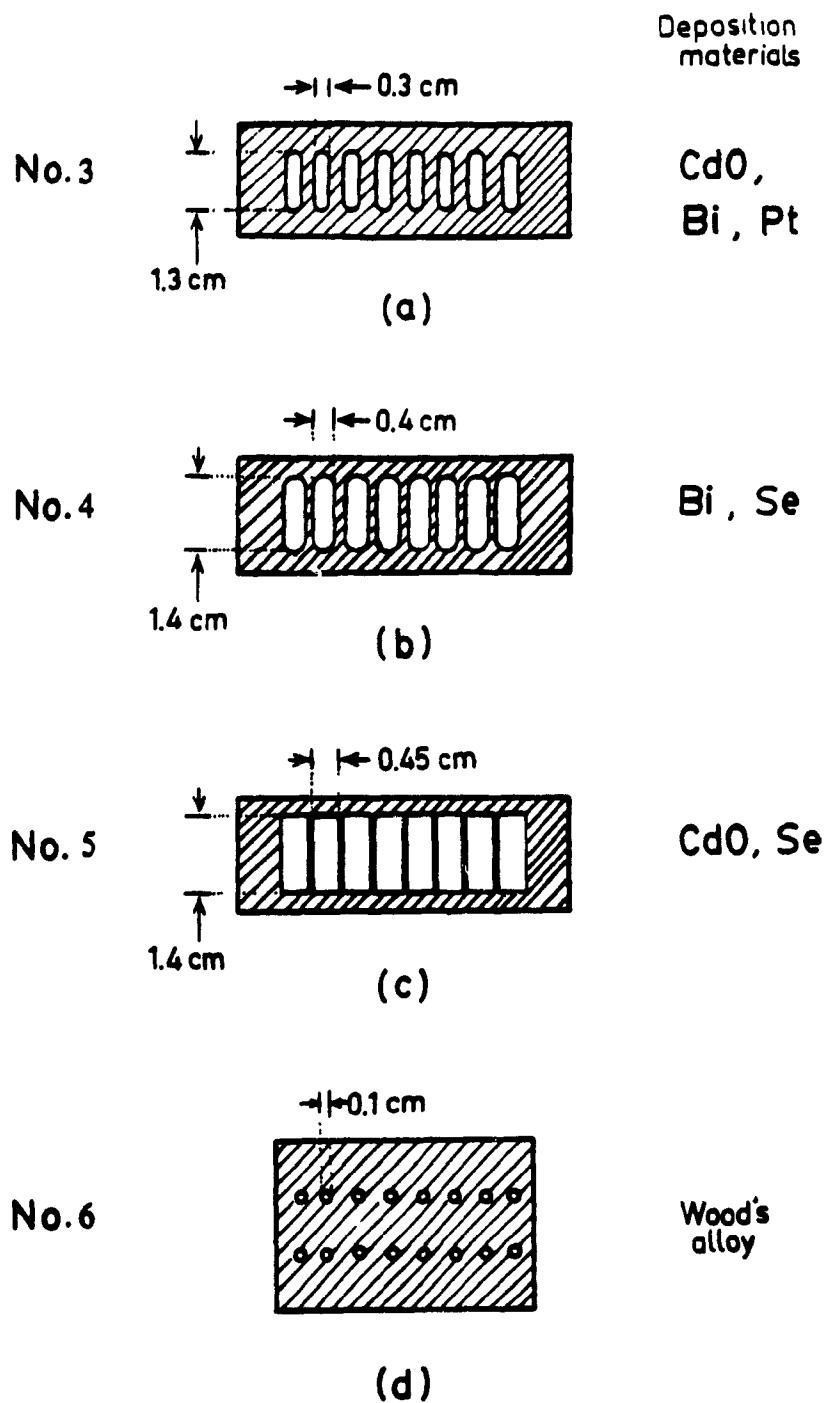


Fig.6.4 Schematic diagram of the four aluminum masks used in the preparation of the panel cells.

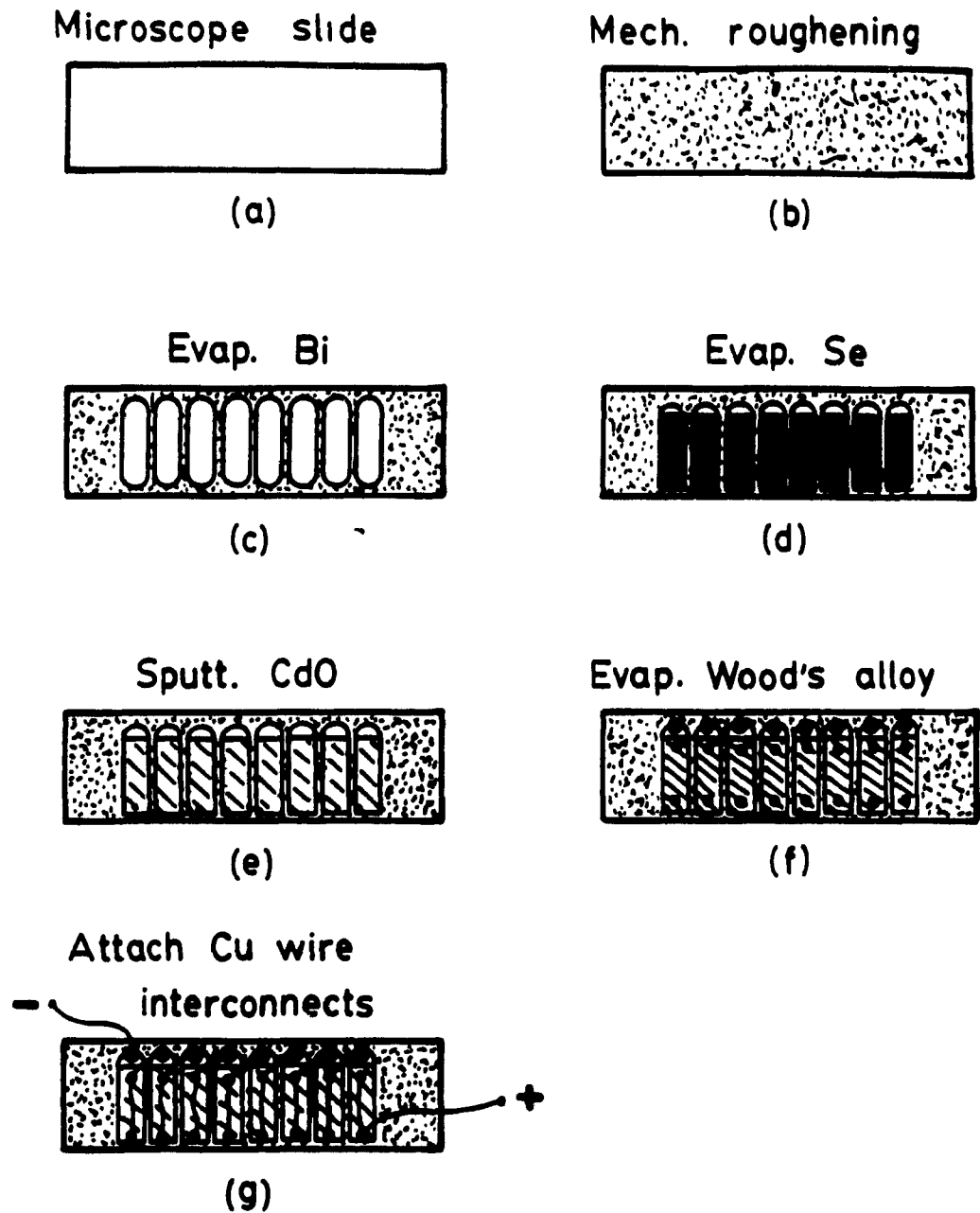


Fig.6.5 Schematic diagram showing the sequence of operations involved in the fabrication of the normal panel structures (with configuration C).

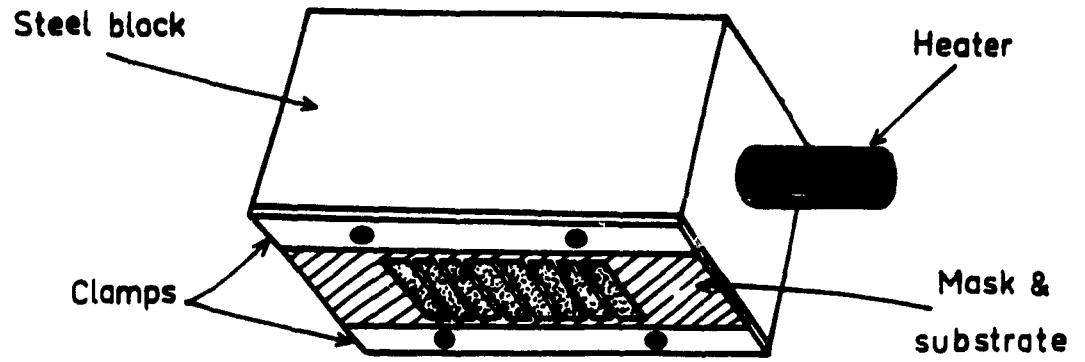


Fig.6.6 Schematic diagram of the panel holder used for the selenium deposition

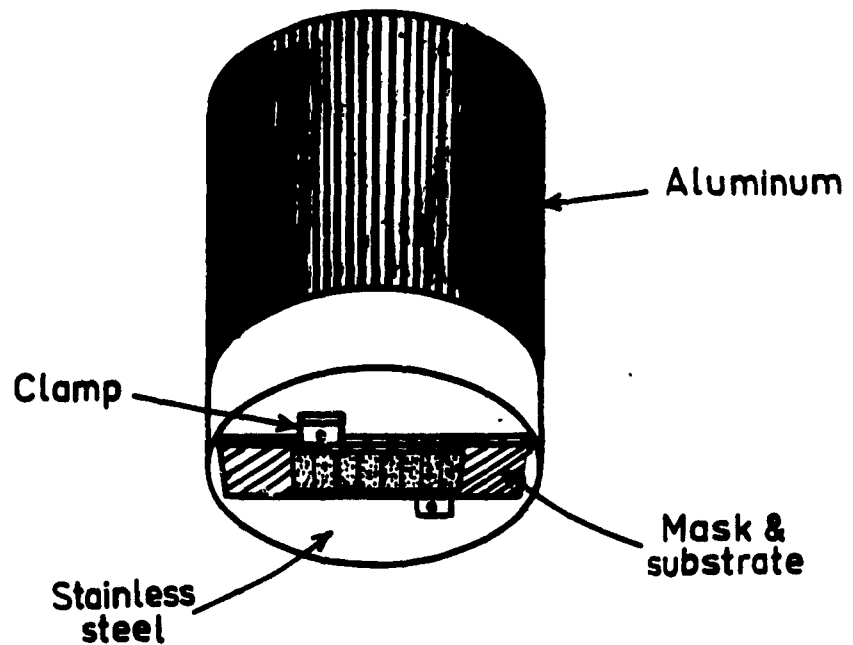
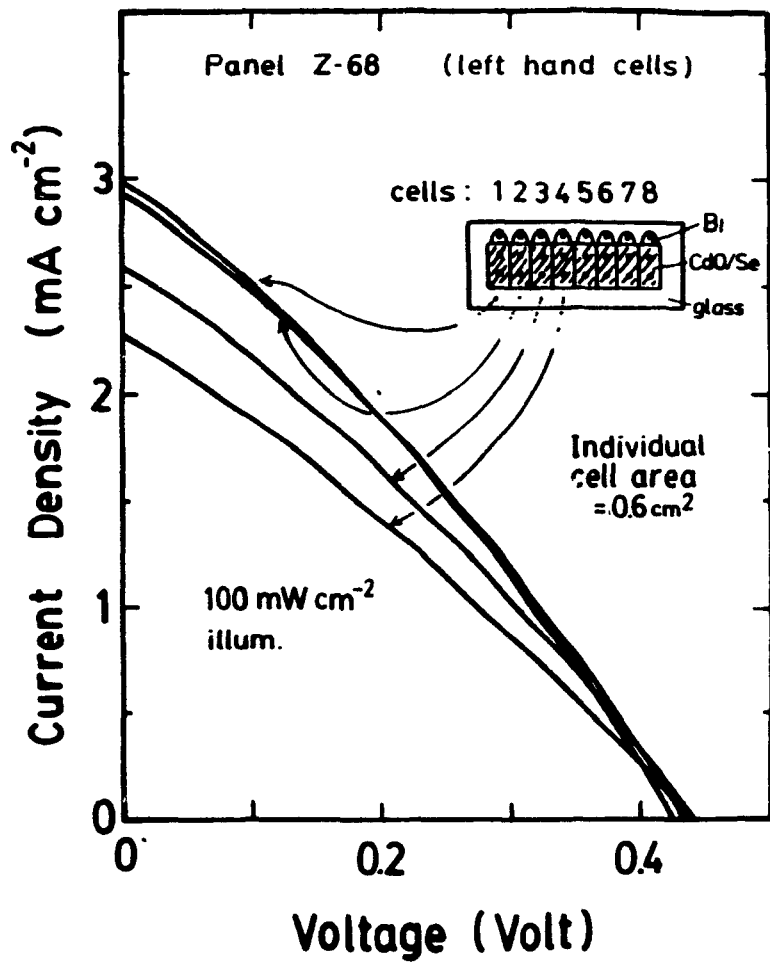
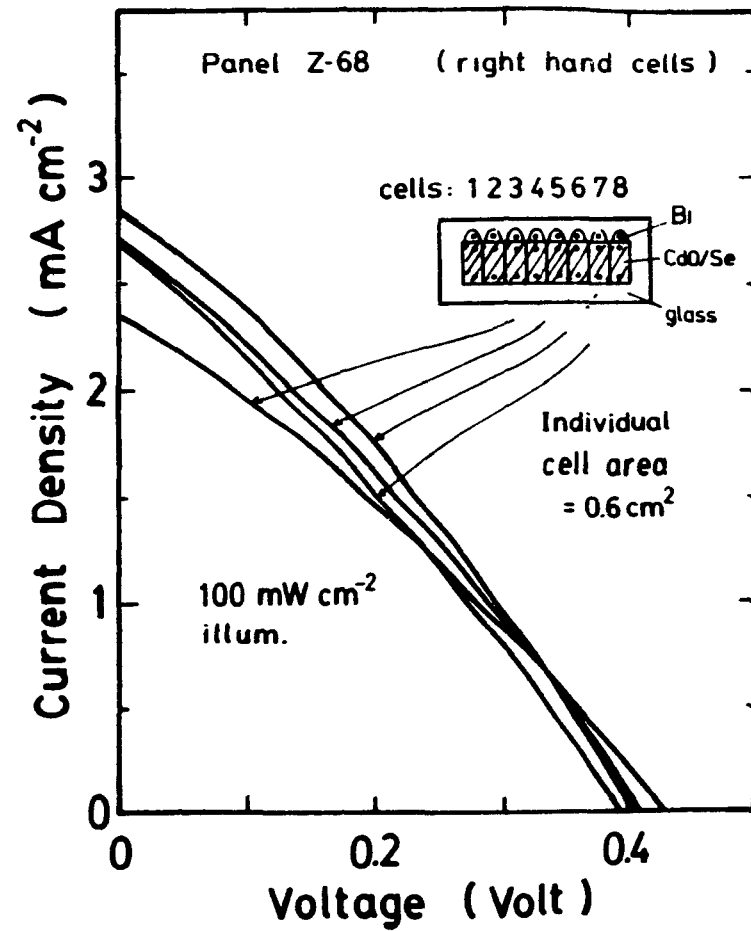


Fig.6.7 Schematic diagram of the panel holder used for the CdO deposition.



(a)



(b)

Fig.6.8 Plot of the illuminated characteristics of the individual cells in panel Z-68.
 (a) Cell numbers 1 to 4,
 (b) Cell numbers 5 to 8.

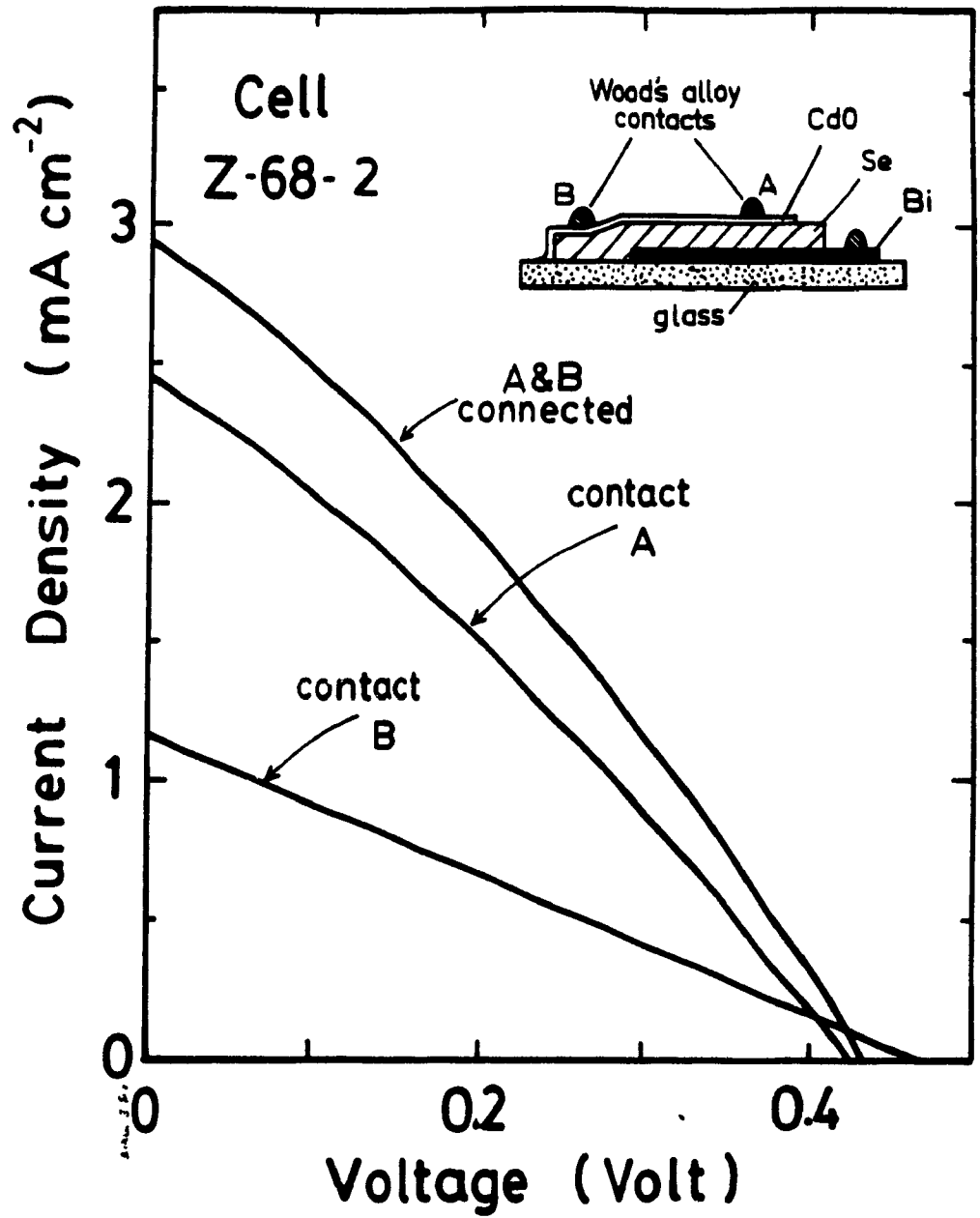


Fig.6.9 Plot of the illuminated characteristics of cell number 2 of panel Z-68, showing the curves for the two contacts separately and together.

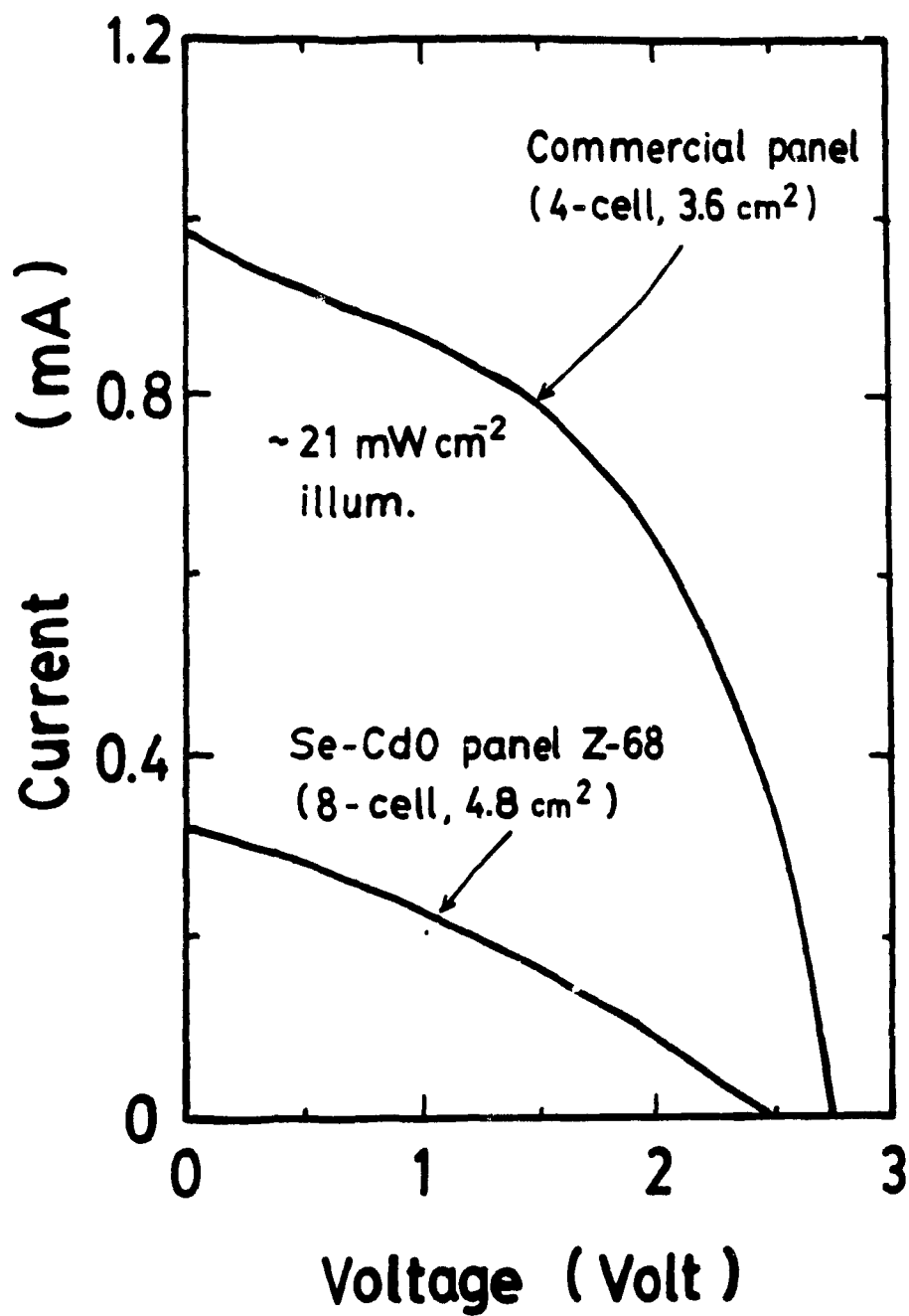


Fig.6.10 Comparison of the current-voltage curves of the Se-CdO panel Z-68 with a commercial panel under low illumination level.

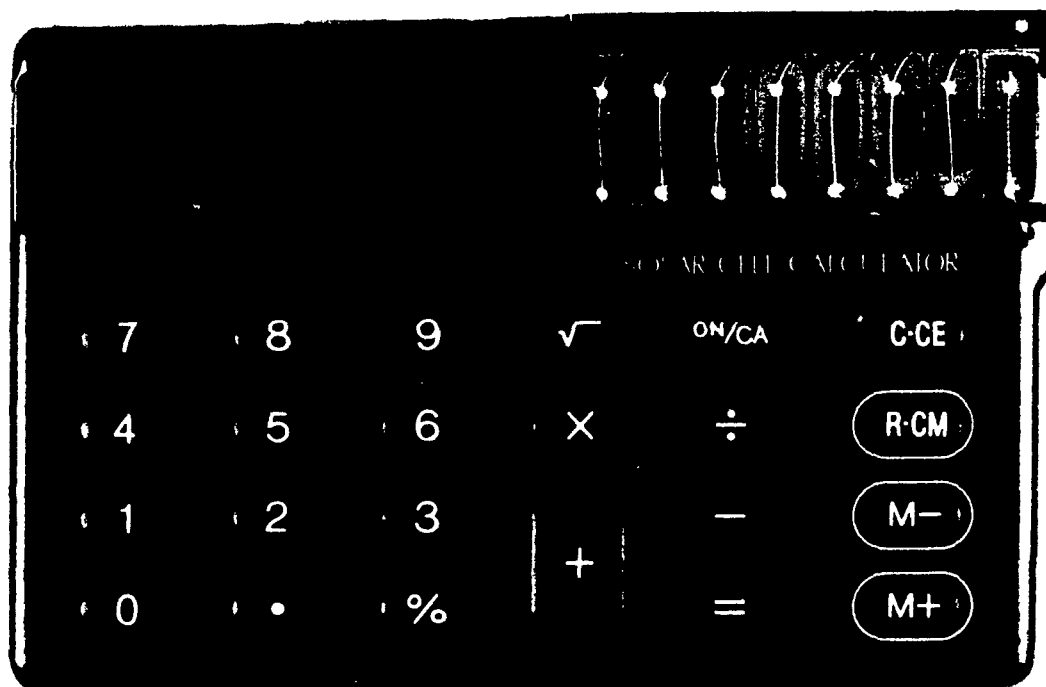


Fig.6.11 Photograph showing the Se-CdO panel Z-68 installed in a commercial pocket calculator.

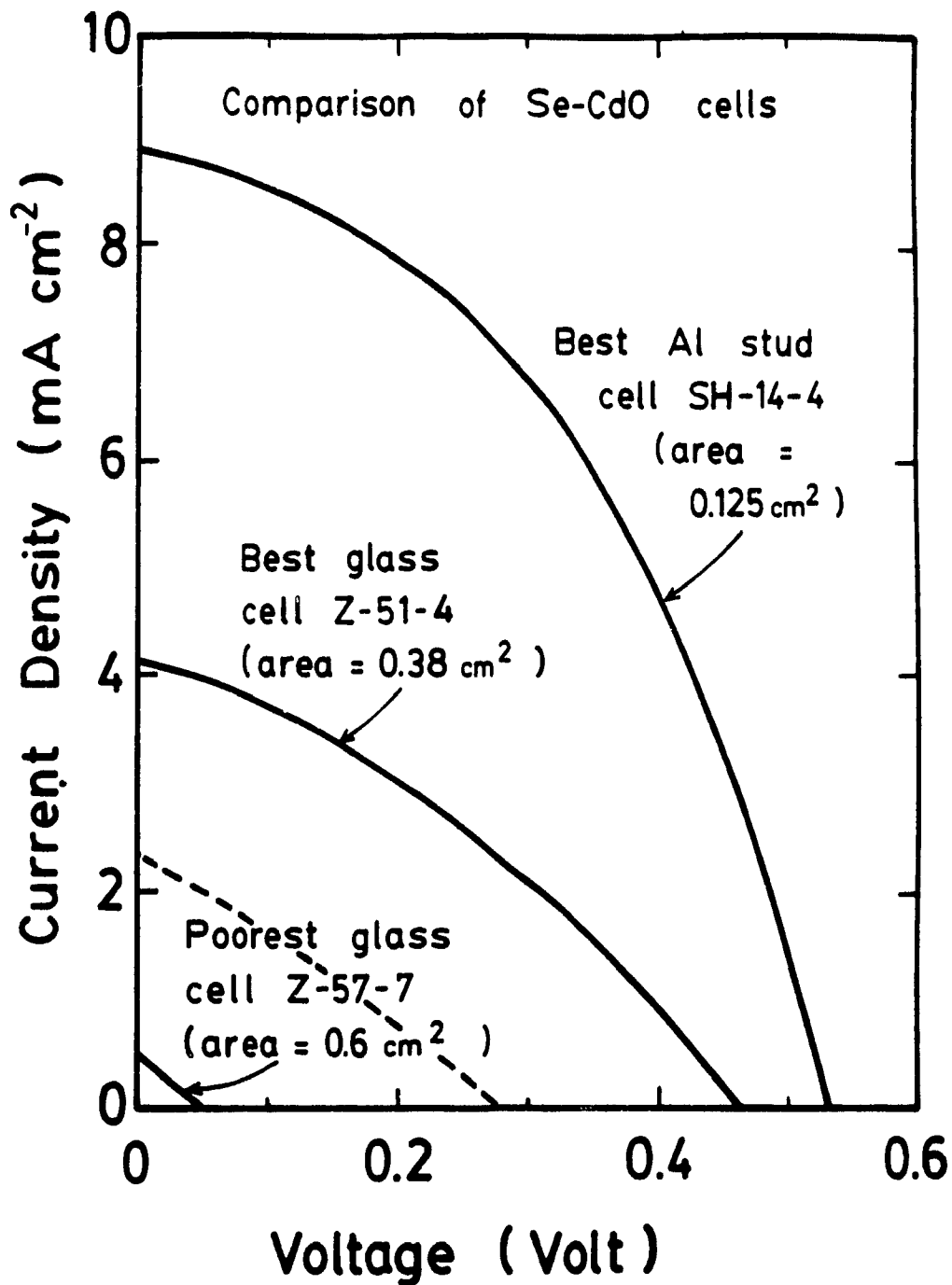
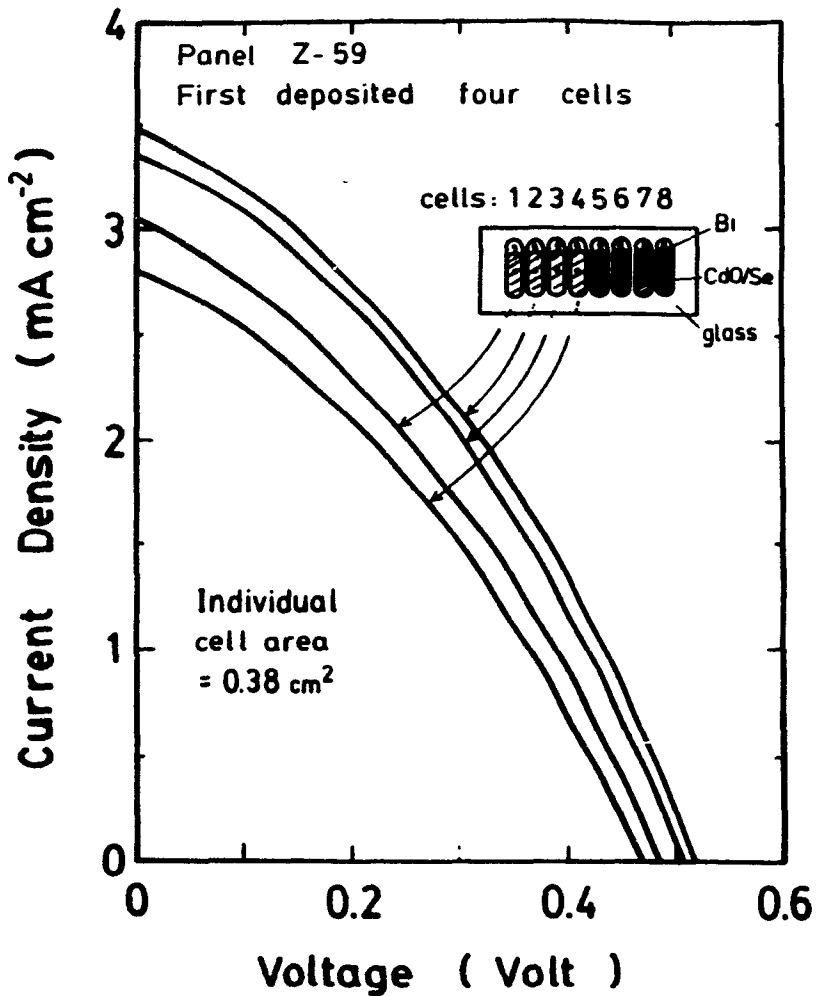
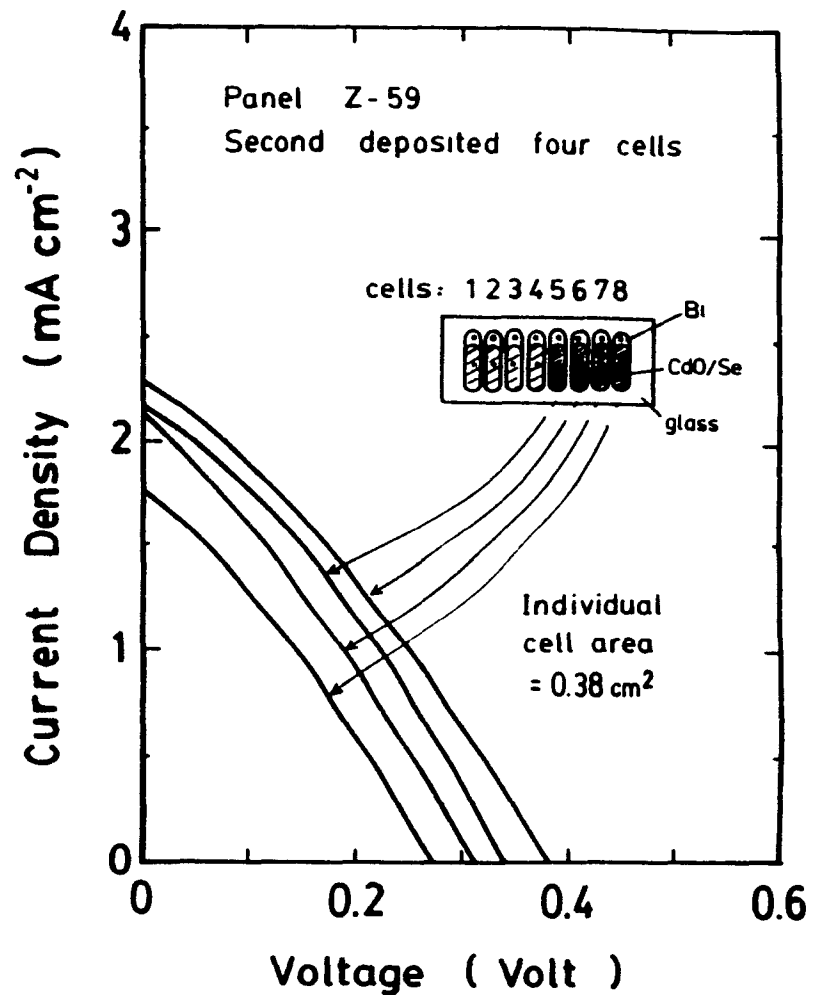


Fig.6.12 Plot of illuminated current density against voltage of the best aluminum stud research cell (SH-14-4) and of the best and the poorest glass substrate cells (Z-51-4 and Z-57-7 respectively). The dashed line represents the average performance for the glass cells.



(a)



(b)

Fig.6.13 Plot of the illuminated characteristics of cells in panel Z-59.
 (a) First deposited CdO areas.
 (b) Second deposited CdO areas.

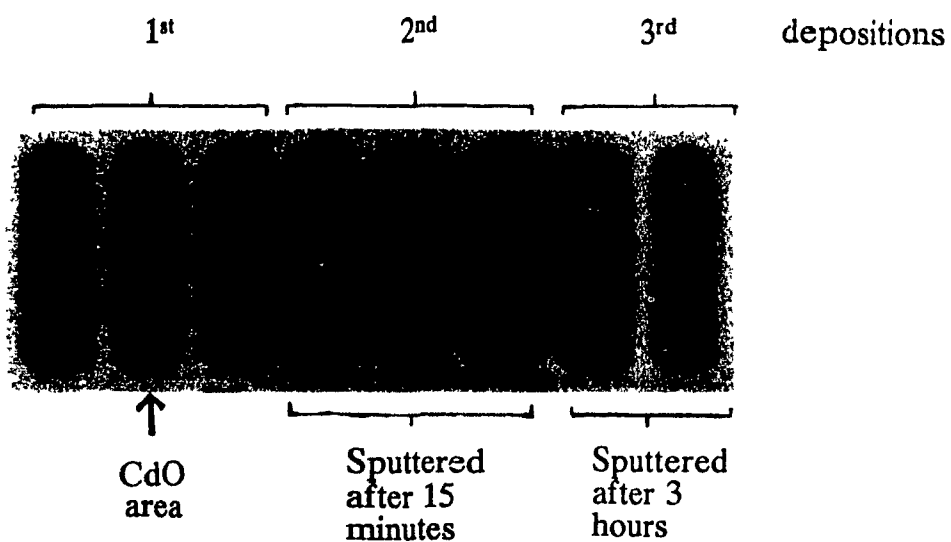


Fig.6.14 Photograph showing CdO areas on glass sequentially deposited by d.c. sputtering after the indicated intervals.

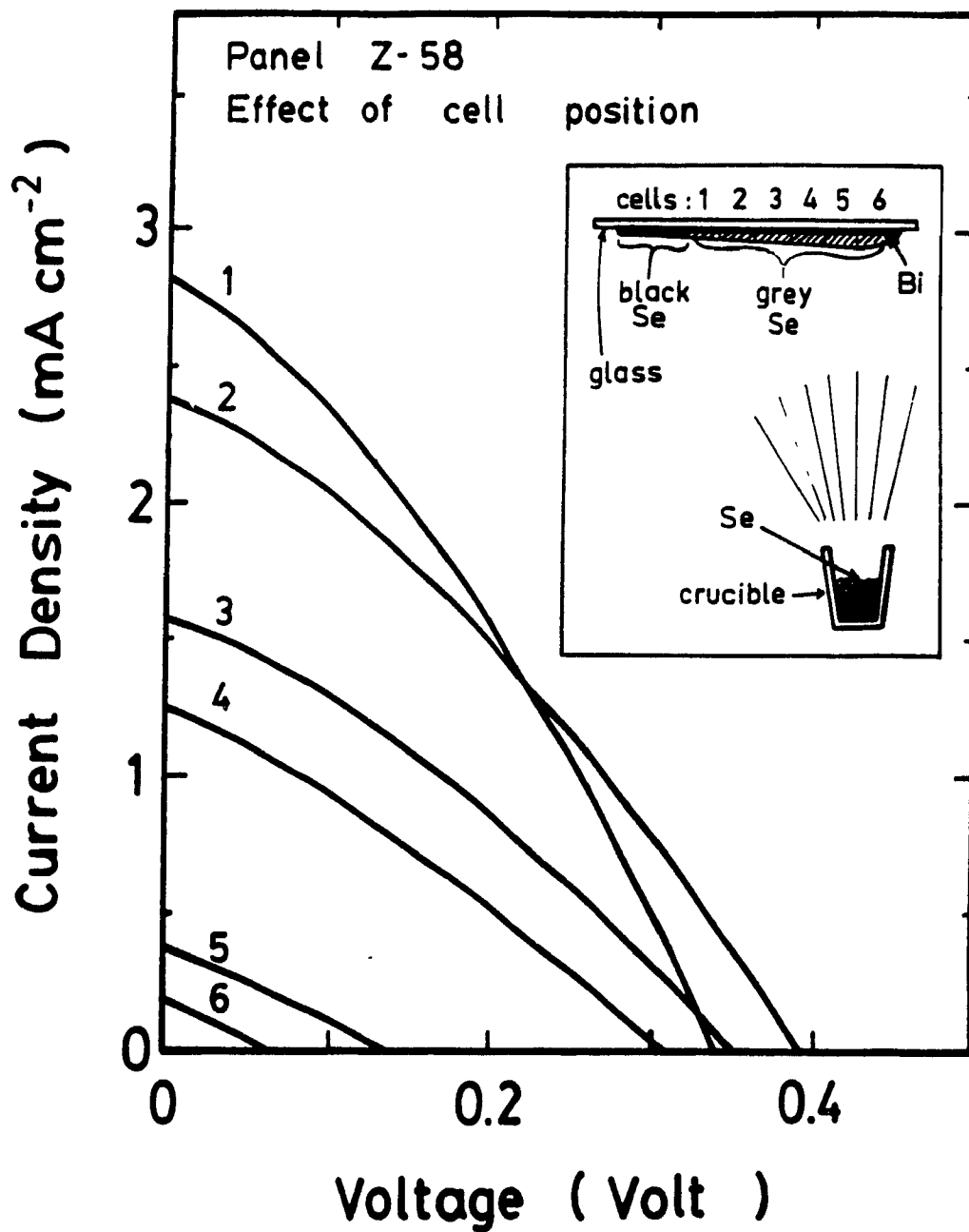


Fig.6.15 Current density-voltage characteristics of six cells in panel Z-58, showing variation in performance with cell position with respect to the source crucible aperture.

Effect of short circuits in panel Z-60

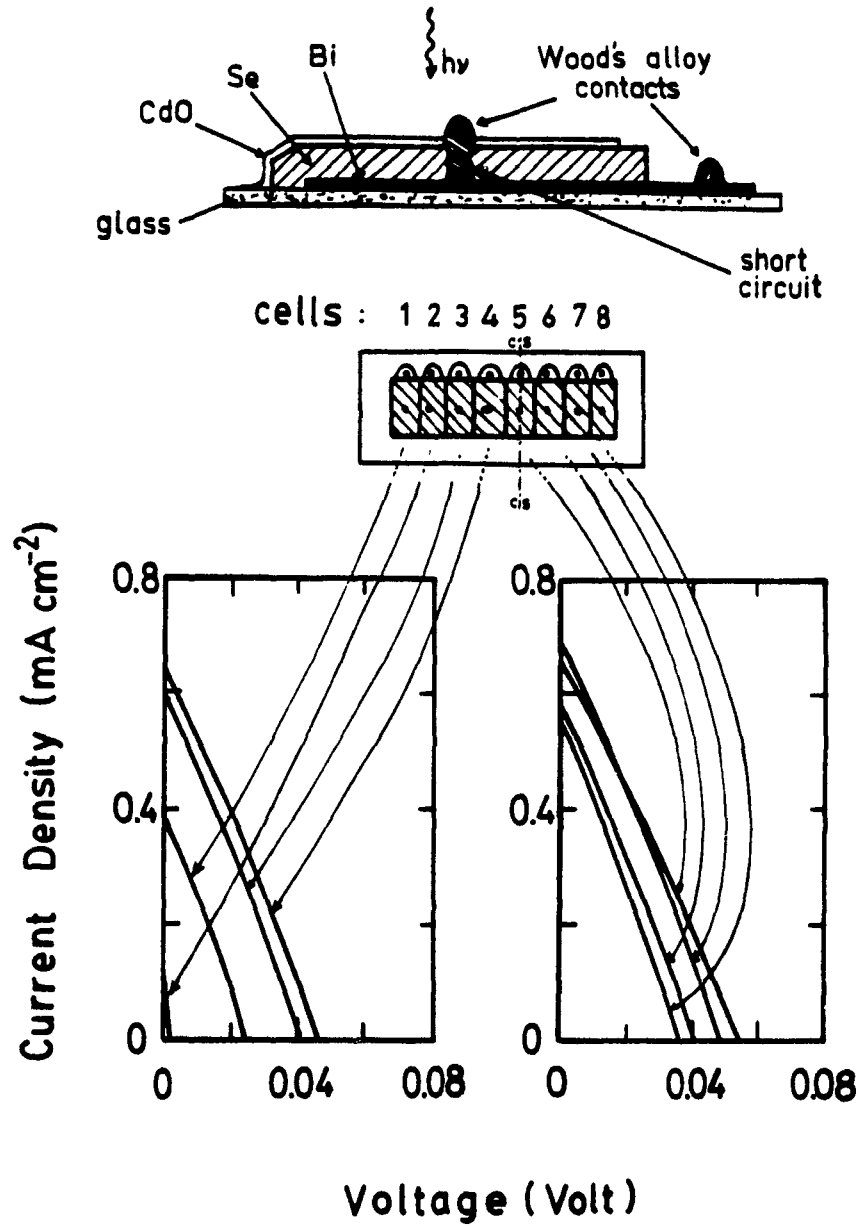


Fig.6.16 Schematic illustration of the short circuit caused by the central Wood's metal contacts of panel Z-60, together with their corresponding j-V curves.

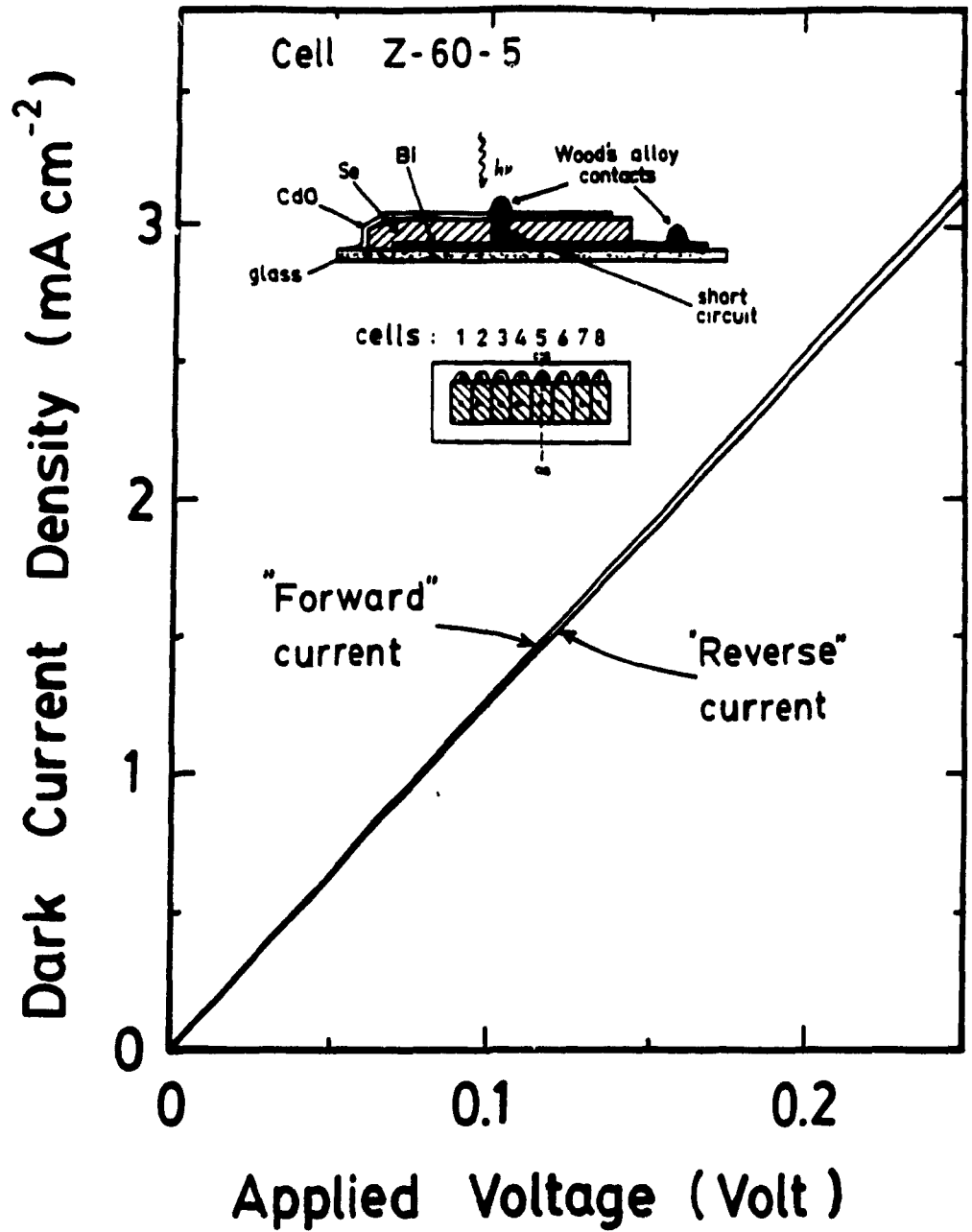


Fig.6.17 Plot of dark j - V characteristics of cell 5 of panel Z-60 showing simply ohmic behavior.

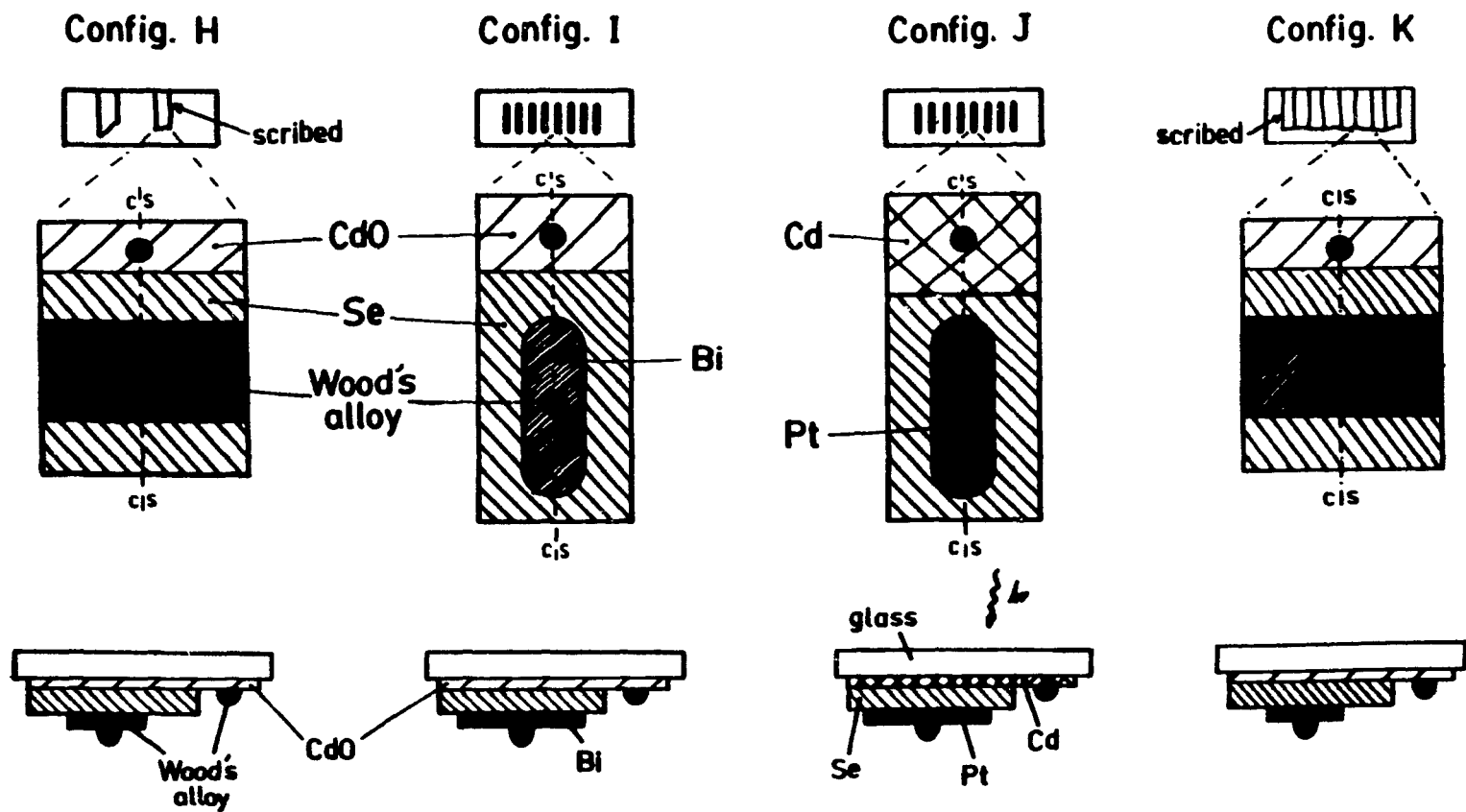


Fig.6.18 Schematic diagram of the four configurations H, I, J and K employed in the inverted panels.

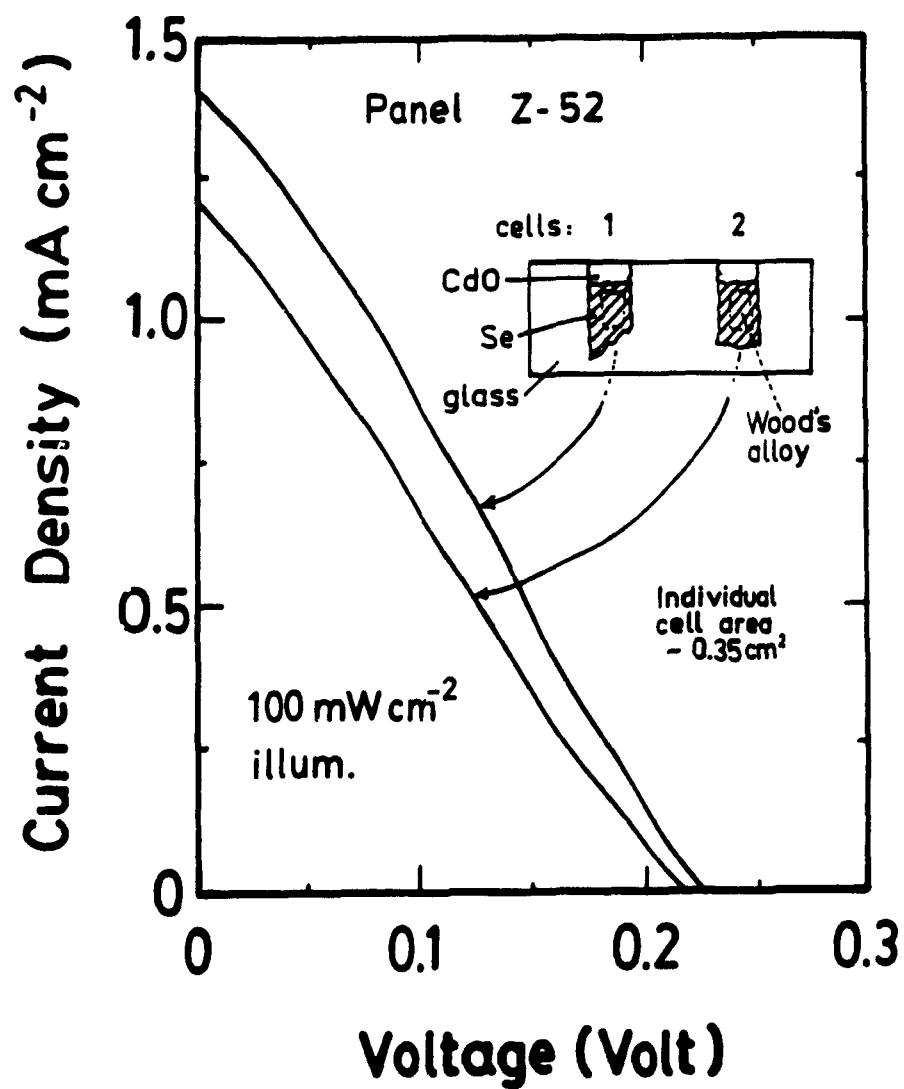


Fig.6.19 Illuminated current density-voltage curves of the two cells in the inverted panel Z-52.

Panel Z-70
Effect of Cd-rich CdO at interface

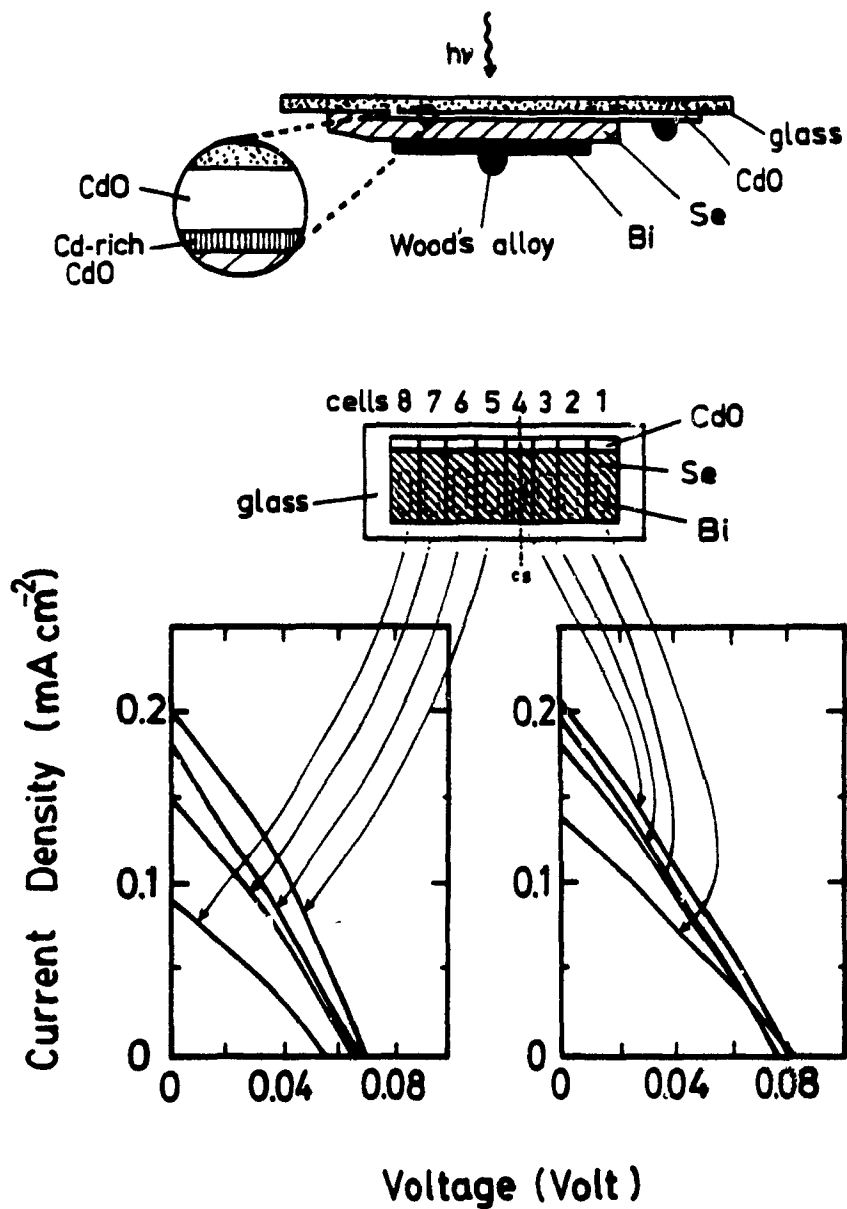


Fig.6.20 Plot of the illuminated characteristics of the eight cells of panel Z-70, showing reduced performance. Shown also is a schematic cross-section of a cell, indicating the Cd-rich CdO layer used to improve the sticking of the crystalline selenium to the CdO film.

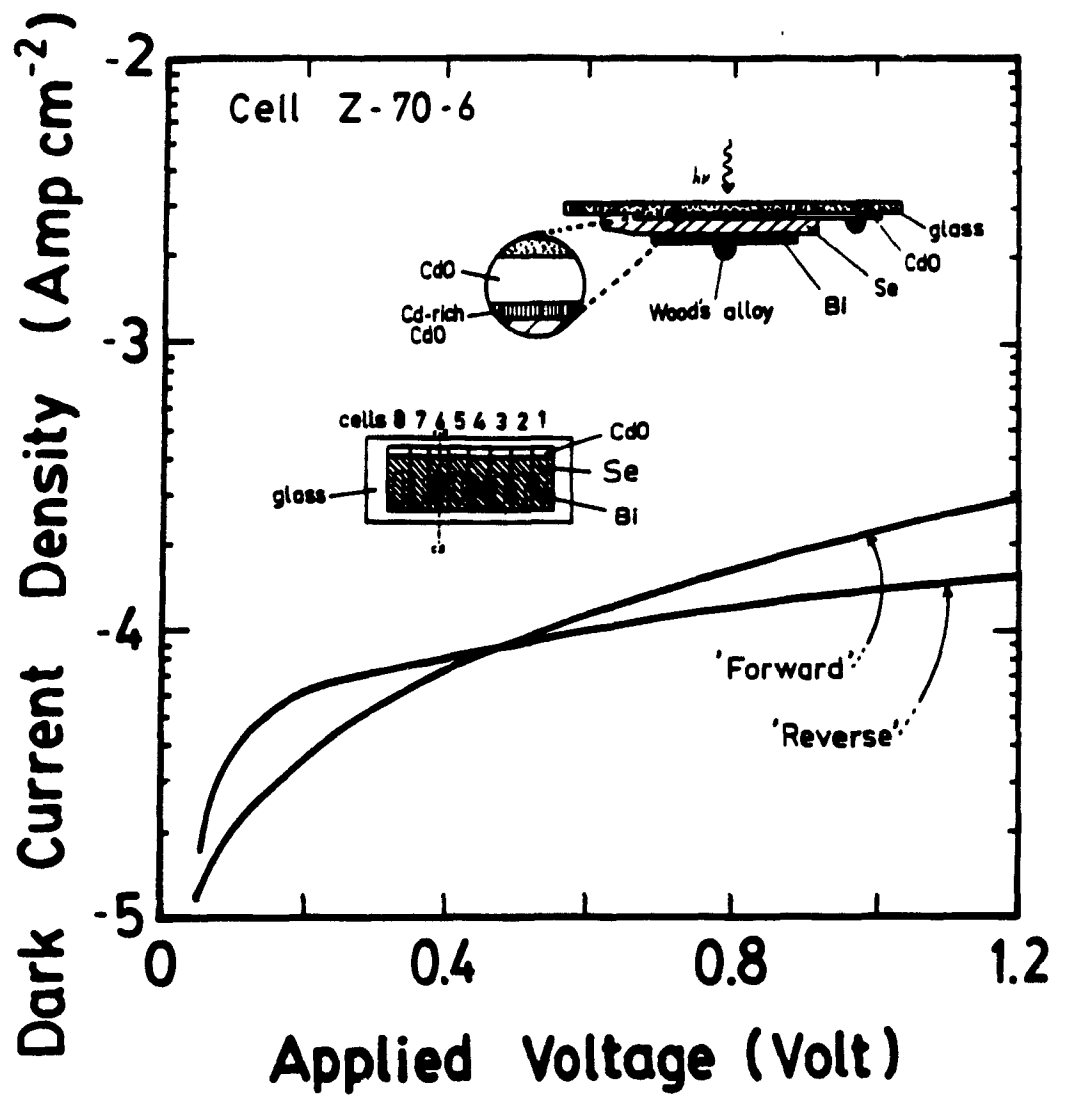


Fig.6.21 Plot of dark current density against voltage of cell number 6 in panel Z-70, showing the possible occurrence of tunnelling at lower voltages.

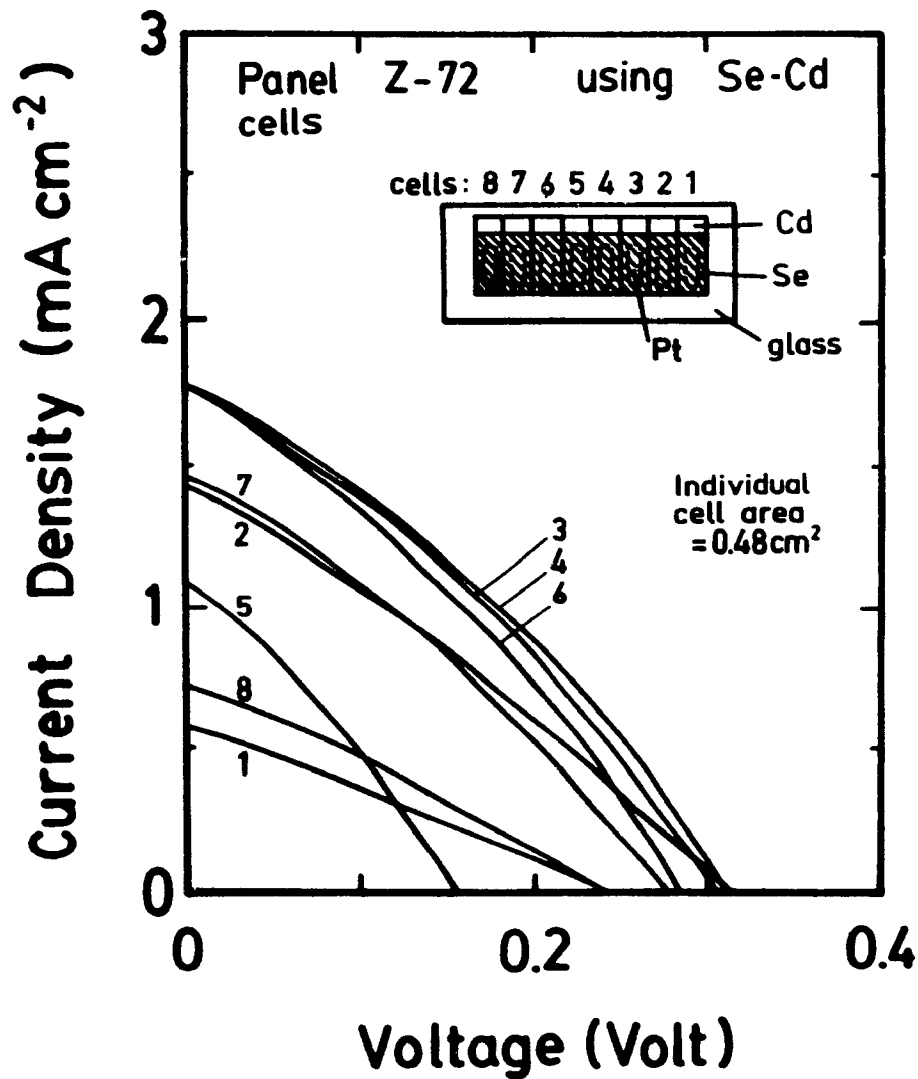


Fig.6.22 Illuminated current density-voltage characteristics of the individual cells of panel Z-72, employing the unconventional Cd-Se-Pt inverted structure.

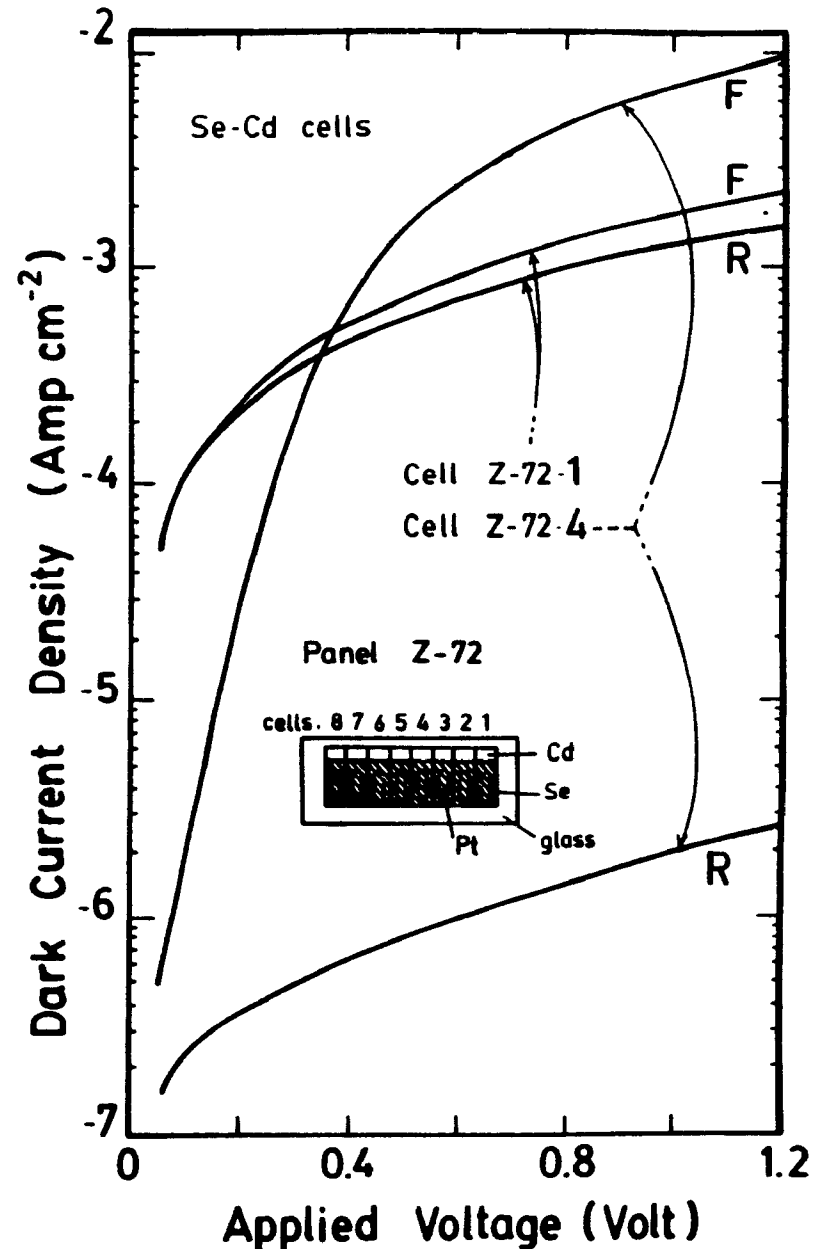


Fig.6.23 Dark current density-voltage curves for cell numbers 1 and 4 of panel Z-72, showing greatly different rectifying behavior.

Chapter 7

OVERALL DISCUSSION OF RESULTS

This chapter gives an overall discussion of the results obtained on the different Se-CdO structures studied in this thesis.

7.1 EFFECT OF SUBSTRATE TEMPERATURE

In the study carried out on the effect of substrate temperature during selenium deposition on cell characteristics in chapter 4, it is clear that crystalline selenium is essential for good photovoltaic performance. Amorphous selenium films, obtained at lower substrate temperatures, such as at 80 and 90°C, yielded barely detectable photovoltaic action, with values of j_{sc} of less than $0.1 \mu\text{Acm}^{-2}$ and V_{oc} values well below 1 mV under 100 mWcm^{-2} illumination. Thus, amorphous selenium is completely unsuitable for photovoltaic devices. It was found that with increasing substrate temperature, at least up to 140°C, both j_{sc} and V_{oc} increased. The temperature limit of 140°C was determined by the re-evaporation of selenium from the substrate, which otherwise would cause the selenium film to be too thin for use in cells, giving rise to short circuits or low shunt resistance values. The initial strong increase of j_{sc} with substrate temperature in the range of 80 to 100°C is due to the amorphous to crystalline transition in the selenium layer. However, the slower progressive increase from about 110 to 140°C is more difficult to explain. It is possible that this increase is due to an increase in the selenium grain size with temperature, although this could not be discerned from microscope observations of the films. The observed increase of dark forward current at 1.0 volt with temperature indicates a decrease of series resistance. This,

in turn, would lead to an increase in the illuminated j_{sc} but would not cause V_{oc} to increase. In fact, no discernible increase in V_{oc} was observed at higher temperature. An alternative explanation is an increase in the electron diffusion length with temperature but this would yield an increase in V_{oc} as well as in j_{sc} . However, this explanation could apply to the lower temperature range, where the amorphous to crystalline transition occurs.

While, at the lower temperature range of 95 to 100°C, the crystallized regions in the selenium were clearly visible and well defined, it was difficult to see the individual grains in films deposited at the higher temperatures between 110 and 140°C. The nucleation for the selenium crystallization resulted in two sizes of crystallization "cells" (which could be spherulites), with one cell about twice the diameter of the other. It is speculated that the larger ones were nucleated during evaporation and the smaller ones at a later stage, possibly during the period of cooling down to room temperature. However, further experiments are needed to determine if this is truly the case.

7.2 CELLS FABRICATED WITH r.f. SPUTTERING

Concerning the results obtained in chapter 5 with r.f. sputtering, it would seem that this is a viable method for depositing the CdO layer in the Se-CdO cells. The overall efficiency of cells prepared by this technique was somewhat lower than that of cells fabricated by d.c. reactive sputtering. It should be pointed out, however, that the work in chapter 5 represents the first time this technique was seriously used in preparing the cells and consequently the deposition conditions were not optimized.

The r.f. sputtering parameters investigated were sputtering pressure, sputtering power and deposition time. The effect of pressure was most interesting in that the stoichiometry of the deposited CdO film was affected in a way similar to that observed in reactive d.c. sputtering. Thus, with increasing sputtering pressure, the CdO resistivity increased monotonically in both the films on glass and in cells. This effect could account for the observed increase in V_{oc} in cells with increasing sputtering pressure. Since the stoichiometry of the target material was presumably fixed and no oxygen was being supplied externally, it is inferred that the sputtering action removes atoms or molecules of cadmium and oxygen separately from the target, which then recombine at the substrate surface. In this case, the deposition rate at the substrate, being controlled by pressure, would affect the degree of stoichiometry of the growing CdO film, as in d.c. reactive sputtering. Results obtained on sputtering power also tend to confirm this explanation, since at very low power settings, much higher resistivity CdO was obtained. This could be due to the greatly reduced deposition rate at the lower sputtering current, whereby there is greater time for the oxygen and cadmium to recombine to produce more stoichiometric and thus, higher resistivity, CdO. Concerning sputtering time, the thickness of the deposited CdO film was confirmed to increase approximately linearly with increasing sputtering time, except for an initial period of some fifteen minutes. Here, the rate was greater, possibly due to the fresh condition of the target surface.

Evidence of an effect of deposition history was obtained in cells and in films deposited on glass. The effect was a decrease in the electrical resistivity of the CdO after continuous sputtering, although the CdO thicknesses were essentially unchanged. While this could be due to an increase in the cadmium to oxygen ratio in the CdO target surface, a more likely cause would seem to be target heating. Despite the fact that the target backing plate was water-cooled, the temperature of

the target surface may still rise if the cooling rate is insufficient. However, further experiments are needed to determine if this is so.

The sputtering yield was greatly increased in using a sintered target over one prepared by hand-pressing, as evidenced by a greater CdO film thickness in a given time. The CdO film thickness was found to increase essentially linearly with power setting, so that this parameter can be used to control film thickness for power levels above about 40 W, where the film resistivity was only weakly dependent on power. The observed initial increase in film thickness with increase of pressure is due to increased ionization of the argon atoms resulting in an increase in the proportion of these ions in the bombarding beam. The subsequent fall of thickness with pressure is due to the reduced mean free path of the sputtered particles and hence to a lower deposition rate. In the present work, the maximum thickness was obtained in the pressure range of 2 to 10 mTorr and therefore this would be a preferred region to carry out the CdO depositions unless stoichiometry control with different pressures is also needed.

The effect of inter-electrode spacing on the r.f. sputtered Se-CdO cells may also be important but it was not investigated in the present work. However, some preliminary runs were carried out with CdO depositions on glass[30], which showed that deposition rate decreased with increasing separation, while film resistivity was more or less unaffected.

7.3 Se-CdO PHOTOVOLTAIC PANELS

In the exploratory work done on the Se-CdO panel structures, the results obtained were quite encouraging. For the first time in this laboratory, a photovoltaic panel was fabricated, employing eight series-connected Se-CdO cells

of the normal type, which was found to operate satisfactorily in a small pocket calculator. The Se-CdO panel was comparable in size to the original "solar panel" used in the calculator, which was believed to employ amorphous silicon. While the short circuit current density of the Se-CdO panel was about one third that of the commercial solar panel, the open circuit voltage was only about 15% less. Since the j_{sc} value in the aluminum stud research cell was about twice that of the panel cell, there is every reason to believe that once the glass-substrate cells are optimized, a Se-CdO based panel can be developed with a performance equal to that of present-day commercial panels employed in calculators.

Besides optimization of the sputtering conditions of the glass-substrate panel cells, an evident improvement in these structures would be the addition of an efficient current collecting grid to replace the dot contacts used. Attempts to deposit Wood's alloy and aluminum stripes on to the CdO were somewhat unsuccessful, since the large ratio of length to thickness in these stripes resulted in high series resistance in the cells and hence reduced performance. Therefore, it is necessary to ensure that the current collecting grid is sufficiently thick so that cell current is not unduly reduced. In relation to the selenium film, improvement is also needed to minimize structural defects in this layer, which are possibly due to the difference in expansion coefficients between selenium and glass.

So far as the author is aware, the present work is the first time photovoltaic action has been reported in an inverted Se-CdO structure, although some similar structures were described in the Japanese literature [31,32]. In this study, the performance of the inverted cells was below that of the normal panel cells in respect of both j_{sc} and V_{oc} . This was more evident in the panels fabricated with a CdO window layer. In these cells, the reduction in j_{sc} is likely to be due to the absence of central metal contacts or stripes on the CdO film, resulting in high

series resistance. Thus, inverted structures with such stripes need to be fabricated to evaluate properly their potential. In the case of the panel with Cd-Se-Pt cells, where the cadmium metal acted as the window layer, the performance was the best among the inverted structures. These cells are all the more interesting because of the lower transparency of cadmium compared with CdO. Furthermore, in this structure, there were no problems with adhesion of the selenium layer to the cadmium film, whereas much difficulty was encountered in depositing selenium onto CdO. Better sticking however, was obtained in the cells where Cd-rich CdO was used. The reason for the generally reduced V_{oc} values in the inverted structures compared to those of the normal panel structures is possibly because the selenium thicknesses in the latter were about twice those in the inverted cells.

Notwithstanding, the lower performance of the inverted cells, they would seem to offer potentially greater advantages over the regular cells. For instance, the CdO layer can be sputtered or heat-treated at a temperature higher than the melting point of selenium, since it is the first layer deposited. Furthermore, the glass substrate with a lower index of refraction than CdO, can reduce the overall reflectance loss in the cells without an additional anti-reflection coating. At the same time, the glass may also serve as a protective cover of the CdO layer and hence reduce any aging process in the cells due to atmospheric exposure.

Chapter 8

CONCLUSIONS AND FUTURE WORK

8.1 CONCLUSIONS

The main conclusions of the present work are summarized as follows:

1. A Se-CdO cell with a conversion efficiency of at least 2%, under simulated solar illumination of 100 mWcm^{-2} , can be fabricated. While this efficiency is not large compared with that of existing solar cells, it is larger than has previously been reported for this type of cell.
2. The illuminated short circuit current density can be increased in these structures by increasing the substrate temperature during the selenium deposition. The increase is strong between about 80 and 100°C but is slower beyond this temperature range, at least up to 140°C . The open circuit voltage also increases rapidly at lower temperature but is more or less unchanged above about 110°C .
3. In depositing selenium as a layer for the cells, two sizes of crystallization region occur at lower substrate temperatures, suggesting nucleation at two different times.
4. Depositing the CdO layer in the Se-CdO cells by r.f. magnetron sputtering from a CdO target, is an alternative method to the d.c. reactive sputtering technique normally employed. However, insufficient results were obtained for a full evaluation of of this technique.
5. The CdO films deposited by r.f. sputtering yield lower shunt resistance in the cells than films prepared by d.c. reactive sputtering. The electrical resistivity of films r.f. sputtered on to glass substrates decreases with increase of sputtering

power and increases with increase of sputtering pressure. This can be understood if atoms of cadmium and oxygen are sputtered separately from the target before recombining at the substrate.

6. A photovoltaic panel consisting of series-connected Se-CdO cells of the normal type can be fabricated to operate satisfactorily as the power source of a small pocket calculator. With sufficient optimization in the fabrication procedure, photovoltaic performance equal to that of present-day amorphous silicon panels under room light should be attainable.

7. The feasibility of an inverted cell structure, where the incident light passes through a transparent substrate, has been demonstrated. Such a device has potential advantages over the normal type structure.

8.2 FUTURE WORK

To improve the Se-CdO cells, much work needs to be done. Some of the more obvious areas for the next phase of studies are as follows.

(a) *Selenium Film Deposition*

1. The selenium film should be deposited at substrate temperatures higher than 140°C to obtain a greater j_{sc} value. In order to accomplish this, methods should be explored to minimize or overcome the re-evaporation of selenium from the substrate at higher temperature. For instance, the selenium may be deposited at a lower temperature and then annealed afterwards beyond 140°C in argon at atmospheric pressure. Alternatively, if the selenium can be deposited on a smooth substrate with sufficient adhesion, then the resultant thinner film deposited above 140°C may still yield sufficient shunt resistance to maintain V_{oc} and obtain

increased j_{sc} at the same time.

2. In the present studies, the selenium used contained about 70 ppm of chlorine. While previous work has indicated some conflicting results obtained with chlorine doping [33,34], it is clear that this element has an important effect on device performance. Accordingly, experiments are needed to determine the optimum level of chlorine doping yielding the best cells.

3. If increased chlorine in the selenium is confirmed to increase performance, cells should be fabricated where the selenium is deposited in two layers; the first should be strongly doped with chlorine to reduce the back contact resistance and the second layer should be undoped or slightly doped to increase the shunt resistance in the cells and hence increase V_{oc} .

4. Experiments should be made to investigate the origin of the two sizes of crystalline regions observed at lower temperatures. For example, the selenium could be deposited at a substrate temperature of 100°C and then cooled rapidly to observe if the smaller type of grain is absent. If so, then this would suggest that nucleation also occurs during the cooling-down period.

5. As a more exploratory idea, it may be interesting to determine if selenium can be deposited by sputtering. If so, such a film might show better adhesion to the substrate and possibly serve as a suitable base on which a second layer could be deposited by evaporation.

(b) CdO Film Deposition

6. While the residual air method was used with d.c. reactive sputtering in this thesis to deposit the CdO layer, future studies should employ the mixed gas technique. This is a simpler method to use and it may yield improved

performance in the cells.

7. Attempts should be made to control the temperature of both the target surface and the substrate surface during sputtering. This can be done by employing new water cooling arrangements or by varying the length of the sputtering periods and the intervals between them.

8. Studies should be made to determine how far the sputtering history of the target affects the deposited CdO film. While some effects may be due to target temperature, other effects may arise from the chemical and physical state of the target surface.

9. The orientation and crystallinity of the deposited CdO may have an effect on cell performance and hence these film properties should be determined by X-ray diffraction.

10. Reactive r.f. sputtering of the CdO in the cells should be investigated using either a cadmium or cadmium oxide target in the presence of mixtures of argon and oxygen.

11. R.f. sputtering from a target consisting of a mixture of CdO and In_2O_3 should be studied to examine how indium-doping of the CdO compares with deviations from stoichiometry to control the resistivity of the deposited window layer in cells.

12. Using r.f. sputtering for depositing the CdO, studies should be carried out of the effects of power level and inter-electrode spacing on cell performance.

(c) Normal and Inverted Panels

13. In respect of panels employing normal Se-CdO cells in series, efforts should be made to improve the cell-to-cell uniformity by appropriate changes in the deposition conditions of both the selenium and the CdO layers. In addition, the deposition parameters of these two layers should be optimized for the glass substrate panels.

14. Further improvement in the performance of the normal cells may be possible by using a thicker layer of bismuth for the back contact to reduce the series resistance. The effectiveness of having a bismuth oxide film underneath the bismuth layer to improve adhesion, should also be investigated.

15. Further work should be done on the inverted structures to improve their performance. In order to reduce series resistance in the cells, a metal grid or stripes should be deposited on the glass substrate prior to CdO deposition. Furthermore, if adhesion can be improved, a thicker layer of selenium should be deposited than was possible in present samples to increase the shunt resistance. Possibly, a very thin film of tellurium between the CdO and selenium may be helpful to promote adhesion between the two layers.

16. Metal stripes of sufficient thickness should be used for cell-to-cell interconnections between panel cells to replace the soldered wires.

BIBLIOGRAPHY

- [1] J.S. Preston, Proc. Roy. Soc. London, Ser. A, **202** , 449 (1950).
- [2] C.H. Champness, S. Fukuda and S. Jatar, Solar Energy Materials, **5** , 391 (1981).
- [3] C.H. Champness and K. Ghoneim, Solar Cells, **13** , 121 (1984).
- [4] C.H. Champness, K. Ghoneim and J.K. Chen, Can. J. Phys., **63** , 767 (1985).
- [5] Y.F. Go, *Variations in the Fabrication of a Se-CdO Photovoltaic Cell*, (McGill University Thesis, Montreal, 1989).
- [6] R.F. Shaw and A.K. Ghosh, Solar Cells, **1** , 431 (1979/80).
- [7] W.R. Grove, Phil. Trans. Roy. Soc. London, Ser. A, **142** , 87 (1852).
- [8] J. Stark, Z. Elektrochem., **14** , 752 (1908); **15** , 509 (1909).
- [9] J.J. Thomson, *Rays of Positive Electricity*, (Longmans, Green and Co., Ltd., London, 1921).
- [10] J.D Cobine, *Gaseous Conductors*, (Dover publishing, New York, 1958).
- [11] L.I. Maissel and R. Glang, *Handbook of Thin Film Technology*, (McGraw Hill, New York, 1970), p. 4-4.
- [12] L.I. Maissel and R. Glang, *Handbook of Thin Film Technology*, (McGraw Hill, New York, 1970), pp. 4-15 to 4-18.
- [13] B. Chapman, *Glow Discharge Processes* (John Wiley and Sons, New York, 1980), pp. 189 and 195.
- [14] N. Laegried and G.K. Wehner, J. Appl. Phys., **32** , 365 (1961).

- [15] J.L. Vossen and W. Kern, *Thin Film Processes* (Academic Press Inc., New York, 1978), p. 61.
- [16] W.Y. Lee and D.W. Oblas, *J. Appl. Phys.*, **46** , 1728 (1975).
- [17] W.D. Westwood, *Prog. Surf. Sci.*, **7** , 71 (1976).
- [18] E. Krikorian and R.J. Sneed, *J. Appl. Phys.*, **37** , 3665 (1966).
- [19] L. Holland, *Vacuum Deposition of Thin Films* (Chapman and Hall Ltd., London, 1966), p. 413.
- [20] K.L. Chopra, *J. Appl. Phys.*, **37** , 3405 (1966).
- [21] D.M. Mattox and J.E. MacDonald, *J. Appl. Phys.*, **34** , 2493 (1963).
- [22] K. Meyer, I. Shuller and C. Falco, *J. Appl. Phys.*, **52** , 5803 (1981).
- [23] L.I. Maissel and R. Glang, *Handbook of Thin Film Technology*, (McGraw Hill, New York, 1970), pp. 4-32 to 4-34.
- [24] S.M. Levitskii, *Sov. Phys.-Tech. Phys.*, **2** , 913 (1957).
- [25] J.L. Vossen and W. Kern, *Thin Film Processes*, (Academic Press Inc., New York, 1978), pp. 157 and 160.
- [26] J.L. Vossen and W. Kern, *Thin Film Processes*, (Academic Press Inc., New York, 1978), p. 49.
- [27] E. Hollands and D.S Campbell, *J. Mat. Sci.*, **3** , 544 (1968).
- [28] S. Schiller, U. Heisig and K. Goedickie, *Thin Solid Films*, **40** , 327 (1977).
- [29] J.L. Vossen and W. Kern, *Thin Film Processes*, (Academic Press Inc., New York, 1978), p. 151.

- [30] Z.A. Shukri, *Studies on Se-CdO Photovoltaic Cells Fabricated by d.c. and r.f. Sputtering*, (McGill University Report, Course 304-677A, Montreal, 1988).
- [31] T. Nakada and A. Kunioka, *Jap. J. Appl. Phys.*, **23**, L587 (1984).
- [32] T. Nakada and A. Kunioka, *Jap. J. Appl. Phys.*, **24**, L536 (1985).
- [33] K. Ghoneim, *Studies on a Se-CdO Photovoltaic Cell* (McGill University Thesis, Montreal, 1983).
- [34] J.K. Chen, *Fabrication of a Se-CdO Photovoltaic Cell using a Mixed Gas Sputtering Technique* (McGill University Thesis, Montreal, 1985).
- [35] M.A. Green, *Solar Cells*, (Prentice-Hall Inc., Englewood Cliffs, N.J., 1982), p. 96.

Appendix

CURRENT DENSITY-VOLTAGE RELATION IN CELLS

The photovoltaic junction cell under illumination, can be represented by the simple equivalent circuit model [35] shown in Fig.A.1. Here, j_{ph} , R_s and R_{sh} represent the photogenerated current density, area series resistance and area shunt resistance in the cell respectively. The output current density j is therefore given by:

$$j = j_{ph} - j_{diode} - j_{shunt}$$

The diode current density is given by:

$$j_{diode} = j_o \left(e^{\frac{q(V+jR_s)}{nkT}} - 1 \right),$$

where n , k , q and T are the ideality factor, the Boltzmann constant, the electronic charge and the absolute temperature respectively. The shunt current density is given by:

$$j_{shunt} = \left(\frac{V+jR_s}{R_{sh}} \right).$$

Therefore, by substitution into the first equation we obtain:

$$j = j_{ph} - j_o \left(e^{\frac{q(V+jR_s)}{nkT}} - 1 \right) - \left(\frac{V+jR_s}{R_{sh}} \right), \quad (\text{A.1})$$

which is the equation describing the illuminated j - V characteristics of a photovoltaic cell. The current density-voltage characteristics in an ~~unilluminated~~ cell is given by equation A.1 with j_{ph} set to zero. However, for the dark characteristics it is customary to express the current as positive when entering the diode in the forward direction. Thus, in this case the forward current density j_f is given by:

$$j_f = j_o \left(e^{\frac{q(V-jR_s)}{nkT}} - 1 \right) + \left(\frac{V-jR_s}{R_{sh}} \right). \quad (\text{A.2})$$

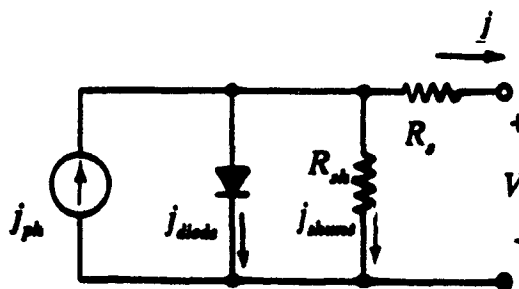


Fig.A.1 Simple equivalent circuit model of a photovoltaic p-n junction cell including parasitic resistances.